MODEL OF CRITICAL HEAT FLUX IN SUBCOOLED FLOW BOILING

Mario P. Fiori

Arthur E. Bergles

Report No. DSR 70281-56

Department of Mechanical Engineering
Engineering Projects Laboratory
Massachusetts Institute of Technology

September 1968

Contract No. Air Force F44620-67-C-0047

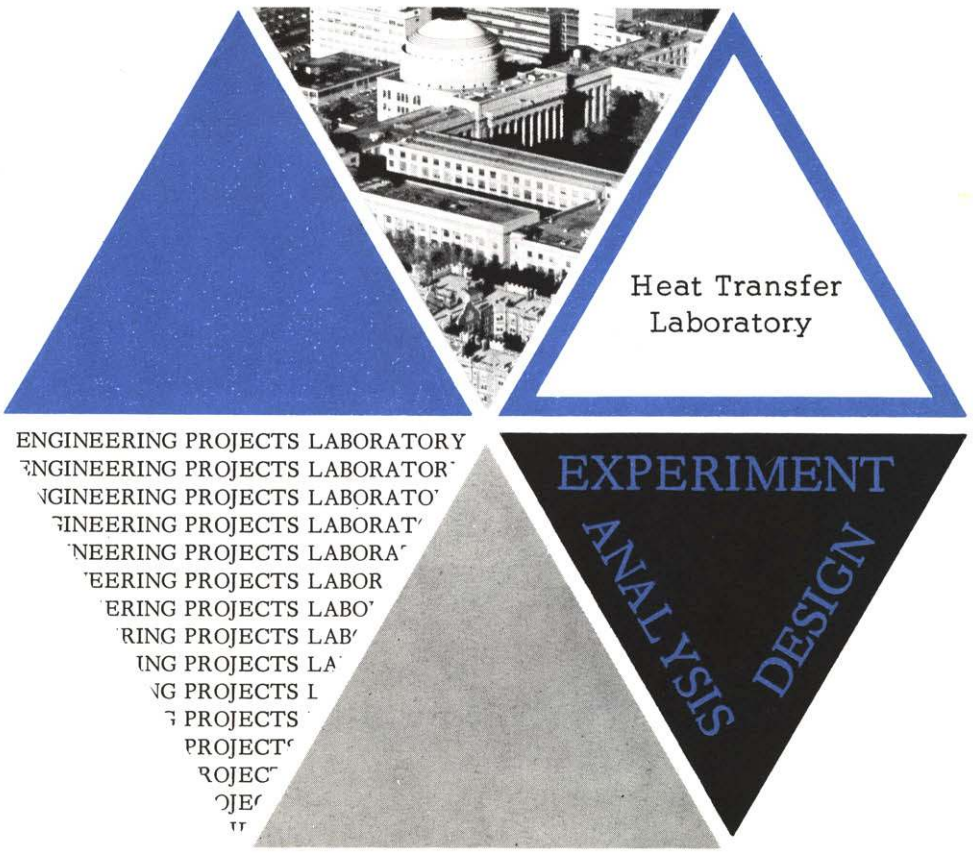

TECHNICAL REPORT NO. 70281 - 56

MODEL OF CRITICAL HEAT FLUX IN SUBCOOLED FLOW BOILING

by

Mario P. Fiori
Arthur E. Bergles

for

Massachusetts Institute of Technology

National Magnet Laboratory

Sponsored by the Solid State Sciences Division

Air Force Office of Scientific Research (OAR)

Air Force Contract F44620-67-C-0047

D.S.R. Project No. 70281

September 1968

Department of Mechanical Engineering

Massachusetts Institute of Technology

Cambridge, Massachusetts 02139

ABSTRACT

The physical phenomenon occurring before and at the critical heat flux (CHF) for subcooled flow boiling has been investigated.

The first phase of this study established the basic nature of the flow structure at CHF. A photographic study of the flow in a glass annular test section was accomplished by using microflash lighting and a Polaroid camera. The results showed that the flow structure at CHF for high heat flux (1×10^6 - 5×10^6 Btu/hr-ft^2), high subcooling (50-110 °F), at low pressures (less than 100 psia) was slug or froth flow depending on the mass velocity. Nucleation was shown to exist in the superheated liquid film. Pin-holes in the burned-out test sections suggested that the CHF condition was extremely localized. Flow regime studies in tubular and annular geometries, using an electrical resistance probe, provided further evidence of the slug or froth nature of the flow, and also showed that dryout of the superheated liquid film was not responsible for CHF.

Since this evidence was contradictory to previously formulated models of CHF, a new model was proposed: Near the CHF condition, nucleation is present in the superheated liquid film near the surface. As a large vapor clot passes over the surface, these nucleating bubbles break the film and cause a stable dry spot which results in an increased local temperature. As the vapor finally passes the site, the dry spot is quenched by the liquid slug, and the temperature drops. At CHF, the volumetric heat generation, slug frequency, and void fraction are such that the temperature rise resulting from the dry spot is greater than the temperature drop during quenching. An unstable situation results where the temperature of this point continues to rise when each vapor clot passes the site until the Leidenfrost temperature is reached, at which point quenching is prevented and destruction is inevitable.

A new method of measuring surface wall temperatures, in conjunction with high speed (Fastax) 16 mm movies, confirmed the microscopic features of the proposed model. At CHF, the wall temperature cyclically increased with the same frequency as the slug-vapor bubble passage. Destruction finally resulted as the temperature increased beyond the Leidenfrost point.

An analytical investigation based on an idealized model demonstrated that the cyclical nature of the temperature increase at CHF could be predicted with appropriate flow pattern inputs. A parametric study using the program indicated that heater thickness and heater material should affect the CHF.

It was shown that the proposed model appears to be consistent with parametric trends, i.e. mass velocity, pressure, subcooling, diameter, length, and surface tension. The model indicated that the CHF for thicker walled tubes, keeping all other conditions the same, would increase. CHF tests were conducted which confirmed that thicker walled tubes (0.078 vs. 0.012 in.) had CHF up to 58 percent higher than thin walled tubes.

ACKNOWLEDGEMENTS

This study was supported by the National Magnet Laboratory of the Massachusetts Institute of Technology which is sponsored by the Solid State Sciences Division of the Air Force Office of Scientific Research. Machine computations were done on the IBM 360 computer located at the M.I.T. Computation Center and on the IBM 1130 computer in the Mechanical Engineering Department, M.I.T.

M. P. Fieri's studies at M.I.T. have been supported by the United States Navy under the Junior Line Officer Advanced Scientific Education Program (BURKE Program).

TABLE OF CONTENTS

List of Figures

LIST OF TABLES

NOMENCLATURE

A = area

c_p = specific heat at constant pressure

D = diameter

D_e = equivalent diameter

E = test section voltage

G = mass velocity

H = enthalpy

H_f = saturation liquid enthalpy

H_{fg} = heat of vaporization

h = heat-transfer coefficient

I = test-section current

k = thermal conductivity

L = axial heated length

P = pressure

q = rate of heat transfer

q_E = rate of heat transfer calculated using test section voltage and current

q_W = rate of heat transfer calculated using First Law of Thermodynamics

r = coordinate shown in Fig. 55

r_b = bubble radius

q/A = heat flux

q/V = internal heat generation rate per unit volume

R_{in} = internal radius of heated section

R_{out} = outside radius of heated section

T = temperature

t = wall thickness

t = time

V = velocity

w = mass flow rate

X = equilibrium steam quality at test section exit

α = thermal diffusivity

α = void fraction

ΔT_{sub} = degrees of subcooling at test section exit

ΔH_{sub} = subcooling enthalpy at test section exit

ρ = fluid density

μ = dynamic viscosity

DIMENSIONLESS GROUPS

Nu = Nusselt number = hD/k

Pr = Prandtl number = $c_p\mu/k$

Re = Reynolds number = GD/μ

SUBSCRIPTS

b = bulk fluid condition

cr = critical condition

e = test section exit condition

fc = forced convection conditions

in = test section inlet condition

q = quench conditions

s = saturation conditions

W = tube wall characteristics

Chapter 1

INTRODUCTION

One of the most important phenomena which limits the thermal performance of high heat flux systems, such as pressurized water reactors, high powered electronic tubes, and high field magnets, is the so-called critical heat flux (CHF) condition, which is characterized by a sharp reduction in ability to transfer heat from the heated surface. This condition is also referred to as burnout, departure from nucleate boiling, or boiling crisis; however, these terms are generally understood to have the same meaning for the high heat flux conditions of interest here. A typical boiling curve for water under subcooled forced-convection conditions is given in Fig. 1; the boiling curve for saturated pool boiling is included for comparison. For a system where heat flux is the independent variable, point A or A' defines the conditions where a sudden rise in surface temperature is observed with a further increase in heat flux. The metal would then continue to overheat, passing through the partial film boiling regime, the Leidenfrost point, D or D', and continue into the film boiling regime. For saturated pool boiling with small wires, the new equilibrium point, C, is generally below the melting point of the heater; however, for flow subcooled boiling this point, C', is above the melting point.

Most emphasis has been devoted to CHF data collection and formulation of empirical correlations to predict the data. Although

some idealized models of the physical conditions at CHF have been proposed, very little experimental work has been undertaken to examine the actual physical situation. A brief review of correlation and modeling work is given in the following sections.

1.1 Parametric Effects on CHF for Water

The principal parameters which have been found to affect subcooled forced convection CHF in round tube and annular test sections with uniform heat flux are pressure, mass velocity, degree of subcooling, and geometry (length and diameters). The trends appear to be independent of the fluid.

Early CHF studies by McAdams [1]* and Gunther [2] found no pressure effect. It is difficult, however, to examine this effect from their limited data. On the basis of more recent data [3, 4, 5] it is generally agreed that $(q/A)_{cr}$ increases up to a maximum for pressures between 300 and 800 psia. Figure 2 presents a composite plot showing this effect.

There also is general agreement that increasing the mass velocity increases CHF for subcooled conditions. This effect is clearly demonstrated by Ornatski's data plotted in Fig. 3 for high pressure and by data of Loosmore and Skinner [6] at low pressures (Fig. 4).

Increased subcooling increases CHF. For convenience in correlation the relation between subcooling and CHF has generally been considered to be linear [7, 8]. Examination of actual data, however, [2, 3, 6, 9] indicates that at low values of subcooling, particularly at low pressures, there exists a decidedly nonlinear relation, since

*Bracketed numbers refer to references listed beginning on page 152.

a minimum heat-flux is generally reached in the subcooled region near zero quality (Fig. 4). Those studies which have considered very high subcooling also demonstrate nonlinearity (Fig. 3). The cross-coupling of mass velocity and subcooling was demonstrated by Longo [10] who noted the increase of CHF with subcooling to be greater when associated with lower velocities.

Bergles [5], and subsequently Loosmore and Skinner [6], both working with pressures below 100 psia, showed that CHF increases as tube diameter decreases. Bergles, using the Zenkevich prediction [11], suggested that above 0.3 in. the diameter might have little effect (Fig. 5). Ornatskii and Vinyarskii [12] showed this effect for pressures between 11 and 61 atm. Doroshchuck and Lantsman [3] similarly found this effect for tube diameters over most of the high pressure range (735 psia to 2500 psia) with exit conditions varying from high subcooling (ΔH_{sub} = 200 Btu/lbm) to bulk boiling.

CHF decreases as L/D is increased to a limiting value (L/D = 10 to 40 [5,4]) above which it has a minor influence; thus L/D is considered only as an entrance effect (Fig. 6).

Limited work has been carried out to define the effect of secondary factors such as surface roughness, gas content, etc. Durant [13] showed up to 100 percent improvement in CHF for knurled surfaces over smooth tubes; however, there appears to have been little work done which would suggest that normal roughness variation has an effect. Doroshchuck and Lantsman [3] have shown that small amounts of dissolved gas in the flow stream has a negligible effect on CHF. Frost [54], in subcooled annular flow experiments, showed CHF decreasing with decreased surface tension.

The possible effects of heater material or heater wall thickness on CHF have received very little attention other than in pool boiling. Lee [14]

examined wall thickness effects in flow bulk boiling and found a 6-8 percent increase in $(q/A)_{cr}$ for the thicker walled tube (0.078 vs. 0.034 in.). Hewitt, et al. [17] found a slight improvement in $(q/A)_{cr}$ for thicker (0.080 vs. 0.036 in.) tube walls for high quality (85 percent) and low pressure (>50 psia) flow. Both Vliet and Leppert [15], for slightly subcooled water flowing normal to a cylinder, and Aladyev, et al. [16], for subcooled forced convection in tubes at high pressures (20 - 200 atm), did not observe any variation of CHF with wall thickness.

The preceding parameter trends refer to stable conditions. Stability of the flow has a very strong influence on CHF [18]. Daleas and Bergles [19] showed that moderate upstream volumes (23 and 94 $in.^3$) of subcooled water have sufficient compressibility to promote oscillatory behavior which produces a large reduction in the subcooled critical heat flux for a single channel. An analytical study [20] and its extension to a wide variety of data demonstrated the conditions under which these system-induced instabilities can be eliminated. General cures for these instabilities are to throttle the flow near the test section's upstream end and to avoid any compressible volumes between the throttle valve and the test section.

1.2 Predicting CHF

Three basic methods for predicting CHF are the empirical method using statistical and curve-fitting techniques, the superposition method, and the prediction method using mathematical models based on hypothesized physical pictures of the events occurring at CHF.

1.2.1 Empirical Analysis of CHF Data

Correlations for CHF resulting from empirical analyses of particular data are usually very limited in application, and often cannot predict another set of data even within the range of applicability. This is understandable considering the fact that CHF for uniformly heated round tubes, is a six dimensional (q/A, G, P, ΔH_{sub}, D, L) problem with cross-coupling of parameters.

A purely statistical method of correlation for predicting CHF has been developed by Jacobs and Merrill [21]. They have proposed a system-describing concept wherein the independent parameters (T_{in}, P, G, D) of the system are used in correlating the CHF data. Twenty-four terms were necessary to correlate the nonlinear and coupling effects of these parameters. Since the physics of the crisis phenomenon is neglected and because the parametric trends cannot be readily deduced from the formula, this method is of little general interest.

A more meaningful method of correlating CHF data involves curve-fitting of data and cross-plotting to obtain the parametric effects. Gunther [2] developed one of the earliest (1950) examples of this type of correlation:

$$(q/A)_{cr} = 0.0135\ V^{0.5}\ \Delta T_{sub}$$

This equation has not been successful in predicting other data, probably due to the fact that Gunther used a very thin walled metal strip as the heated surface. Mirshak [7], using similar techniques of cross-plotting data, also showed a pressure effect.

Another example of a correlation using this method of curve-fitting is that of Macbeth [22]. He used a combination of physical reasoning, by assuming the local conditions hypothesis (CHF for bulk boiling is a function of G, D, X, P), and a statistical approach, by examining more than 5,000 world data points. A reasonably accurate correlation was achieved for the bulk boiling regime, but he also states that the correlation equations are applicable in the subcooled region. This, however, is questionable since he extrapolates the linear $(q/A)_{cr}$ - X_e curve from the quality region into a known nonlinear subcooled region.

A more fundamental approach to CHF prediction centers around finding certain dimensionless groups which describe the data. Both Zenkevich [4] and Griffith [23] attempted to use this method to account for different fluids.

1.2.2. Method of Superposition

Several investigators have suggested that CHF for forced convection can be predicted by superimposing a convective term on the CHF for pool boiling. Gambill [24], in a very extensive study, demonstrated this technique by using a pool boiling correlation, an appropriate convective heat-transfer coefficient and Bernath's [25] wall temperature correlation. It has been shown that Bernath's correlation is incorrect [26]; thus the physical basis for the correlation is insecure. Gambill's correlation predicts a wide variety of data; however, it is still not especially general since the data for small diameter tubes are not well

predicted [5,6]. Levy [27] independently developed a similar superposition method which, however, used the more accurate method recommended by Jens and Lottes [28] to get the wall temperature.

Using superposition, it is tacitly assumed that convection and pool boiling, two highly nonlinear systems, do not interact. Since this is not physically reasonable, the success of the correlations must be regarded as fortuitous. One of the reasons they work quite well is because the heat flux level is generally set by the dominant convective term.

All the correlations mentioned in this section are sometimes useful for specific design purposes; however, all the above methods suffer from the fact that they do not explain the physical situation contributing to subcooled flow boiling crisis. The desire to go beyond merely correlating CHF data and to begin to understand the physics of the crisis has prompted several investigators to propose models which supposedly represent the physical situation. Three interesting and well-known pictures of CHF are discussed in the next section.

1.3 Discussion of Earlier Critical Heat Flux Models

1.3.1 Hydrodynamic Analysis of Chang [29]

It has been shown by Zuber et al. [30] and others that the critical heat flux in pool boiling is a hydrodynamically-oriented phenomenon which can be compared to a traffic jam where the bubbles leaving the surface are so numerous that colder liquid cannot reach the surface. Chang, in agreement with this pool CHF picture, extends it to forced convection flow.

Chang proposes that the bubbles generated on the heated surface either break away from the surface or collapse on it. At the critical condition, the bubbles do not collapse but agglomerate on the surface. He considers the bubbles to be moving in the field of a very viscous, or even non-Newtonian fluid, and at CHF the bubbles achieve a critical velocity normal to the surface. He finds this velocity by taking a force balance on a bubble, and then claims that the critical heat flux is the sum of the sensible heat flux transferred by liquid convection and the latent heat flux transported by the bubbles (See Fig.7).

Chang does not explain how the various empirical constants are chosen, and his comparison with the experimental results of other investigators is extremely limited, especially for water. In addition, it does not appear that the physical picture is accurate, as will be commented upon further in Sect. 1.3.4.

1.3.2 Sequential Rate Process of Bankoff [31]

Bankoff presents a model for subcooled critical heat flux, Fig. 8, postulating a turbulent bubble layer on the wall surface and a single-phase turbulent liquid core. He assumes a sequential rate process where the heat is transferred from the wall to the bubble layer, through the bubble layer and from the outer surface of the bubble layer to the core. The critical condition occurs when the core is unable to remove the heat as fast as it can be transmitted by the wall layer, resulting in a marked increase in bubble size and population, which in turn results

in bubble coalescence and dryout.

Bankoff has related his entire work to the empirical data of Gunther [2] who examined bubble lifetime, population, maximum bubble radius, and average fraction of surface covered by the bubbles. The heat balance expressions which were derived showed good agreement with Gunther's $(q/A)_{cr}$ data. They were not tested for any other data because the experimental bubble data were not available. Bankoff's physical picture, as shown in Sect. 1.3.4 also does not appear to represent the physical situation at CHF.

1.3.3 Tong's Model of Subcooled CHF [32]

Figure 9 shows a schematic of Tong's [32] postulated model of subcooled CHF. There is a superheated layer next to the wall above which exists a bubble layer and turbulent core. It is suggested that CHF is an overheating of the surface which starts with the formation of a hot patch underneath a bubble layer. The model is used to develop a method to relate nonuniform to uniform heat flux data, rather than predict $(q/A)_{cr}$.

1.3.4 Critical Review of the Three Proposed Physical Conditions at CHF

In each picture of CHF, the authors assumed that a bubbly-type flow exists near the heated wall while the flow core is liquid. This presumably resulted from the belief that at high subcoolings the void fractions are very low.

In fact, the void fractions at high subcoolings and high heat fluxes are actually very large. Jordan and Leppert [33] reported voids

of 50 percent; Styrikovich [34, 35],at pressures below 126 psia, near 30 to 40 percent; and Sato [36] noted voids of 40 to 50 percent at low subcoolings. The flow patterns which have been observed for subcooled boiling [37, 36, 38, 39] have have been variously described as slug, froth, wispy annular, and clotting vapor. The evident conclusion is that the postulated clear bubble boundary layer near CHF does not exist.

The implication of the models that there is a dryout of the superheated film under a vapor bubble blanket has not been substantiated. Kirby [38] using a resistance-type measuring device showed that at the CHF, the superheated liquid film thickness was not appreciably reduced. Styrikovich using both a scanning beta ray [40] and a salt water deposition [35] technique, showed that at CHF the water mass reaching the wall was greater than the mass evaporating from the wall.

1.4 Motivation for this Study

Until recently the major work conducted in CHF studies has been predominantly concerned with data collection and correlation. Although the principal parametric effects on CHF are well known and can usually be predicted with a reasonable degree of accuracy, the actual physical situation at the critical condition is still unknown. The few models which have been proposed do not accurately nor adequately describe the conditions at CHF, nor do they explain all the parametric effects.

Most work concerning the microscopic nature of boiling has been limited to the experimentally more tractable region of nucleate pool

boiling. For example, Cooper and Lloyd [41] examined the conditions under a nucleating bubble and confirmed the existence of a microlayer under it. Dougall [42], using the Marcus [43] thermocouple setup, measured eddy temperatures resulting from nucleating bubbles for subcooled pool conditions. Bobst [44] and Semeria [45] examined, up to CHF, the temperature profiles adjacent to the heated surface. With the exceptions of Gunther [2] who did a photographic study, and more recently Kirby [46], using photography and a resistance probe, very little detailed work has been accomplished in examining the processes occurring at CHF in subcooled forced-convection boiling. With high heat fluxes (1×10^6 - 4×10^6 Btu/hr-ft^2) and large subcoolings (50-140 °F) especially at low pressures (less than 100 psia), no work beyond data collection can be found. Thus the main purpose of this study is to determine the actual physical phenomenon occurring at CHF.

Chapter 2

PRELIMINARY STUDY OF THE FLOW STRUCTURE AT CHF

Since there appeared to be confusion regarding the physical picture at the CHF condition, the first phase of the research effort was designed to establish the basic nature of the flow structure at CHF. With the results of this phase, discussed in this chapter, a model of CHF was postulated, Chapter 3. During the second experimental phase (Chapter 4), the microscopic details of the water and heated surface conditions were examined in order to provide the necessary proof to substantiate the proposed model.

2.1 General Experimental Program

The experiments were conducted with the low pressure water test loop located in the M.I.T. Heat Transfer Laboratory, and described in Appendix A. Degassed and deionized distilled water in vertical upflow was used to cool the direct-current heated metal test sections. Both annular and tubular test sections were considered. The annular section consisted of either a glass or insulated metal outer tube together with a heated stainless steel inner tube. The tubular section was also fabricated from stainless steel tubing, and was fitted with power bushings and appropriate instrumentation. In Appendix A, Section A.2, a detailed description of both types of test sections is given.

The following table lists the experimental conditions examined during the program:

Table 2-1

Range of Variables

D_e	=	0.094 - 0.25 in.
t	=	0.012 - 0.078 in.
L	=	1.4 - 10.0 in.
P	=	25 - 90 psia
G	=	$0.5 \times 10^6 - 7.5 \times 10^6$ lbm/hr-ft^2
ΔH_{sub}	=	50 - 100 Btu/lbm
$(q/A)_{cr}$	=	$1.0 \times 10^6 - 5.5 \times 10^6$ Btu/hr-ft^2

2.2 Flow Visualization at CHF

Using the glass annular test section, a photographic flow regime study was conducted. Test runs were made by setting the flow rate, inlet temperature,and exit pressure. The power was then increased in steps until CHF. Polaroid photos were taken of the boiling phenomenon at the exit end of the test section after each increase in power. Details of the photographic techniques are described in Section A.4 of Appendix A. The photographic evidence was of excellent quality, and permitted an evaluation of the physical picture at CHF. The data and comments for this series of annular flow regime tests are presented in Appendix E, Table E-1. The salient features of these visual observations are indicated in representative photographs given in Fig. 10.

Photo I (Fig. 10) shows two large irregular vapor bubbles near the

exit of the heated section. This is an indication of the high void fraction typically observed at highly subcooled conditions. It can be observed that nucleation is occurring in the superheated liquid layer under the bubbles. As the heat flux is increased, the nucleation persists and the void fraction increases significantly (Photo II). Photo III was taken at the start of the CHF condition. The bright spot indicates that the surface is glowing red, signifying that the local surface temperature has already gone beyond the Leidenfrost point. This hot patch was subsequently seen to spread quickly (1 - 2 sec) over the entire circumference as the test section was melted and the electric current was broken. The liquid drops on the outside of the glass tube resulted from a small water leak in an exit plenum fitting. The CHF condition was also captured at a higher mass velocity as shown in Photo IV.

At higher mass velocity (Photo V) the phase distribution can no longer clearly be characterized as slug. The flow is more highly agitated and the bubbles are somewhat smaller; however, nucleation can also be seen beneath the bubbles. The CHF condition occurred when the heat flux was increased by two percent.

For one CHF test an Ampex Video Tape system, described in Section A.4 of Appendix A, was used to record an entire experiment from the initial power rise to complete destruction. The complete video tape is on file in the M.I.T. Heat Transfer Laboratory. Photos VI and VII (Fig. 11), are taken of a television monitor displaying the video tape. In VI the circular bright spot, indicating localized film boiling, is evident. Photo VII shows the same hot patch slightly larger

after a short time span (0.1 sec.), the flow pattern again is basically of a vapor clot or slug nature. Because of the low camera speed (20fps), analytical examination of flow velocities and void fractions is impossible. However, the video tape does show the flow regime, nucleation on the heated surface, and the localized growth of the hot spot. This experiment appears to be the first time that video has been tried, and it appears to be a useful technique for flow visualization.

From this preliminary evidence, it appeared that the CHF condition for subcooled flow boiling is of a very localized nature. The flow configuration can be described as having large vapor clots between approximately equal sized liquid slugs. Nucleation exists on the wall under both the vapor clots and the liquid slugs. This vapor clot-liquid slug pattern exists just before and continues during the physical destruction of the heated section. The vapor film over the CHF point apparently does not perceptibly alter the gross flow pattern as was observed in the video tape. In order to verify that the flow pattern is slug-like for all CHFs, and to examine the superheated liquid layer under the vapor clots, further tests were made with an electrical resistance flow probe.

2.3 Flow Regime Studies

The flow regime probe, developed by Fiori and Bergles [37] for low pressure diabatic flow regime studies, measures the resistance between the exposed metal tip and the heated surface (Fig.50). If water

bridges the gap, the resistance is relatively low and a high voltage reading is observed on an oscilloscope. The observed voltage will be essentially zero when pure vapor bridges the gap. Thus, by observing the voltage level and voltage fluctuations, the flow configuration at the exit end of the heated section can be determined. Section A.2 (Appendix A) describes the probe circuitry and the test sections used with the probe.

2.3.1 Probe Signal Interpretation

A thorough discussion of probe interpretation for all flow regimes which exist at low pressure subcooled conditions can be found in [37]. Only three flow regimes, bubbly , slug, and froth were found to exist prior to and at the subcooled CHFs recorded in this study. Bubbly flow is characterized by small bubbles dispersed in the subcooled liquid. Slug flow consists of large, irregular bubbles, whose size is on the order of the diameter of the tube or gap of the annulus with somewhat continuous slugs of water between them. The bubble, unlike the adiabatic, bullet-shaped, Taylor type, is a vapor clot without a definite head or tail, and the slugs have small bubbles dispersed throughout. As the velocity of flow is increased (somewhere between $2 \times 10^6 - 3 \times 10^6$ lbm/hr-ft^2), the flow pattern changes to what has been called froth flow [37,47]. The flow now consists of many chunks of vapor more or less evenly distributed in the liquid. Although bubbles are also present, it cannot be referred to as bubbly flow because of the large size of the irregular vapor bubbles. Fig. 12 gives a schematic illustration of slug and froth flow as has been

observed visually in the present (glass annulus) and previous (tube with exit sight section [37]) studies. Bubbly flow is not shown since it does not occur at CHF.

A probe located in the center of the tube at the exit of the heated section, gave the signals shown in the oscilloscope photographs in Figs. 13 and 14.

Photo I (Fig. 13) shows the probe trace for forced convection of water with zero power to the test section. Incipient boiling cannot be detected with this probe, but bubbly flow gave the characteristic trace shown in Photo II. The base or zero volt line in the photos would be the signal for complete vapor (infinite resistance). For this series of tests, even in the clearly defined slug flow, the probe signal never approached the base line. This indicates that a secondary current path existed between the probe and tube wall, probably through a tear in the teflon tubing insulation. However, this did not cause any interpretation problems. Photo III shows the bubbly to slug transition. Small blips, larger than the bubbly flow variations, indicate a small void, not wide enough to completely cross the probe wall distance. Fully developed slug flow is shown in Photos IV, V, VI (Fig. 14) on different time scales. Above a mass flow rate of 2.0×10^6 lbm/hr-ft^2 there exists a confused vapor-clotted flow called froth. For one particular run, Photo VII shows the bubbly trace while Photo VIII shows the froth trace. Photo IX, just before CHF, indicates that some vapor agglomerates

sufficiently to cause the vapor to bridge the gap. The frequency of these large deflections in froth flow were extremely low, as is evidenced in Photo IX.

2.3.2 Tube Flow Regime Results

The tubular flow regime tests were conducted to show that similar flow structures exist in straight tube flow as that previously observed in annular flow. The effects of velocity, exit pressure, quality, length, and diameter on the flow regimes were examined. The values of the variables were so chosen so that they could be compared to the results of the previous flow regime work [37]. Figs. 15-18 show the flow regime data in terms of mass velocity and quality, and Table E-2 lists the sets of runs completed during this section of the experimental program.

It is seen in all these figures, called flow regime maps, that bubbly and slug or froth flow occurred in the highly subcooled region. The transition from bubbly to froth was not as clear as the bubbly to slug transition. For the 0.242 in. tube, slug flow appeared to exist up to $G = 2.5 \times 10^6$. The transition lines on the maps are drawn continuously from the low G, bubble to slug (BTS) transition to the high G, bubbly to froth (BTF) transitions. The several CHF points obtained are also plotted on these curves, and it is observed that the flow pattern was slug or froth in each case.

In the four maps, the transition, BTS or BTF, occurs at greater subcooling or lower quality as the velocity of the flow is increased. Using previous data [37] in Fig. 16, it is seen that the BTS transition occurs at higher qualities as the inlet temperature is increased.

Composite plots of these transition lines, Figs. 19 - 21, clearly show the effects of pressure, length, and diameter. Increasing the pressure from 40 psia to 90 psia shifted the flow regime boundary to lower qualities as seen in Fig. 19. Figure 20 shows that the smaller L/D caused the transition to occur at greater subcooling. The diameter effect in Fig. 21 indicates that for smaller diameters the transition is at lower subcoolings.

The parametric effects of the present study are consistent with [37] and are also consistent with the effects on CHF as described in Chapter V. This study also conclusively shows that the flow regime near or at CHF for high heat flux,high subcooling conditions is slug or froth flow.

2.3.3 Annular Test Section Flow Regime Results

An annular test section was designed and built which allowed the mounting of an electrical resistance probe on the outer metal tube. A micrometer mechanical drive system allowed movement of the probe up to the heated wall, hence allowing the examination of the flow regimes in the bulk flow and also in the superheated liquid film next to the heater. A complete description of this test section is in Section A.2. A traversing electric probe of this type has been extensively used to determine the characteristics of the liquid film in two-phase annular flow of high pressure water [48].

By moving the probe across the annular gap, for the test conditions listed in Table E-1, it was found that slug flow exists up to 0.002 to 0.003 in. from the wall at or close to the CHF condition. From the observed bubbly signal as the probe was moved closer to the wall, it was concluded that nucleation exists in the superheated liquid film next to the wall. Representative photos (Fig. 22) of the oscilloscope trace show that slug flow exists at 0.011 in. (Photo I) and at 0.0015 in. (Photo II) from the surface. A very confused bubbly flow signal at 0.001 in. is shown in Photo III.

Besides the obvious advantage of being able to examine the film flow structure with this moveable probe, it was found that a mean film thickness could also be measured. By adjusting the distance of the probe from the wall, a point could be estimated which was the boundary between the liquid film bubbly region and the bulk flow slug region, i.e. the superheated film thickness. Although no attempt was made to define exactly the film thickness, the distance from the wall recorded for the bubbly flow regime could probably be regarded as a minimum film thickness. A few of these points are plotted on a critical film thickness versus heat flux curve (Fig. 23) which was recently presented by Kirby [38]. He used an electrical conductance method of measuring the film thickness directly downstream of his heated section for subcooled flow boiling in an annular test section. An extrapolation of his curve to the present data probably is not valid.

However, since the present film thickness values are certainly of the same order of magnitude, it appears that the electrical resistance probe, positioned directly above the heated section, can be used for film thickness measurements.

It is obvious from the different studies described in this chapter that the actual flow structure or hydrodynamic conditions are very different from those postulated by Chang, Tong, and Bankoff. This probably is the reason that their models are very limited and cannot predict all the parametric effects which were mentioned in Chapter 1. Thus it is necessary to formulate a new model of the CHF condition in light of the experimental evidence so far presented.

Chapter 3

CRITICAL HEAT FLUX MODEL FOR SUBCOOLED FLOW BOILING

With the preliminary results of the present work discussed in the previous chapter, a new model of the physical processes occurring before and at CHF is postulated.

Referring to Fig.1, as the heat flux is raised to the CHF condition, the following situation exists: The void fraction is very high, perhaps greater than 20 percent on a time-averaged basis; however, on a local instantaneous basis, α can easily be greater than 50 percent as shown in Fig. 10, Photo II. The flow pattern is either slug or froth flow as described previously.

Next to the heated surface is a superheated liquid layer in which violent nucleation exists due to the high heat flux level. Regardless of whether the bulk flow conditions are predominately vapor or water, nucleation continues. This observation is also consistent with the observations of Hsu et al. [49], using water, and Berenson [50], with Freon 113, both reporting that nucleation exists in slug and low quality annular flow.

When a liquid slug passes by, the bubble trajectory is similar to that usually observed in subcooled flow boiling. The bubbles leave the surface and condense as they flow downstream. However, when a vapor clot passes over the surface, it is reasonable to assume that the nucleating bubbles disrupt the liquid film and cause a dry spot.

This film breakdown could not be directly observed in the present tests, due to the very turbulent flow boiling covering the surface. However, Hewitt and Lacey [51, 52] have observed that nucleate boiling can produce breakup of liquid films in annular two-phase flow, which represents essentially the same flow regime on a local basis.

The forces acting at the liquid-vapor interface are probably such that the small dry spot remains stable, and probably grows, as the vapor clot passes over. The heater temperature meanwhile increases, with the rate of increase primarily depending on the rate of heat generation per unit volume, the size of the dry spot, and the heat capacity of the metal. After the vapor has moved past the small dry spot, the dry spot can no longer remain stable, but must be quenched by the liquid slug. Below CHF this sequence of events is continuously repeated, causing a cyclical overheating and quenching of the surface as shown schematically in Fig. 24.

CHF and destruction will result when the temperature rise, ΔT_{rise}, due to the dry spot,is greater than the temperature drop, ΔT_{quench}, resulting from the quench. The net surface temperature change is then positive after passage of each vapor bubble and liquid slug combination. When the surface temperature reaches the Leidenfrost temperature [53], stable film boiling exists, whereupon the surface temperature increases to adjust itself to point C' on the boiling curve (Fig. 1). Since the equilibrium temperature is beyond

the melting point, physical destruction of the heater occurs. Figure 25 illustrates this proposed CHF mechanism.

This picture of an extremely localized overheating at CHF explains why Kirby [46] noted a substantial average film thickness at CHF, and also why Styrikovich [35] saw water predominately covering the surface during the critical condition.

The fact that nucleation and slug flow can exist [37] and CHF not result for some conditions of subcooled flow boiling can be explained by referring to heat flux level. When slug flow is observed with low heat fluxes, (long L/D, low G, high T_{in}),the intensity of nucleate boiling is insufficient to break through the liquid film. Even if a dry spot is produced, the ΔT_{rise} would be small due to the low rate of volumetric heat generation.

In order to verify the model, it was necessary to use experimental methods to examine the CHF phenomenon in greater detail. The following chapter will discuss the details and results of this phase of the experimental program.

Chapter 4

RESULTS OF THE DETAILED EXAMINATION OF THE CHF MECHANISM

A new method of measuring the surface wall temperatures has been used, in conjunction with high-speed Fastax movies and Contaflex 35 mm photography, to test the assumption of a cyclically varying surface temperature. A computer program was also developed to test the validity of the proposed physical picture. The results of these tests and of the analytical approach are discussed in this chapter.

4.1 Microflash Photography with Simultaneous Temperature Recordings

The glass annular test section was used for this study to allow visual observation of the heated section, and also to simplify the construction of the wall thermocouple. A copper-constantan 0.010 in. thermocouple was drawn through a hole in the 0.035 in. heated wall so that the bead would be flush with the water side of the heated section. The thermocouple was located at the most probable axial location of CHF, approximately 1/4 in. from the exit of the heated section as shown in Fig. 47. The thermocouple signal then was continuously recorded on an oscillograph recorder. While the temperature traces were being recorded, microflash photos or Fastax movies (1200 frames per sec), were taken of the flow. A detailed description of the thermocouple installation and the test techniques used is presented in Sections A.2 and A.3 of Appendix A.

Figures 26 and 27 show three microflash (Contaflex) photos with the simultaneous temperature traces. A signal is seen in each trace

which corresponds to the microflash discharge and hence the photograph. The horizontal lines on the trace are 0.1 seconds apart. The absolute wall temperatures are estimated from McAdams' [1] correlation as discussed in detail in Appendix C. The heat fluxes in all cases were within 85 percent of CHF. Since the primary purpose was to relate the temperature trace to the configuration, CHF was avoided for most of this series of tests.

Photo I shows a bubble about to pass the wall thermocouple. The wall temperature is at a minimum since water is covering the surface. During the next 0.03 sec, the temperature rise results from the approximately 1-1/2 in. long vapor bubble passing the thermocouple at roughly 50 in./sec. Since void fraction data could not be taken, it was difficult to get the exact flow velocity at the exit. Photo II shows the surface again covered by liquid and the wall temperature, during the microflash discharge was also a minimum, confirming the presence of water on the surface. The small bubbles seen upstream of the exit caused the slight temperature variations following the discharge signal. Approximately 0.06 sec later the temperature rise seen on the trace resulted from the larger bubble at the bottom of the photo. Photo III (Fig. 27) shows the vapor void directly above the thermocouple. The corresponding trace shows the surface temperature to be a maximum. The water slug, which quickly follows, quenches the surface. From these photos and traces, then, the relationship between slug flow and the temperature variation has been established.

Photos IV and V, without temperature traces, again clearly show the high-void, slug nature of the flow with nucleation in the superheated film. These photos were taken at 87 and 90 percent of the CHF condition recorded in Fig. 28. However, the flow conditions were such that the temperature rise, associated with a vapor clot passing the thermocouple, finally exceeded the temperature drop due to the quenching slug. The cyclically increasing temperature is observed in Fig. 28 until film boiling and destruction result. Figure 29 shows the observed fluctuations of this CHF trace on an expanded scale. The computed curve resulted from the analytical study of CHF discussed in Section 4.4.

4.2 Fastax Movie Results

A Wollensak 16mm Fastax camera was used to photograph the flow during CHF runs. Preliminary black and white movies without the thermocouple instrumentation showed that slug flow exists at high subcoolings and is extremely violent and unstable to the point of actually causing momentary (0.001 sec) flow stoppage. With this film, however, there was not enough contrast to clearly distinguish details of the flow structure. Color film was then tried since other investigators studying flow boiling [55] have had more success with it. In all the Fastax work with the simultaneous wall thermocouple instrumentation, Ektachrome film was used.

One thousand feet of colored movies, 40 sec real time, were taken.

Seven hundred feet were of suitable quality for interpretation, and a twenty-minute movie was made of the useable footage. A listing of the titles used for this film and a short commentary which explains the purposes and results of each test are reproduced in Appendix D. Table E-3 lists all the tests, including the movie runs, completed during this phase of the study.

Because the camera was in operation for only 4 sec, the recording of an actual CHF condition was only partially successful. Starting the camera at the onset of the critical condition, i.e. at the time that the cyclical rise of wall temperature began, was the basic experimental difficulty encountered. Attempts at forcing CHF while starting the camera did not work. The attempt to start the camera when the recorder first showed the CHF temperature variation had limited success. By the time the camera was started, the CHF condition had progressed to film boiling as evidenced in Test T-15. The films of tests T-14 and T-15, being representative, will be discussed in detail to show the method of analysis used and the results obtained.

Previous films showed slug flow with large void fractions and flow instabilities in the nature of momentary flow reversals and stoppage. In order to see whether this flow stoppage was inherent in the flow or whether it resulted from the 90 degree change of flow direction, the straight-through-flow, exit plenum chamber was built (See Appendix A, Section A.2). Test T-14 was run to 98 percent

of the critical heat flux with the new exit chamber. The movie was taken and another film was placed in the camera, continuing the same run to burnout (Test T-15). From these films, it was determined that the flow stoppage also occurred with the new exit plenum; consequently the observed flow stoppage was an internal flow, rather than system, instability.

A time-motion study of the film, using a Kodak Time-Motion Analysis Projector, although tedious, was very straightforward. A 60 cycle (120 flashes per sec) timing light inside the camera, produced a mark every 0.00833 sec on one edge of the 16mm film. Using the number of frames counted between marks and the number of marks, the two curves in Fig. 30 were drawn. The reference or zero frame was the central frame of the first time mark.

Fig. 31 is the actual wall temperature trace for run T-14. The camera was running for approximately 1.9 seconds before the timing light was turned on. The fact that the camera increased in speed from 1350 to 1500 frames per second (Fig. 30) did not cause any difficulties in film analysis. A random sample of vapor clots from the film were recorded and compared to the temperature trace. Likewise, several points on the trace were checked to see whether they coincided with the particular frames of the film found by using Fig. 30. In both cases, movie to trace or trace to movie, a temperature rise coincided with a vapor clot and a temperature drop with a slug quenching the surface. Fig. 32 shows the temperature trace for Test T-15.

The rapidly fluctuating temperature trace shows the cyclically increasing temperature at the CHF condition. It is interesting to note that the power was increased 21.5 seconds previous to CHF. Thus a reasonable steady state was achieved and the heat flux was probably at point A' on the boiling curve (Fig. 1). The CHF condition was triggered by either a slight power perturbation, or more probably, a random flow perturbation in the form of a large vapor clot. The movie camera was turned on 0.6 seconds after the CHF condition started. Thus, the resulting exceptionally fine quality film, and the only one showing the actual destruction of the test section, showed only the already oxidized and darkened area under the vapor film. As the film boiling expanded circumferentially, and less so axially, the charred color turned to a pale red, cherry red, and finally yellow before melting. The slug flow continued in the test section and did not appear to be greatly affected by the local film boiling.

A rough measure of the average void fraction was determined in the following manner. The velocity of the flow at the exit was calculated by measuring the distance a particular vapor patch moved over several frames of film. An arithmetic average velocity was then calculated using the several velocities calculated at various times in the film. Then, knowing the inlet velocity, and assuming no slip, the average void fraction at the exit was calculated. Two assumptions implicit in this method are that the rate of condensation at the vapor-

liquid interface is negligible and that the flow velocity does not change radically during the camera run time (3.5 to 4.0 seconds). For Test T-14 the void fraction was calculated to be 25 percent. Such a large void fraction is consistant with the data of Styrikovich [40] and Jordan [33], and with others mentioned previously.

4.3 Pin-Holes in Destroyed Test Sections

Small pin-holes are noticed in some of the destroyed test sections of the annular flow tests (Fig.33). The observation of these holes was possible because of the particular geometry and experimental setup that was used. The inside of the tube was open to the atmosphere through the inlet copper shorting tube, as described in A.2. Thus when the localized temperature of the heated wall exceeded its melting point, the higher pressure on the flow side forced water through the pin-hole, which in turn cooled the pin-hole circumference. If the shutdown of power was slow, more holes developed as film boiling spread, and complete fracture resulted. Conduction losses through the exit shorting bar normally caused the burnout point to be approximately 1/4 in. from the end rather than at the end.

With the wall temperature trace being continuously monitored, the onset of CHF was immediately noticed and frequently allowed sufficiently rapid shutdown of the power. Thus, referring to Fig. 33, it is seen that the test sections sometimes did not completely fracture near the exit but merely blew out the molten metal, producing the pin-holes. This evidence further substantiates the existence of an

extremely localized dry patch at CHF.

4.4 Analytical Results

A set of differential equations were written to describe the proposed physical situation at CHF. It was felt that a good correlation between the solution to these equations and the experimental results would indicate that the proposed model correctly described the actual physical phenomenon at CHF.

Since the bubble size on the heater wall is much smaller than the test section radius(See Fig.54), it was assumed that the wall could be treated as a flat plate. The differential conduction equations for a flat plate with internal heat generation and time-varying boundary conditions were approximated in the computer program by using finite difference equations. The time-varying wall temperatures are actually calculated by a method best described as a marching time solution. Given an initial wall temperature distribution, time is incremented and a new distribution is found. This new distribution is then used for the succeeding time increment. By selecting the proper boundary conditions at a particular time, the unsteady nature of the problem is solved. A detailed discussion of the computer program is presented in Appendix C.

Before comparing the computed and experimental temperature variations, it appears appropriate to briefly discuss the physical significance of the thermocouple measurements. Because of its large size (0.010 - 0.013 in.), the wall thermocouple cannot be expected to accurately respond to the temperature change underneath a nucleating bubble only

0.001 to 0.002 in. in diameter. The measured temperature at CHF (Figs. 28 and 32)is a result of the overheating and quenching of the metal surrounding the thermocouple; hence, the temperature represents an average value of the temperature variation around the thermocouple.

The computer program calculates the temperature variation assuming a fixed dry spot area and no thermocouple hole in the metal. In other words, an infinitely small thermocouple on the surface would measure the calculated variations. Nonetheless, this idealized solution of the average temperature variation proved extremely useful.

The necessary inputs to the computer program, obtained from the data and from the observed flow structure of the experiments, are; (q/A), ΔH_{sub}, T_{in}, P_e, appropriate test section geometry, frequency of the slug-clot passage, and the percent of the slug-clot conbination which is vapor. The latter two values set the time variation of the boundary conditions which simulate the overheating-quenching cycle. An assumed dry spot size is another input parameter. In Figs.29 and 34 two particular temperature variations generated by the computer program (See Table E-4 for the computer input values) are compared with the corresponding temperature variations recorded by the oscillograph. The remarkable agreement between the calculated and measured temperatures is viewed as further evidence that the proposed physical picture correctly describes the actual phenomenon occurring at CHF.

Although the program probably cannot, for the present at least,

be used as a prediction tool as discussed in 5.2, it can be used in predicting the general trends resulting from varying wall thickness, heater metals, and dry spot area. For instance, it was verified that increasing the dry spot area or decreasing the tube wall thickness, all other conditions remaining the same, will cause greater surface temperature rises. With a higher thermal conductivity material, molybdenum, the calculated temperature rises were shown to be much smaller than for stainless steel, for the same flow conditions and heat flux. Table E-4 lists the inputs and the resulting temperature rises for representative runs showing these effects.

4.5 Summary of the Detailed Experimental and Analytical Studies

The postulated cyclical temperature rise and drop, with the rise being greater than the drop, has been observed during the CHF phenomenon. The pin-holes observed in some burned-out test sections verifies that the overheating is extremely localized. The computer analysis further supports the proposed model, since the surface temperature variations can be calculated using appropriate input data.

The proposed model can be further tested by examining its ability to predict the effects of the various parameters on CHF. Chapter 5 will examine this aspect of the model.

Chapter 5

PROPOSED MODEL AND PARAMETRIC EFFECTS ON CHF IN TUBES

In this chapter it will be shown how the proposed model appears to be consistent with all the parametric effects. The model as a prediction tool will be discussed in the final section.

5.1 Parametric Trends and the Model

For discussion purposes the mathematics involved in describing the proposed physical situation can be simplified. It will be assumed that when the surface is covered by the passing vapor clot, the temperature rise of the surface under the dry spot will be governed only by heat generation in the tube wall. It will be assumed that the section under the dry spot is completely insulated, thus neglecting the heat transfer to the vapor on the cooled side. This also neglects the conduction losses which occur with the local overheating. For these conditions, i.e., total surface insulation and heat generation in the tube wall, a simple relationship between time and temperature change can be derived. Thus, whenever the surface is covered by a vapor clot, the formula

$$\Delta T_{rise} = (q/V)\ \Delta t/\rho\ c_p$$

applies. This equation, because of the simplified assumptions, overestimates the temperature rise for a given time interval. Thus, a longer Δt would be necessary for a given ΔT_{rise} in the actual physical situation. For discussion purposes, however, this equation is satisfactory.

The temperature drop, ΔT_{quench}, which is due to the liquid slug, partially depends on the temperature of the water and the duration of the slug over the nucleating point. Other factors such as nucleate boiling bubble size, dry patch stability,and flow regimes also effect the temperature variations. With this discussion in mind, the parametric effects noted in Chapter 1 will now be examined.

5.1.1 Mass Velocity

In Section 1.1 it was found that $(q/A)_{cr}$ increases with mass velocity as P, ΔH_{sub}, L, and D remain constant. Several factors appear to be important to the explanation of this effect by means of the proposed model.

The first factor relates to the establishment of the slug or froth flow regime. Figs. 15-18 show that the flow regime transitions and slug or froth flow occur at higher subcoolings as G increases. Replotting the BTS or BTF lines of Fig. 15 on q/A versus ΔH_{sub} coordinates (Fig. 35) shows that the transitions also occur at higher heat fluxes for increased mass velocities. Thus q/A must increase sufficiently for the necessary flow conditions of the model to exist.

The increased flow velocity also decreases the time span during which the vapor clot covers the stable dry spot. This in turn limits the temperature rise before the surface is rewetted by the slug. At the same time, the turbulence level increases. This increased

turbulence allows colder liquid to quench the surface even though the mixed-mean enthalpy of the bulk flow might be the same as that for a lower G. For an increased G, then, a higher q/A, hence q/V, is necessary before the surface temperature rise, ΔT_{rise}, is greater than the temperature drop, ΔT_{quench}.

An analytical attack on the dry spot stability, as explained in Section 5.3, is extremely difficult. It is probable, however, that the increased film velocity under the vapor void will prevent a stable dry spot. Only a higher q/A would be able to counteract this increased film velocity effect.

5.1.2 Subcooling

In Figs. 3 and 4 it was noted that $(q/A)_{cr}$ increases with ΔH_{sub}, holding P, G, L, and D constant. The flow regimes which result, Figs. 15-18 and [37], indicate that with increased subcooling, a higher q/A is necessary to generate sufficient vapor and develop the slug or froth flow regimes. For example, the $(q/A)_{cr}$ at point 1 in Fig. 36 would not be sufficient to cause the slug or froth regime for operating line 2. Once the flow regime is established, the quenching effect is still greater than the insulating effect because of the colder quenching liquid at the higher subcoolings. The volumetric heat generation will have to increase sufficiently to counterbalance this subcooled liquid effect.

Instead of continuously decreasing as ΔH_{sub} decreases, $(q/A)_{cr}$ has a minimum near zero subcooling, particularly at low pressures

[5,6,36]. Large voids exist in the slug flow regime for these particular conditions [37]. Consequently a higher throughput velocity results from this increased void fraction. The arguments used to describe the mass velocity effect can now be similarly applied here. The increased velocity, therefore, explains why the $(q/A)_{cr}$ achieves a minimum.

5.1.3 Pressure

CHF increases with pressure up to 300 - 800 psia as shown in Fig. 2. Using the model, the observed increases of CHF with pressure can be explained satisfactorily. Fig. 37 illustrates that the heat flux must be increased in order to achieve slug flow as the pressure is increased from 30 to 100 psia, while keeping G, L, D and H_{in} constant.

Since the bubbles are smaller at higher pressures, the bubble population must increase to have sufficient vapor for slug or froth flow. This is effected by increasing the heat flux. For the same subcooling, the surface temperature rise is smaller at high pressures because of the greater conduction losses from under the smaller diameter dry spot,i.e. smaller initial bubble size. Using the computer model, a comparison of two different dry spot sizes confirmed that the temperature rise would be less for the smaller dry spot (Table E-4). Thus to reach the critical condition, $\Delta T_{rise} > \Delta T_{quench}$, q/V or q/A must be increased.

Although the proposed model does suggest that CHF increases with P, it appears that the model, for the present at least, does not show why CHF should decrease again at very high pressure (Fig. 2). This may imply that the model is limited to the low pressure range

5.1.4 Diameter

CHF increases with decreasing diameter as shown in Fig. 5. However, this plot is not suitable for a realistic assessment of the percentage increase in $(q/A)_{cr}$, since the parametric distortion is not accounted for. The diameter effect can best be depicted by holding G, P, L/D, and H_{in} constant as shown in Fig. 38. CHF is still substantially increased with the smaller diameter tube; however, the percentage increase is less than would be implied by comparing at constant H_{out}, as in Fig. 5.

It appears to be reasonable to assume that the void fraction, for similar local flow conditions, increases as the tube diameter decreases. Bubble size and development of the bubble boundary layer should be relatively independent of tube size; hence, the void fraction should be larger for the smaller diameter tube as sketched in Fig. 39. This produces a significantly higher velocity in the smaller tube, with the result that $(q/A)_{cr}$ should be increased in accordance with the arguments advanced in Sections 5.1.1 and 5.1.2.

This qualitative description is, however, in apparent disagreement with the flow regime boundaries indicated in Fig. 21, which imply that the larger tube has the higher void fraction. This inconsistency can

be resolved by noting that the formation of slug flow is probably suppressed in the smaller tube due to the much shorter transit time (shorter length and higher velocity). The flow regime observations are accurate; however, in this case they are not indicative of the void fraction.

5.1.5 Length

Length does not represent a major effect on $(q/A)_{cr}$ for L/D greater than about 35 [5], keeping G, P, ΔH_{sub} and D constant. For L/D less than 35, $(q/A)_{cr}$ increases with decreasing L. The transit time through the shorter tube is decreased to such an extent that agglomeration of the bubbles is prevented; slug or froth flow is thus suppressed. In addition, the high single-phase entrance heat-transfer effect probably delays boiling until further into the tube. A higher heat flux is thus necessary to counter these two effects.

5.1.6 Surface Tension

Surface tension (σ) effects are normally of secondary importance since they appear only when additives are used to substantially decrease the surface tension. Several investigators [5, 54, 70] have clearly shown that CHF decreases with decreasing surface tension. Frost [54] found, by means of high speed movies, that the amount of vapor generated in pure water with reduced σ, compared to that generated in pure water at the same heat flux, is much greater. Thus a lower heat flux is necessary to create the flow conditions of the model.

5.1.7 Wall Thickness and Thermal Diffusivity

The effects of these two variables on CHF have had minimal experimental examination. The proposed model is inherently related

to the volumetric heat generation and any substantial increase of q/V will certainly allow ΔT_{rise} to be greater than ΔT_{quench} for equal time spans, all other conditions being identical. For identical heat fluxes, all other variables the same, the thin-walled tube will have a greater q/V. Thus the ΔT_{rise} will be larger than that of the thicker walled tube. This indicates that the thicker walled tube could maintain a higher q/V before the critical condition is reached. This was seen to be the case in testing the computer program using two different wall thicknesses (Table E-4).

Since the available evidence of a wall thickness effect [14,15,16,17] was contradictary and inapplicable to the present subcooled flow conditions, a series of CHF tests were conducted to test this proposed wall effect. Table E-5 lists the twelve tests which were conducted for the wall thicknesses of 0.012 in. and 0.078 in. The data are plotted in Fig. 40. The points which should be compared are on the same operating line, i.e. G, P, H_{in} are the same. The increase of $(q/A)_{cr}$ with the 0.078 in. wall is dramatic. At the lower velocity the $(q/A)_{cr}$ increased 58 percent, while at the highest velocity, $(q/A)_{cr}$ increased 6 percent.

Heat conduction improves with an increased thermal diffusivity, α. Thus for a given heat flux, the temperature rise under a dry spot would be less for the high α metal. This implies that the surface can withstand a higher q/A before serious overheating occurs. Thus metals like aluminum and molybdenum would be expected to have a higher CHF, all other conditions being the

same. A comparison of stainless steel (α = 0.172 ft^2/hr) and molybdenum (α = 2.07 ft^2/hr), using the computer program, showed that the surface temperature rise for molybdenum is substantially decreased (Table E-4).

5.2 Comparison of CHF Data with Other Experimenters

To show that the values of $(q/A)_{cr}$ found during this entire study were representative of that of other published data was difficult for annular flow due to a lack of data for comparable test conditions. The annular CHF data of Frost [54] , which probably best match the conditions of the present data are in good agreement with present data as shown in Fig. 41. Figure 42 indicates that the present tube data are comparable to those previously taken at M.I.T. for approximately the same conditions. This comparison indicates that the present data are entirely representative of typical stable CHF data.

5.3 CHF Model as a Prediction Tool

Much of the previous discussion of parametric effects is based on a combination of experimental fact and physical intuition. To analytically predict $(q/A)_{cr}$ by means of the model, specifically by use of the computer program, is possible in principle. A method of iteration is envisioned, whereby, for a given system and operating conditions, a check is made to verify that slug or froth flow exists. Then it would be necessary to show that the dry spot initiated by violent nucleate boiling is stable for the particular

conditions. If it is, the final check would be to see whether ΔT_{rise} is greater than ΔT_{quench}; If so, then $q/A \geq (q/A)_{cr}$. The heat flux would be incremented, starting from a low value, until the necessary conditions of flow regime, dry spot stability, and temperature increase are satisfied.

Unfortunately,none of these interelated conditions have yet been examined or understood in any detail. For example, there are presently only two extensive studies of flow regimes near CHF: Bergles and Suo [47] for pressures greater than 500 psia, and Fiori and Bergles [37] for pressures below 100 psia. Both works, however, are experimental and examine the gross changes of flow regime with changing flow conditions. The mechanisms causing a particular flow regime and the cross-coupling effects of geometry, flow conditions, and heat flux have not yet been resolved. Thus, since no adequate theory exists which can relate the system parameters to the flow regimes, it would be necessary to conduct more flow regime studies to delineate the slug or froth flow regimes for a variety of conditions.

Another necessary step for the CHF prediction technique is to show that the dry spot under the vapor bubble is stable. Much has been written [51, 58, 64, 65] about the formation and stability of a dry patch formed in nucleation or dryout of a two-phase annular flow. In the present study, it is assumed that the film under a vapor void is quite similar to annular flow; thus the previous works should have application here. A recent study by McPherson [56] is

representative of the approach used in attacking the film stability problem. McPherson considered six forces acting on a liquid film upstream of a dry patch. He summed up the axial contributions of these forces, and for different assumed film velocity profiles, showed that the resultant force, F, determined whether the dry patch was stable ($F = 0$), was rewetted ($F > 0$), or grew upstream ($F < 0$). He points out that his theory is still inadequate since he does not know such physical parameters as film surface temperature at the triple interface or the contact angle. His force equation does show that increased film (hence flow) velocities contribute to a positive axial force, and thus film recovery. Although this qualitative evidence supports the arguments used in the discussion of parametric effects, quantitative dry spot stability analysis is presently impossible.

To calculate the wall temperature it is necessary to know the size of the dry spot and the time interval or frequency of the dry spot occurrence. The dry spot size is probably related to the nucleating bubble size. Unfortunately, representative studies [57, 58, 59, 60] of bubble growth are for conditions far removed from the high heat flux, subcooled forced convection conditions of the present study. Thus the dry spot size must be assumed.

There is no method to predict the frequency of slug or froth flow. Thus the necessary time intervals can only be approximated, perhaps by use of an estimate of the size of the vapor clot and the

throughput velocity. If the size of the clot is represented by a characteristic dimension, diameter for instance, and if the void fraction determines the throughput velocity, the time variations can be approximated. In void fraction predictions for subcooled flow, two flow regimes are commonly assumed [61, 62, 63], i.e., a wall voidage (First) region and a bulk voidage (Second) region. Figure 43 suggests that void fraction data have not been taken for the conditions of interest in this study. Thus it appears that only with experimental measurements, possibly using techniques developed in this work, can the time span be determined.

It is obvious from this discussion that CHF cannot be predicted analytically using first principles. If it is desired to develop a prediction method in the light of the actual physical conditions shown to exist at CHF, much more fundamental research would have to be conducted.

Chapter 6

CONCLUSIONS

A new model of the CHF phenomenon in subcooled flow boiling has been formulated. Near the CHF condition, and as a large vapor clot passes over the heated surface, nucleating bubbles break the superheated liquid film and cause a stable dry spot. This results in an increasing local surface temperature until the vapor passes the site and the dry spot is quenched by a liquid slug. At CHF, the volumetric heat generation, slug frequency, and void fraction are such that the temperature rise resulting from the dry spot is greater than the temperature drop during quenching. An unstable situation results where the temperature of this point continues to rise after each vapor clot passes the site, until the Leidenfrost temperature is reached, at which point quenching is prevented and destruction is generally inevitable.

The experimental evidence obtained with water at pressures below 100 psia, which supports the validity of this CHF model is:

1. The flow regime for high subcooling CHF conditions for tube and annular geometries is either slug or froth.
2. Nucleation exists in the liquid film underneath the vapor clots.
3. The extremely localized nature of the CHF phenomenon was observed by colored movies, still picture photography, and the pin-holes in the destroyed test sections.

4. The cyclically increasing surface temperature, described by the model, was shown to exist at CHF.

5. $(q/A)_{cr}$ increased with tube wall thickness.

The transient heat conduction equation for the tube wall was solved for a variety of flow conditions utilizing experimental flow structure information. The wall temperature oscillations with increasing average temperature, were duplicated at CHF; thus the mathematical formulation supported the model. To use this program as a prediction tool is presently impossible since the necessary program input information concerning the flow structure cannot be predicted.

By means of the model, the parametric effects of mass velocity, pressure, subcooling, diameter, length, tube material, and tube wall thickness can be reasonably explained. A comparative study was made to resolve the influence of tube wall thickness; increasing wall thickness should increase $(q/A)_{cr}$ according to the model. It was found that $(q/A)_{cr}$ was increased by up to 58 percent when the wall thickness was increased from 0.012 to 0.078 in. This wall effect can probably explain some of the differences in data between different investigations which may have used equal tube diameters but different wall thicknesses.

Several new experimental techniques have been developed to examine the subcooled CHF condition. A thermocouple at the heat transfer surface provided an excellent indication of the temperature fluctuations. The traversing electrical flow regime probe allowed examination of the liquid film layer, and probably can be used in measuring

film thicknesses. A television video system was used for the first time in a CHF study and found to be a very versatile experimental device.

The desire to use this new and accurate picture of the CHF condition for subcooled flow boiling as a prediction tool has shown the necessity of detailed flow structure studies. Work in bubble dynamics and film stability must also be extended to the present conditions. For further understanding of the CHF phenomenon, it appears that emphasis should be placed on the microscopic nature of CHF rather than on simply collecting more CHF data.

Appendix A

EXPERIMENTAL FACILITIES AND TECHNIQUES

A.1 Description of Apparatus

A.1.1 Hydraulic System

The experimental facility used was the low-pressure test loop located in the MIT Heat Transfer Laboratory. The basic apparatus was designed and constructed in 1961 [5].

A schematic of the loop is presented in Fig. 44. The loop is designed to accept vertical and horizontal test sections. The pipings and fittings are made of brass and stainless steel for corrosion resistance. Rayon-reinforced rubber hose is used where flexible connections are required. Distilled water is circulated by a Westco bronze, two-stage, regenerative pump providing a discharge pressure of 260 psig at 3.6 gpm. The pump is driven through a flexible coupling by a 3-hp Allis-Chalmers induction motor. A Fulflo filter is installed at the pump inlet. Pressure fluctuations at the outlet of the pump are damped out by means of a 2.6-gal Greer accumulator charged with nitrogen to an initial pressure of 40 psig. This accumulator contains a flexible bladder-type separator which prevents the nitrogen from being absorbed by the system water. After the accumulator, the flow splits into the by-pass line and the test-section line.

In the test-section line, fluid flows through a Fischer-Porter flowrator followed by a preheater, thence through a Hoke metering valve and the test section, after which it

merges with fluid from the by-pass line. The flow then goes through the heat exchanger and returns to the pump. The pre-heater consists of four Chromalox heaters of approximately 6 kw each. Three of these are controlled simply with "off-on" switches while the fourth can provide a continuous range from 0 to 6 kw by means of a bank of two variacs mounted on the test bench. For the majority of tests, these preheaters were not used since it was necessary to use the coldest water temperature available to achieve the high subcoolings of the experiments. Quick-action Jamesbury ball valves are installed before the inlet to the flowrator and after the exit from the test section. The exit valve is also used to adjust the test-section pressure.

Flow through the by-pass line is controlled by a ball valve, on each side of which there is a 300-psig pressure gage. Pump operating pressures, and hence the pressure upstream of the test section, is controlled by this valve.

The heat exchanger is a counterflow type with system water flowing in the inner tube and city water in the outer annulus. Hence the lower temperature limit was determined by the city water supply and season of the year. Test-section inlet temperatures varied from 38°F in the winter to 70° F in the summer. A Fulflo filter is installed on the city water line to reduce scale formation in the exchanger.

The distilled water was deionized continously by passing a portion of the flow through four mixed-bed resin demineralizer units. A 4.7-gal degassing tank is provided with five electrical heaters (3-200 vac and 2-100 vac). This tank also serves as a surge tank. A 15-gal stainless-steel storage tank for filling the system is mounted directly above the degassing tank and can be filled with distilled water from standard 5-gal bottles with a small Hypro pump.

A.1.2 Power Supply

Test-section electrical power is provided by two 36-kw dc generators connected in series. Each generator is rated at 12 volts and 3000 amperes. The power control console permits coarse or fine control from 0 to 24 volts. A water-cooled shunt installed in parallel with the test section protects the generators against the shock of the sudden open circuit which occurs at burnout. Power is transmitted from the main bus to the test section by water-cooled power leads. Rubber hose connected both inlet and exit chamber plenums to the main loop in order to electrically isolate the test section. The test section was then separately grounded.

A.1.3 Instrumentation

The basic temperature measurements were measured by copper-constantan thermocouples made from 30-gauge Leeds and Northrup duplex wire. The test-section inlet temperature was measured by

a thermocouple directly in the fluid stream, upstream of the heated section. Details are shown in the schematics of the various test sections.

All pressures were read on Bourdon-type gages located as shown in Fig. 44. The test-section inlet and exit pressures were measured with Helicoid 8-1/2 in. gages of 200 psig and 100 psig, respectively. Both are specified to an accurary of $\pm$ 0.25% of full scale.

A variety of metering tubes and floats, which could be installed interchangeably in the basic Fischer-Porter flow-meter housing, provided measurement of the test-section flow from 1.5 to 4000 lbm/hr.

The voltage drop across the test section was read directly, either on a Weston multiple-range dc voltmeter with specified accuracy of $\pm$ 1/2 percent or on a USC Digitec, Digital D.C. Voltmeter Model 204 with a specified accuracy of .1 percent. The current flow was determined by using the Minneapolis-Honeywell, Brown recorder to measure the voltage drop across a calibrated shunt (60.17 amp/mv) in series with the test section.

A.2 Description of Test Sections and Their Instrumentation

Both annular and straight tube test sections were used for the experimental program. Appendix E lists the test data and the dimensions of all the test sections.

A.2.1 The Glass Annular Test Section

Fig. 45 shows the schematic of the annular glass test section. Pressure and temperature measurements were made in the plenums. Precision-bore pyrex tubing was used. The Hoke metering valve was placed immediately before the entrance plenum to eliminate premature burnouts due to the effects of system compressibility as described by Maulbetsch [20].

To determine whether the 90° change of flow direction in the exit plenum affected the slug flow regime, the exit plenum was redesigned. Fig. 46 shows the changes made. The flow now is straight-through and the power connection enters from the side. The vertical shorting bar is pushed into the horizontal bar and is held tight by a set screw. This design was exceptionally versatile and allowed for very good centering of the heated section inside the glass annulus.

The heated section of 304 SS, 0.242 in. i.d. and 0.035 in. wall was 10 in. long. Silver-soldered to both ends were copper tubes, 0.312 in. o.d. and 0.187 in i.d. Power connections were made to the copper tubes by means of brass or aluminum bushings.

These annular test sections had special surface temperature instrumentation. A 0.0135 in. hole was drilled through the 0.035 in. SS wall approximately 1/4 in. from the end of the heated section. Copper-constantan 36 gage wire with teflon insulation was used for the thermocouple. A nominal bead size of 0.014 in. was produced

by the Dynatech Model 116 Thermocouple Welder. Figure 47 illustrates the construction details. The wire leads were fed through the hole, pulled through the inside of the SS tube and out through the copper tube. Teflon tubing, 0.030 in. diameter, was slipped over the thermocouple wire and then the bead was epoxied onto the SS tube by high thermal conductivity,0.975 Btu/hr-ft-F°, Eccobond Paste 99 made by Emerson and Cummings, Inc. Eccobond Solder 58c, a silver based epoxy, was also used with a thermal conductivity greater than 16.6. Temperature observations were more difficult to interpret with the silver epoxy, probably because of its very low volumetric resistivity (less than 2×10^{-3} ohm-cm) which allowed the thermocouple to pick up much more d.c. generator noise and general a.c. noise. Consequently, Eccobond 99 was used for most tests. The thermocouple reading probably had impressed on it part of the voltage gradient existing across the test section. This did not cause any problems however, since the desired signal was the amplitude of the temperature fluctuation rather than an absolute value of the temperature level.

Figure 48 shows the schematic setup of the instrumentation. The 36 gage wire was connected to 30 gage wire which was led to a differential operational amplifier. The temperature signal was split, part of it going through the amplifier and the rest bypassing it. The signals were placed on separate galvonometers in the Recording Oscillograph of Consolidated Electrodynamics Corporation. The Type 5-124 oscillograph is a multi-channel, portable, direct-recording photographic type instrument. It uses 7-inch wide print-out recording paper and provides up to 18 individual channels of data.

A.2.2 Metal Annulus

To examine the flow regimes at CHF, the electric probe (described in detail by Fiori and Bergles [37])was mounted on the outside metal tube of the annular geometry. Fig. 49 illustrates the probe mounting. Note that the metal tube was electrically insulated from both flow plenums.

The probe was constructed from 0.013 in. spring wire insulated by teflon tubing, increasing the overall size to 0.025 in. The hypordermic steel tubes surrounding the probe gave it sufficient rigidity that the probe position could be determined to within 0.0005 in.

The probe measures the resistance between its exposed tip and the metal wall. When water is in the tube, the voltage across the 5 megohm resistor, shown in Fig. 50, is maximum. With high resistance caused by vapor in the tube, the voltage is at a minimum. The amplitude of the voltage signal depends upon the water conductivity, which is a function of water impurities and water temperature. Since the shape rather than the signal amplitude is important, no attempt was made to maintain the conductivity at a particular value. It was always above 0.3 meghohm-cm as measured by a Barnstead Purity Meter, at ambient conditions.

A.2.3 Straight Tube Test Sections

Figure 51 illustrates the test section used to test the wall thickness effect. The power bushings were made of brass and the

pressure tap hole at the exit end of the tube was 0.015 in. in diameter.

Figure 52 shows the straight tube with a fixed probe mounted separately. This test section was used to verify that the flow regimes existing in annular test sections also existed inside round tubes. Several tests were continued to CHF. The probe mounting allowed rapid changing of test sections without rebuilding the probe after each CHF run. Special plugs were silver soldered into the combined exit test section to accommodate the 0.094 in. tubes. The probe instrumentation was similar to that used for the annulus.

A.3 Experimental Procedure

A.3.1 General Loop Operation

After the test section was installed, the loop and degassing tank were filled with water from the supply tank. The water in the degassing tank was then brought to a boil while the loop water was circulated with the heat exchanger coolant off. The degassing tank vent was closed when the tank began to boil, and the pressure in the tank was allowed to increase to a level of from 6 to 15 psig. This placed the pump inlet above atmospheric pressure, and prevented air from being drawn in around the pump seals. Degassing was then accomplished by by-passing a portion of the cool loop water into the top of the vigorously boiling degassing tank. This was continued until the temperature of the loop rose to approximately $180^{\circ}F$.

A standard Winkler analysis described by Brown [65] and Lopina [66] indicated that this method of degassing reduced the air content to less than .2 cc air/liter. After degassing, the loop water was adjusted to the desired inlet temperature, and the desired pressures were set. The generators also were started and allowed to warm up. Regardless of the purpose of a particular run, the voltage drop across the test section, the current, pressure at the exit, and the inlet temperature were always recorded. Such values as inlet pressure, exit temperature, picture number, water conductivity, and pressure on the upstream side of the Hoke metering valve were often recorded.

A.3.2 Annular Test Section Procedures

The oscillograph recorder was calibrated for every test using the surface temperature thermocouple. With the generators on, but without power in the test section, the temperature of the water was changed by means of the preheaters. The exit temperature obtained from the Brown Recorder was used as a basis for calibrating the trace of the oscillograph galvonometers. The amplification for the wall thermocouple signal varied for each test, but usually was near 30. A 0.1 mv thermocouple signal normally was equivalent to a 0.1 in. horizontal deflection using the 7-324 galvonometer. After being reduced over a 1200 ohm resistor, the unamplified signal led to a 7-339 galvonometer. The calibration remained fairly constant giving an 0.1 in. deflection for a 0.5 mv temperature change. Absolute temperature measurements with the wall

thermocouple could not be made because of d.c. pickup, electric field, and other disturbances, a very good description of which is contained in a paper by Green and Hunt [67]. Since the temperature variation was of primary concern, the only serious interference with the desired signal was 60 cycle a.c. noise. This was minimized by proper shielding and grounding of equipment, and never was strong enough to seriously interfere with signal interpretation.

The recorder paper speed of 4 in./sec was the optimum speed both for economy and for signal clarity and interpretation. The recorder was on during all changes of power and when steady state was achieved. Near CHF, the recorder was on continuously to guarantee recording the temperature trace at CHF.

Placing the flow regime probe signal on the recorder met with some succuss. Figure 53 shows a trace having both the thermocouple and flow regime probe signals. It was very difficult to eliminate all the a.c. noise on the probe signal, consequently only the large vapor slugs could be clearly distinguished. Only one test used the probe and thermocouple simultaneously.

Whenever Fastax movies were taken, a 2 v signal activated a 3-326 galvonometer to indicate on the recording paper the camera

motor startup and the start of the film timing light. This allowed time synchronization of the movie with the thermocouple signal. For single picture studies, a signal deflected the 3-339 galvonometer whenever the microflash discharged.

The actual operational procedure to obtain a movie slightly before or at CHF required coordinated action of the test team. The power was increased in .5 to 1 volt increments until the power was approximately 85 percent of CHF. The violent downstream pipe vibrations and exit pressure ocsillations indicated that slug flow existed and that CHF was being approached. The recorder was turned on for continuous operation, and the trace was marked after every incremental (.3-.4 volts) change in power. The camera, and approximately .5 seconds later the film timing marker, were turned on when it appeared that CHF was imminent. Various attempts were made to force the critical condition as the camera was turned on,but due to a very limited camera run (4 secs), CHF was never filmed using this method. The method finally used was to increment the voltage by .6 to .8 volts and simultaneously start the camera.

The time for a normal test, beginning with the first power increase to the test section until destruction, averaged approximately one hour.

A.3.3 Tube Flow Regime and CHF Studies

The procedures for raising power and data accumulation were similar to those of the annular tests. The oscillograph recorder was not used for these tests. By means of the Techtronix 564 storage oscilloscope, representative flow regime probe signals could be stored and photographed using a Polaroid Techtronix camera system. Because the primary purpose of these tests was to gather flow regime information, CHF, except for several instances, was avoided.

The tube wall thickness experiments were all carried to CHF. T_{in}, T_b, w, P_e, E, and I were recorded for each power increase. Power was slowly increased in order to avoid any power surges and possible premature destruction.

A.4 Photographic Techniques

Although there were seven phases of the photographic study as listed in Table E-6, they can be divided into four categories: oscilloscope photography, microflash photography, movie (Fastax) photography, and video tape photography.

A.4.1 Oscilloscope Photography

Two types of oscilloscopes were used. The Techtronix 502 scope showed a continuous probe signal. Since the trace could not be stored, several photographs at any particular power setting desired were necessary to obtain the representative flow regime signal. The camera used Type 47 Polaroid

film and the settings were f4.0 at 1/30 sec.

The Techtronix 564 scope and Polaroid pack film camera had the definite advantage of saving the representative trace for photographing. Various combinations of f-stops and speeds, using Type 107 Polaroid film, gave excellent results. This oscilloscope and camera proved to be a superior experimental tool for the flow regime studies.

A.4.2 Microflash Photography

Polaroid and 35 mm cameras were used in conjunction with the glass annular test section. A General Radio Company Type 1530-A Microflash was used to illuminate the test section. The 2-microsecond light pulse effectively stopped the motion of the flow. The camera, mounted on a tripod, triggered the microflash simultaneously with its shutter release. The films used for the 35 mm Contaflex 3 camera were the colored ASA 40 Kodachrome II and the black and white ASA 400 Tri-X Panchromatic film. Type 42 film was used with the Polaroid camera. Close-up lenses for the particular camera allowed the camera to be within 4 inches of the heated section. The relatively high f-stop (f-8) for the black and white films gave a sufficient depth of field in all cases. The colored slides were slightly too dark for the light and lens setup which was available. Consequently most of the still photography was in black and white.

The microflash was positioned below the camera and was covered by a heavy tissue paper which diffused the light. The background behind the test section was black felt. The oscillograph was used with the 35 mm photography, and a signal blip appeared whenever the microflash discharged.

A.4.3 Movie (Fastax) Photography

The Wollensak 16 mm Fastax camera was used for both experimental movie phases. The first phase, using 16 mm Tri-X Negative Kodak Type 7233 film, was an attempt to photograph, at high speeds (4,000 frames per sec), an area less than 3/8 in. square at the probable burnout point. Several difficulties were experienced during this photographic attempt. For instance, it was extremely difficult to obtain sufficient lighting on the subject since the lens, only 3/4 in. away from the subject, blocked the light. Also the depth of field was extremely small due to the large f-stops necessary. The black and white film itself had drawbacks since the various shades of grey were difficult to interpret. Because of these drawbacks, colored movies, using Ektrachrome Film Type 7242 EF, were taken at 30 cm from the subject. Using this distance, the field of view was increased to almost 3-1/2 inches of the test section.

Three G.E. Photospot 500 W DXB bulbs allowed an f-8 lens setting at 1200 frames per sec. The motor voltage set at 40 vac

gave a camera speed of approximately 1200 fps. The camera, operated remotely, was started by the experimenter who monitored the continuous oscillograph temperature trace. A signal appeared on the oscillograph trace as the camera was turned on and also as the timing light was activated. The timing device consists of a neon glow lamp enclosed in a small housing mounted under the drive sprocket in the camera housing. A small lens in the top of the housing focuses the light on the edge of the film and produces 120 flashes per second. These marks on the film provided an accurate means of calculating film speed and contributed to the interpretation of the oscillograph trace.

A.4.4 Video Tape Photography

An Ampex Model VR-7100 Video Tape System was used to record one experiment, and the tape recording is on file in the Heat Transfer Laboratory, MIT. The primary advantage of such a system for experimental purposes is that a continuous record of the experiment is obtained. Thus there is no need to guess when burnout will occur in order to film the phenomenon. The major, and basically the only, fault of this television system is that its application can only be qualitative. The photographic speed, 20 frames per sec, is so slow that time-motion studies are impossible for the experimental conditions examined.

Appendix B

DATA REDUCTION

The experimental data obtained was reduced by programs written in FORTRAN IV, and run on the M.I.T. Mechanical Engineering Department IBM 1130-Computer. Different programs were used depending on the particular need. Thus the following discussion will cover the calculation programs only in a general manner.

The input data always contained the inlet and outlet temperature, exit pressure, voltage across the test section, and voltage across the current shunt (60.17 amps = 1 mv). The temperatures were converted from millivolts to degrees by means of a subroutine developed by Scott[68] who fitted eleven fourth-order polynomials to the copper-constantan thermocouple tables. The test section power was determined from the current and voltage measurements

$$q_E = E\ I$$

A heat balance to compare q_E with q_W,

$$q_W = w\ c_p\ (T_b - T_{in}),$$

showed agreement within five percent for all CHF data.

The quality, X, was calculated using

$$X = \frac{q_E/w + H_{in} - H_f}{H_{fg}}$$

The inlet enthalpy, H_{in}, was taken directly from tables read into the computer. The other thermodynamic properties of steam were calculated using the polynomials derived by Todreas [69].

The heat generation per unit volume, q/V, is assumed uniform, and for the annular test section is

$$q/V = \frac{q/A \; 2 \; R_{out}}{(R_{out}^{2} - R_{in}^{2})}$$

Where

R_{out} = the cold side radius

R_{in} = the hot side radius

Appendix C

COMPUTER STUDY OF CHF MODEL

C.1 Applicable Theory

The cyclical overheating and quenching of the heated surface at the location of CHF can be described by the time-dependent differential heat-conduction equation and appropriate boundary conditions. For the purposes of the following discussion, the dry spot will be considered to be underneath a bubble. Figure 54 shows the heated wall with the bubble insulating the surface. Since the dry spot radius is small in comparison to the curvature of the tube wall, a flat-plate geometry is assumed as shown in Fig. 55. Hence, the actual coordinate in radial direction is labeled z.

The governing differential equation for the flat plate geometry with the origin under the bubble, is:

$$\frac{1}{r}\frac{\partial}{\partial r}\left(r\frac{\partial T}{\partial r}\right) + \frac{\partial^2 T}{\partial z^2} + \frac{1}{r^2}\frac{\partial^2 T}{\partial \theta^2} + \frac{(q/V)}{k} = \frac{1}{\alpha}\frac{\partial T}{\partial t} \qquad (1)$$

For this equation, the metal properties are independent of temperature and the heat source is uniform. The temperature variation about the center of the dry spot is assumed to be symmetric, hence:

$$\frac{\partial^2 T}{\partial \theta^2} = 0 \qquad (2)$$

and also,

$$\frac{\partial T}{\partial r} = 0 \qquad \text{at } r = 0 \qquad (3)$$

The hot surface is adiabatic, giving

$$\frac{\partial T}{\partial z} = 0 \qquad \text{at z corresponding to } R_{in} \qquad (4)$$

The influence of the temperature variation resulting from the dry spot is assumed to be negligible at $r = r_c$ and hence,

$$\frac{\partial T}{\partial r} = 0 \qquad \text{at } r = r_c \tag{5}$$

The value of r_c is discussed in Section C.3.

On the water side ($z \sim R_{out}$) the boundary conditions depend on time. During a time span Δt_{rise}, the bubble is on the surface and for $r \leq r_b$

$$-k \frac{\partial T}{\partial z} = h_s(T_W - T_s) \tag{6}$$

and for $r_c \geq r > r_b$

$$-k \frac{\partial T}{\partial z} = h_b(T_W - T_b) \tag{7}$$

Without the bubble, during a time span Δt_{quench}, the conditions are for $r \leq b$,

$$-k \frac{\partial T}{\partial z} = h_q (T_W - T_q) \tag{8}$$

and $r_c \geq r \geq r_b$

$$-k \frac{\partial T}{\partial z} = h_b(T_W - T_b) \tag{9}$$

It is impossible to arrive at an exact solution to this problem, and even with further assumptions, an approximate analytical solution would be extremely difficult. Thus a numerical method of solution is necessary to solve this time-dependent problem.

C.2 Discussion of Computer Program

The Fortran IV program, listed in Section C.4, computes the temperature variation in the wall as a function of time. To account for the

different boundary conditions, the tube wall is divided into ten areas as shown in Fig. 56. The method of analysis is centered around the finite-difference equations, derived from heat balances taken about the nodes in each area. There are two sets of equations for the areas labeled 1, 2, 3 and 8. The applicable set depends on whether the surface has a dry spot on it as the vapor void passes over, or whether it is being quenched by the slug. For the node illustrated in Fig. 56, the finite-difference equation is,

$$T'(i, j) = \alpha\cdot\Delta t \{T(i, j)[1/(\alpha\cdot\Delta t) - 2/\Delta r^2 - \frac{2}{(\Delta z)^2}]$$
$$+ T(i - 1, j)\left[\frac{1}{\Delta r^2} - \frac{.5}{\Delta r\cdot R(i)}\right]$$
$$+ T(i + 1, j)\left[\frac{1}{\Delta r^2} + \frac{.5}{\Delta r\cdot R(i)}\right]$$
$$+ \frac{T(i, j + 1)}{\Delta z^2} + \frac{T(i, j - 1)}{\Delta z^2} + \frac{(q/V)}{k}\} \qquad (10)$$

T', the temperature for the new time, is calculated from the five old temperatures, T, surrounding the node (i, j). In the Fortran IV language, the above equation is written as,

```
TB(1,J) = A*(TA(I,J) * (1./A - Z.*C - Z*B)
        + TA(I -1,J)*(B-D) + TA(I+1,J) * (B+D)
        +TA(I,J+1) * C  + TA(I,J-1) * C + 2.*E)          (11)
```

with

A =	AlPHA * HT	HR =	ΔR
B =	$1/HR^2$	HZ =	ΔZ
C =	$1/HZ^2$	HT =	Δt
D =	.5/(R(I) * HR)	E =	(q/V)/2 * k

A marching time solution can best describe the method used in solving for the time-varying wall temperatures. With a given initial temperature distribution, the time is incremented and a new temperature at every node is found. These temperatures then are are used to find the temperatures for the succeeding time increment. By selecting the proper boundary equations at a particular time, the unsteady nature of the problem is resolved.

The basic program can go through three cycles of heating and quenching; these cycles simulate the passage of three slugs over the surface. The program is applicable to tubes and annuli and is written to allow flexibility in examining many variations and approximation of the important parameters. Stability of the solution is assured by selecting the proper time increment, HT, which guarantees that all temperature coefficients in the finite-difference equations are positive. The detailed discussion of the assumptions used in the program to simulate the actual physical conditions at CHF are discussed in the next section.

C.3 Discussion of Assumptions

The initial temperature distribution is found by using the

one-dimensional, steady-state conduction equation in the z direction,

$$\frac{\partial^2 T}{\partial z^2} + \frac{(q/V)}{k} = 0 \tag{12}$$

With the boundary conditions, for the annular test section,

$$\frac{\partial T}{\partial z} = 0 \qquad \text{at } z = R_{in} \tag{13}$$

and

$$T(R_{out}) = T_W \tag{14}$$

The solution to these equations is

$$T(z) = T_W + \frac{(q/V)}{2k} \left(R(z)^2 + 2R_{in}\, R(z) + R_{out}^2 - 2R_{in} \cdot R_{out}\right) \tag{15}$$

This temperature distribution is assumed to be the same function of z across the wall at any position, r, at initial time zero. Such a temperature distribution also satisfies all the initial boundary conditions in the two dimensions.

The initial surface temperature, T_W, is found from the McAdams' [1] correlation for subcooled boiling,

$$T_W - T_s = \left(\frac{q/A}{.19}\right)^{.259} \tag{16}$$

This correlation has been found [65] to describe very well data for forced convection, fully-developed boiling from stainless steel.

The heat transfer coefficient, h_b, for the forced convection boiling, is

$$h_b = \frac{(q/A)}{(T_W - T_b)} \tag{17}$$

T_b is the bulk fluid temperature at the exit and is found from the first law equation,

$$T_b = T_{in} + q/(w \cdot c_p) \tag{18}$$

The heat transfer coefficient for steam, h_s, is chosen to be a very low value (h_s = 20 Btu/hr-ft^2 °F) so as to simulate an almost insulated surface.

The use of the heat transfer coefficient, h_q, simulates the quenching of the dry spot area. Fig. 57 shows the variation of h with time. The solid line shows the actual variation and the broken line shows the assumed variation. The water is heated until its temperature is sufficient for incipient boiling. The coefficient continues to increase with increasing nucleation and remains constant in the fully-developed region. This rapid change of h_q is assumed to vary linearly with time, giving

$$h_q = h_{fc} + \{ \frac{h_b - h_{fc}}{\Delta t_{quench}} \} \quad t \tag{19}$$

The Δt_{quench} is the time during which the slug covers the surface.

The forced-convection heat transfer coefficient, h_{fc}, is calculated using the well known McAdams [1] correlation

$$Nu = 0.023\ Re^{.8}\ Pr^{.4} \tag{20}$$

The program was written so that the water quenching temperature and the temperature of the water film above areas 3 and 8 during a vapor clot passage can be changed. Since these temperatures were not known and since $(T_b - T_W)$ is considered to be the heat transfer driving force, the water temperatures were assumed to be equal to the bulk temperature, T_b.

The equations for the saturation temperature, T_s as a function of pressure were obtained from Todreas [69].

A discussion of the input and output variables, their Fortran names and their significance will conclude this section.

For the first of three input data cards, the four variables are:

BRAD - The assumed dry spot radius in inches. This size is held constant since it is impossible to predict the rate of growth of the dry spot for the conditions under investigation.

IDIV - is one less than the number of nodes under the dry spot. Its value determines the grid spacing in the "r" direction.

HLEN - is the heated length in inches.

MC - is the number of nodes in the r direction. It was determined that 20 nodes were sufficient for this problem because it was

shown that the dry spot did not influence the temperature at the 20th node.

The second data card requires:

ALPHA - is the thermal diffusivity of the metal test section in ft^2/hr at 350 °F.

COND in Btu/hr-ft °F is the thermal conductivity of the metal at 350 °F.

RAIN - is the inside diameter of the glass annulus in inches and is zero if tube data is used. It is used to find the flow area.

Z - is a dummy variable, sometimes used in the basic program for logic operations, iterations or any other particular need.

The third card consisted of the actual data. NO is another dummy variable serving a similar function as Z.

FREQ - is the frequency of the slugs passing the thermocouple. The value is obtained from the oscilloscope flow-regime probe traces, from the thermocouple oscillograph traces, or from the colored Fastax movies.

TIN is the bulk inlet water temperature.

P is the exit pressure in psia.

QONA is the heat flux ($\times 10^{-6}$) for the particular test.

SFRAC is the percent of time that the vapor is over the thermocouple during one cycle. The size of the vapor void, and hence water slug, could thus be altered while the frequency remained constant.

RIN and ROUT are the inner and outer radii, in inches, of the heated

tube, regardless of the test configuration.

w is the mass flow rate in lb/hr.

The output is printed after every fifteenth repetition of the temperature calculations. It contains the time, the arithmetic average of the four nodes about ($r = 0$, $z \sim R_{out}$ or R_{in}), the temperatures along the surface and those along the axis under the dry spot.

C.4 COMPUTER PROGRAM OF MODEL (FORTRAN IV)

```
      DIMENSION RR(15),TA(50,15),TB(50,15),TIMES(1200),TAV(1200),R(100)
      DIMENSION TA1(15)

      READ(5,1) IR, IP
    1 FORMAT (2I1)
      READ(IR,222)BRAD,IDIV,HLEN,MC
  222 FORMAT(F5.4,5X,I2,5X,F5.2,5X,I2)
  228 READ(IR,227)ALPHA,COND,RAIN,Z
  227 FORMAT(4F8.5)
  111 READ(IR,2)NO,FREQ,TIN,P,QONA,SFRAC,RIN,ROUT,W
    2 FORMAT(I1,10X,3F6.2,F6.3,F4.2,2F5.3,F5.0*
      IF(NO-1) 300,112,112
  112 WRITE(IP,3)NO,FREQ,TIN,P,QONA,SFRAC,RIN,ROUT,W
    3 FORMAT(1H1,3HNO=I1,2X,5HFREQ=F6.2,3X,4HTIN=F6.2,3X,2HP=F6.2,3X,
     1 5HQONA=F6.3,'MILLION',3X, 6HSFRAC=F4.2,3X,4HRIN=F5.3,3X,4HRIN=
     2F5.3,3X,2HW=F5.0//)
C HEATED LENGTH  IS AL IN FEET.
      AL=HLEN/12.
      PI=3.14138
      RI = RIN/12.
      RO = ROUT/12.
      IF(RAIN)601,601,611
  611 WRITE(IP,612)RIN,ROUT,HLEN,RAIN
  612 FORMAT(10X,'THE TEST SECTION IS AN ANNULUS,WITH DIMENSIONS(IN INCH
     1ES)  '/1X,'THE METAL TUBE INSIDE RADIUS',2X,F6.4,4X,'THE METAL TUB
     2E OUTSIDE RADIUS ',F6.4/1X,'THE HEATED LENGTH IS 'F6.3,12X,
     3'THE INSIDE RADIUS OF THE ANNULUS ',F6.4//)
      HAREA = PI*RO*2.*AL
      GO TO 777
  601 WRITE(IP,636)RIN,ROUT,HLEN
  636 FORMAT(10X,'THE TEST SECTION IS A ROUND TUBE WITH DIMENSIONS (IN I
     1NCHES)'/1X,'THE METAL TUBE INSIDE RADIUS',2X,F6.4,4X,'THE METAL TU
     2BE OUTSIDE RADIUS ',F6.4/1X'THE HEATED LENGTH IS 'F6.3,/)
      HAREA=PI*2.*RI*AL
  777 BRAD1=BRAD/12.
      QONA = QONA*1.E6
C THE ASSUMED BUBBLE RADIUS IS BRAD
      CODIV = IDIV
```

```
C THE INCREMENT OF DISTANCE IN THE RHO DIRECTION
      HR=BRAD1/CODIV
C MB IS THE END NODE FOR THE BUBBLE
      MB=IDIV + 1
      WRITE(IP,221)HLEN,BRAD,MB,MC
  221 FORMAT(1X,'THE HEATED LENGTH IS ',F5.2,5X,'THE DRY SPOT RADIUS IS
     1',F5.3,' INCHES',5X,'THE NUMBER OF NODES UNDER BUBBLE IS ',I2/
     21X,'THE NUMBER OF NODES IN THE RHO DIRECTION IS',I2/)
      HZ=(RO-RI)/14.
      HSTE= 20.
C HMC IS THE MC ADAMS FORCED CONVECTION HEAT TRANSFER COEEFICIENT.
      HMC=2370.
C
      IF (P-450.) 301,310,310
  301 PS = ALOG(10.*P)
      TS= 3.5157890E 1+2.4592588E+1*PS +2.1182069*(PS**2)
     1-3.4144740E-1*(PS**3)  +1.5741642E-1*(PS**4)
     2 -3.1329585E-2*(PS**5)    +3.8658282E-3*(PS**6)
     3 -2.4991784E-4*(PS**7)    +6.8401559E-5*(PS**8)
      GO TO 5
C
  310 PS = ALOG(P)
      TS= 1.1545164E+4  -8.3860182E+3*PS +2.4777661E+3*(PS**2)
     1 -3.6344271E+2*(PS**3)     +2.6690978E+1*(PS**4
     2 )   -7.8073813E-1*(PS**5)
C
    5 DTSAT = (QONA/.19)**.259
       TW= TS+DTSAT
      TSTE = TS
      TWAT = TIN + QONA*HAREA/W
      DTSUB = TS-TWAT
      HWATW = QONA / (TW-TWAT)
C HWATS IS THE COEFFICIENT FOR WATER WHEN LIQUID FILM COVERS SURFACE.
      HWATS = HWATW
      TWATS = TWAT
      B = 1./(HR*HR)
      C = 1./(HZ*HZ)
      QVOL1= QONA*2.*RO/(RO*RO-RI*RI)
       QVOL= QONA/(RO-RI)
      WRITE(IP,10002)QVOL1,QVOL
10002 FORMAT(1X,'THE VOLUMETRIC HEAT STRENGTH FOR A CURVED SURFACE IS ',
     1E11.4 /1X, 'THE VOLUMETRIC HEAT STRENGTH FOR A FLAT PLATE IS ',
     2E11.4//)
C FREQUENCY OF SLUGS PER SEC (FREQ) IS CONVERTED TO PERIOD IN HRS.
      PERIO = 1./(FREQ*3.6E3)
C SLOPE IS FOR THE TIME VARIATION OF HWATQ
      SLOPE = (HWATW-HMC)/(PERIO*(1.-SFRAC))
C CHECKING FOR STABILITY
      DIV = 200.
C HT IS THE TIME INCREMENT.
    6 HT = PERIO/DIV
      A = ALPHA * HT
      STAB = 2.* A * ( HWATW/(COND*HZ) + 2.*B  +C)
      IF (1-STAB) 7,8,8
    8 HTS = HT*3.6E6
      WRITE(IP,9)QONA,HWATW,DTSUB,TWAT,HTS,DIV,TS ,HR,HZ
    9 FORMAT(1X, 5HQONA=E11.4,3X,6HHWATW=F6.0,3X, 6HDTSUB=F6.2,3X,
     15HTWAT=F6.2/1X, 'STABILITY CRITERIA IS SATISFIED. HTS=',
     2F6.3,'MSECS',5X, 'THE PERIOD IS DIVIDED BY DIV =',F6.1,2X,
     33HTS=F6.2/1X,3HHR=F9.7,'FT',5X,3HHZ=F9.7,'FT'//)
      GO TO 99
    7 DIV = DIV + 10.
      GO TO 6
C NOW CALCULATE THE VARIOUS POINTS IN THE Z DIRECTION IN ORDER TO GET
C THE INITIAL TEMP DISTRIBUTION. (THIS IS THE ACTUAL RADIAL DIRECTION.)
      IF(RAIN)999,999,99
   99 DO 991 J=1,15
      RR(J)=RO-(J-1)*HZ
C CALCULATE THE INITAL TEMP DISTR IF CURVED PLATE
      TA1(J)  = TW +QVOL1/(4.*COND)*(-RR(J)**2+2.*RI*RI*
     1ALOG(RR(J)/RO) + RO*RO)
C NOW CALCULATE THE INITIAL TEMP DISTRIBUTION IN Z DIRECTION.
  991 TA(1,J) = TW + QVOL/(2.*COND)*(-RR(J)**2 + 2.*RI*RR(J) + RO*RO
     1 -2.*RI*RO)
         GO TO 10000
  999 DO 998 J=1,15
C MUST REVERSE THE ORDER OF J FOR A TUBE
        RR(J) = RI + (J-1)*HZ
         TA(1,J)= TW + QVOL/(2.*COND)*(-RR(J) **2 + 2.*RO*RR(J)
     1 + RI*RI -2.*RO*RI)
        TA1(J) = TW + QVOL1/(4.*COND)* (-RR(J) ** 2 + RI*RI
     1 + RO*RO*2.*ALOG(RR(J)/RI))
  998 CONTINUE
10000 DO 100 I=2,MC
      DO 100 J=1,15
  100 TA(I,J) = TA(1,J)
      TIMES(1) = 0.0
      WRITE(IP,993) (TA(1,J),J=1,15),(TA1(J),J=1,15)
  993 FORMAT(1X,'TEMPERATURE DISTRIBUTION USED IN PROGRAM'/
     11X,'TB(1,J)=',15F7.2/
     2 1X,'TEMPERATURE DISTRIBUTION ASSUMING A CURVED SURFACE VIS FLAT'/
     32X,'TA1(J)=',15F7.2//)
C GO THROUGH TWO CYCLES FOR EACH RUN
      N=2.*DIV + 1.2
      TIME = 0.0
      TIME1 = 0.0
      L=1
      R(MC)=(MC-1)*HR
      F=(R(MC)-HR/2.)/(R(MC)-HR/4.)
      DO 10  K = 2,N
C TIMES FOR EXTERNAL USE IN MSECS.
      TIME = TIME + HT
      TIMES(K) = TIME * 3.6E6
        TIME1=TIME1+HT
      DO 11 J=1,15
      DO 12 I=1,MC
      R(I) = (I-1)*HR
      IF(I-1)104,104,103
  103 D = .5/(R(I)*HR)
  104 E = QVOL/(2.*COND)
C CHECKS WHETHER ON THE FIRST ROW
      IF(J-1) 138,138,14
C CHECKS FOR WHETHER BUBBLE OR WATER ON THE SURFACE
  138 IF(TIME - 3.*PERIO)139,139,135
  135 CALL EXIT
  139 IF(TIME - (3.-SFRAC/2.)*PERIO)140,140,13
  140 IF(TIME- (2.+SFRAC/2.)*PERIO)141,141,201
  141 IF(TIME- (2.-SFRAC/2.)*PERIO) 142,142,13
  142 IF(TIME-(1.+SFRAC/2.)*PERIO)143,143,201
```

```
  143 IF(TIME-(1.-SFRAC/2.)*PERIO)144,144,13
  144 IF (TIME-(SFRAC/2.*PERIO))13,13,201
   13 TIME1 = -HT
C IF IT IS THE BUBBLE IT CAN BE IN AREA 1,2,3
      IF(I-1)15,15,16
C EQT 15 IS THE EQUATION FOR REGION 1 WITH BUBBLES OVER IT.
   15 TB(I,J) = 2.*A*( TA(I,J)*(.5/A - 2.*B- C - HSTE / (COND*HZ))
     1+ 2.*B* TA(I+1,J)  + C * TA(I,J+1) + E + HSTE  *TSTE /(COND*HZ))
      GO TO 12
C IF STILL UNDER BUBBLE BUT NOT AT (1,1),THUS IN AREA 2
   16 IF (I-MB) 17,17,18
   17 TB(I,J) = 2.*A*( TA (I,J) * ( .5/A - HSTE/(COND*HZ) - B - C)
     1 + HSTE * TSTE / (COND*HZ) + TA(I-1,J)*.5*(B-D)
     2 + TA(I+1,J) *.5*(B+D)   + TA(I,J+1)*C + E)
      GO TO 12
C IF SLUG ON SURFACE IN AREA 8
   18 IF(I-MC)181,182,182
  182 TB(I,J) = 2.*A*(TA(I,J)*( .5 / A - F * B - C - HWATS/(COND*HZ))
     1 + TA(I,J+1)*C + HWATS*TWATS/(COND*HZ)+ F * B * TA(I-1,J) + E)
      GO TO 12
C IF SLUG ON SURFACE,IN AREA 3 WITH LIQUID FILM COVERING THE REMAINING SURFACE
  181 TB(I,J) = 2.*A*( TA (I,J) * ( .5/A -HWATS/(COND*HZ) - B - C)
     1 + HWATS*TWATS / (COND*HZ) + TA(I-1,J)*.5*(B-D)
     2 + TA(I+1,J) *.5*(B + D) + TA(I,J+1)*C + E)
      GO TO 12
C HWATQ IS THE HEAT TRANSFER COEFFICIENT FOR QUENCHING AT THE HOT SPOT
C HWATQ IS A LINEAR FUNCTION OF TIME
  201 HWATQ = HMC+ SLOPE * TIME1
      TWATQ=TWAT
      IF(I-1)202,202,203
C EQUATION FOR NODE 1 WITH WATER ON IT
  202 TB(I,J) = 2.*A*( TA(I,J)*(.5/A - 2.*B- C - HWATQ/ (COND*HZ))
     1+ 2.*B* TA(I+1,J)  + C * TA(I,J+1) + E + HWATQ*TWATQ /(COND*HZ))
      GO TO 12
  203 IF(I-MB) 2031,2031,2032
C FOR THE QUENCHED SURFACE UNDER THE BUBBLE
 2031 TB(I,J) = 2.*A*( TA (I,J) * ( .5/A -HWATQ/(COND*HZ) - B - C)
     1+TWATQ*HWATQ   / (COND*HZ) + TA(I-1,J)*.5*(B-D)
     2 + TA(I+1,J) *.5*(B+D)   + TA(I,J+1)*C + E)
      GO TO 12
 2032 IF(I-MC)204,205,205
C EQUATION FOR NODE MC,1
  205 TB(I,J) = 2.*A*(TA(I,J)*( .5 / A - F * B - C - HWATW/(COND*HZ))
     1 + TA(I,J+1)*C + HWATW*TWAT/(COND*HZ) + F * B * TA(I-1,J) + E)
      GO TO 12
C EQUATIONS FOR ALL NODES ON SURFACE EXCEPT THE ENDS AND UNDER THE BUBBLE
  204 TB(I,J) = 2.*A*( TA (I,J) * ( .5/A -HWATW/(COND*HZ) - B - C)
     1 +TWAT*HWATW   / (COND*HZ) + TA(I-1,J)*.5*(B-D)
     2 + TA(I+1,J) *.5*(B+D)   + TA(I,J+1)*C + E)
C THE PREVIOUS TWO EQUATIONS COVER AREAS 1,2,3
      GO TO 12
C THE FOLLOWING IF STATEMENTS CHECK FOR NODES IN ROW 15,THE ADIABATIC WALL
   14 IF (J-15)22,21,21
   21 IF ( I-1) 23,23,24
C FOLLOWING FORMULA FOR AREA 6
   23 TB(I,J) = 2.*A* ( TA(I,J)*(.5/A - C - 2.*B)
     1 + TA(I,J-1) * C + TA(I+1,J) * 2. * B  +E)
      GO TO 12
C THE FOLLOWING FORMULA FOR AREA 10
   24 IF(I-MC)241,242,242
  242 TB(I,J) = A*(TA(I,J)*(1./A - F*B*2. - C*2.)+ TA(I-1,J)*F*B*2.
     1 + TA(I,J-1) * C * 2. + 2. *E)
      GO TO 12
C FOLLOWING FORMULA FOR AREA 7
  241 TB(I,J) = 2.*A*( TA(I,J)*(.5/A - B - C ) + TA(I+1,J)*.5*(B+D)
     1 +TA(I-1,J) *.5*(B-D) + TA(I,J-1) * C + E)
      GO TO 12
   22 IF ( I - 1 ) 25,25,26
C FOLLOWING FORMULA FOR AREA 4
   25 TB(I,J) = A * ( TA(I,J)* (1./A - 2.*C - 4.*B) + TA(I,J-1)*C
     1 + TA(I,J+1) * C + TA(I+1,J)*4.*B +2.*E)
      GO TO 12
   26 IF(I-MC)261,262,262
C FOLLOWING EQUATION FOR AREA 9
  262 TB(I,J) = 2.*A*(TA(I,J)*(.5/A -F * B - C ) + F*B*TA(I-1,J)
     1 + .5*C*TA(I,J+1)  + .5*C*TA(I,J-1) + E )
      GO TO 12
C THE FOLLOWING FORMULA FOR ALL INTERNAL NODES
  261 TB(I,J) = A* (TA(I,J) * (1./A - 2.*C - 2.*B) + TA(I,J+1)*C
     1 + TA(I-1,J)*(B-D) + TA(I+1,J)* (B+D) + TA(I,J-1)*C +2.*E)
   12 CONTINUE
   11 CONTINUE
C THE AVERAGE TEMPERATURE OF FOUR NODES ABOUT (0.0)
      L=L+1
      IF(L-15)32,31,32
   31 TAV(K) = (TA(1,1)+ TA(1,2) + TA(2,1) + TA(2,2) ) / 4.
      WRITE(IP,27) TIMES(K),TAV(K),  (TB(I,1),I=1,15), (TB(1,J), J=1,15)
   27 FORMAT(1X,'ELAPSED TIME=',F7.3,'MSECS',4X,'THE MEAN TEMP,TAV=',
     1F7.2/1X,'TB(I,1)',1X,15F7.2/1X,'TB(1,J)',1X,15F7.2//)
      L=0
   32 DO 30 J=1,15
       DO 30 I =1,MC
   30 TA(I,J) = TB(I,J)
   10 CONTINUE
      IF(Z)1111,1111,112
 1111 GO TO 111
  300 CALL EXIT
      END
```

TYPICAL DATA

```
C  FIRST CARD IS A MACHINE INSTRUCTION
56
.002        1      2.82       20
.172       10.3
2           150.   66.     27.7 3.58  .52 .047 .052 178.
```

Appendix D

MOVIE TITLES AND DESCRIPTION

The titles for the 20-minute forced-convection movie taken during this study and presently on file in the M.I.T. Heat Transfer Laboratory are listed below.

Title No.	Caption
1	Slug Flow and Subcooled Burnout
2	M.P. Fiori A.E. Bergles Heat Transfer Laboratory Massachusetts Institute of Technology 1967-1968
3	Test Conditions Vertical Upflow of Water In An Annular Test Section 0.546 in. o.d. (glass) 0.312 in. o.d. (heated test section) DC Resistance Heating of Inner 304 SS Tube
4	Heat Flux = 1.12×10^6 Btu/hr-ft^2 Flow Rate = 918 lbm/hr Exit Subcooling = 113^0F Pressure = 40 Psia Precent of CHF = 85 percent
5	Camera Speed 1200 Frames Per Sec
6	Heat Flux = 1.65×10^6 Btu/hr-ft^2 Flow Rate = 1040 lbm/hr Exit Subcooling = 101^0F Pressure = 49 Psia Percent of CHF = 98 percent
7	Camera Speed 1500 Frames Per Sec
8	Heat Flux = 939×10^6 Btu/hr-ft^2 Flow Rate = 614 lbm/hr Exit Subcooling = 83^0F Pressure = 29 Psia Percent of CHF = 85 percent

Title No.	Caption
9	Camera Speed 1500 Frames Per Sec
10	Heat Flux = 1.57 x 10^6Btu/hr-ft^2 Flow Rate = 918 lbm/hr Exit Subcooling = 121^{0}F Pressure = 88 Psia Percent of CHF = 92 percent
11	Camera Speed 1300 Frames Per Sec
12	Heat Flux = 1.12 x 10^6Btu/hr-ft^2 Flow Rate = 918 lbm/hr Exit Subcooling = 75^{0}F Pressure = 37 Psia Percent of CHF = 92 percent
13	Camera Speed 1300 Frames Per Sec
14	Heat Flux = 1.665 x 10^6Btu/hr-ft^2 Flow Rate = 1040 lbm/hr Exit Subcooling = 101^{0}F Pressure = 40 Psia Percent of CHF = 100 percent
15	Camera Speed 1300 Frames Per Sec
16	Blue Flash Results From Current Arcing As Test Section Melts and Breaks the Circuit
17	Conclusions 1. Slug Flow Exists at Subcooled Burnout
18	2. Nucleation Exists in the Liquid Film Under the Bubble
19	3. The Film is Broken by a Nucleating Bubble Causing a Dry Spot, Surface Overheating and Burnout
20	The End

A short descriptive paper accompanies the film. This paper is reproduced on the next two pages.

Description of 16 mm Fastax movie titled "Slug Flow and Subcooled Burnout"

This movie was made in the Heat Transfer Laboratory at M.I.T. using a Fastax movie camera. The movies were part of a thorough examination of the physical conditions existing at CHF. The results of the entire research effort are presented in Fiori, M.P., "Model of Critical Heat Flux in Subcooled Flow Boiling", PhD Thesis, M.I.T., September 1968.

The first film, test T-16, only part of which is included in this movie, was taken in order to show that slug flow existed upstream of the test section exit. The length of the test section photographed is twice that of the other runs. The conclusions are that at only 85% of CHF, slug flow exists along the greater part of the heated tube length.

The second film, Test T-14, slightly dark, clearly shows slug flow and momentary flow stoppage which results from the flow rather than system characteristics. The orange or discolored metal at the exit is the copper shorting tube silver-soldered onto the stainless steel.

The third film, Test T-13, again at high subcoolings, shows a similar flow situation, i.e., extremely high void fractions at high subcoolings (83^{o}F for T-13).

The fourth film, Test T-2, shows the first successful movie run. The yardstick, missing here, was added for all the following tests. Flow stoppage and instability is noted. The exit plenum design, causing a 90 degree change of flow, was suspected of causing these instabilities. The redesigned straight-through-flow exit plenum showed that the momentary reversal was inherent with slug flow.

The fifth film, Test T-17, was taken for relatively low subcooling ($75^{o}F$). The very high void fraction is obvious.

The final film, Test T-15, is the only film actually showing the destruction of the test section. The critical condition has already passed and the heated wall already is covered by the insulating vapor. Note that the flow regime is not appreciably altered. The blue flash results from the circuit breaking a current of nearly 1400 amperes.

TABLE E-1

ANNULAR FLOW REGIME TESTS

O.D. of Heated Section = 0.312 in.

Test	P (psia)	$(q/A)_{cr}$ x 10^{-6} Btu/hr-ft^2	G x 10^{-6} lbm/hr-ft^2	ΔT_{sub} °F	L in.	Annular Gap in.	Purpose and Comments
1	21.5	.564	.4	42	8-7/8	0.091	Microflash (Polaroid)
2	40.5	1.30	1.1	110	9-3/4	0.091	Photo of flow in glass annulus at CHF
3	43.5	1.37	1.1	90	9-3/4	0.091	
4	33.7	.891	.7	71	9-13/32	0.091	
5	47.7	1.17	.91	126	8-11/32	0.091	Black and white Fastax movie
6	37.4	1.08	.91	93	7-1/16	0.091	
7	67	1.86	1.25	95	10	0.102	
8	68	1.37	1.0	111	10	0.102	
9	73	1.69	1.25	99	10	0.102	
10	74	2.02	1.25	87	10	0.102	
11	67	1.63	1.08	84	10	0.102	Video tape

TABLE E-2

Range of Variables for Tube Flow Regime Studies

Fig.	L/D	D in.	P_e psia	G x 10^{-6} lbm/hr-ft^2
15	30	0.242	90	.7 - 3.4
16	30	0.242	40	.5 - 3.4
17	15	0.094	30	1.12 - 6.72
18	30	0.094	30	1.12 - 6.72

The data listed below are for those tube flow regime tests (F series tests) which were continued to the CHF condition.

Test	P (psia)	G x 10^{-6} (lbm/hr-ft^2	$(q/A)_{cr}$x10^{-6} (Btu/hr-ft^2)	ΔT_{sub} °F	D in.	L/D	Flow Regime at CHF
1	42	1.5	1.75	66	0.242	30	SLUG
2	53	3.4	3.23	88	0.242	30	SLUG
3	92	2.5	2.76	111	0.242	30	FROTH
4	87	3.0	3.21	105	0.242	30	FROTH
5	28	3.69	3.58	63	0.094	30	FROTH
6	29	2.24	4.06	67	0.094	15	FROTH
7	29	6.72	7.03	116	0.094	15	FROTH

TABLE E-3

Data of Wall Thermocouple Tests

The P-series tests were conducted to photographically examine the flow regimes and simultaneously record the wall surface temperatures. Only those q/A's with asterick are at CHF. The q/A was normally increased only until slug flow was shown to exist. A Contaflex 35 mm camera was used.

DIMENSIONS:
L = 10.0 in. O.D. = 0.312 in. Gap = 0.112 in.

Test	P psia	q/A x 10^{-6} Btu/hr-ft^2	G x 10^{-6} lbm/hr-ft^2	ΔH_{sub} Btu/lbm	Comments
P1	38	1.18	.88	120	
P2	35	1.30	.88	105	
P3	39	1.02	.59	91	
P4	35	1.50	1.0	92	
P5	40	1.47	.88	90	
P6	32	.936	.59	88	Photo I in Fig. 26
P7	58	1.08	.59	108	Photo II in Fig. 26
P8	51	1.34	.88	116	Photo III in Fig. 27
P9	33	1.16	.88	106	
P10	32	1.33*	1.0	99	
P11	48	1.53	1.0	107	
P12**	29	1.1*	.59	43	
P13	35	1.27	.88	80	Photo IV & V, Fig.27

** See Figs. 28 and 29 for CHF Wall Temperature Trace

TABLE E-3 CONT.

The T-series tests were those using the wall thermocouple instrumentation simultaneouslv with Fastax movies or with the flow regime probe. Only those tests continued to CHF are recorded here.

DIMENSIONS: L = 10 in.,O.D. = 0.312 in., Gap Between Inner and Outer Tube of Annulus as Noted

Test	P psia	$(q/A)_{cr} \times 10^{-6}$ Btu/hr-ft^2	$G \times 10^{-6}$ lbm/hr-ft^2	ΔT_{sub} °F	Annular Gap in.	Comments
T1	61	1.633	1.08	103	0.095	
T2	87	1.71	1.08	121	0.095	1st Color movie
T4	49	1.289	.75	85	0.102	Flow regime probe
T5	58	1.27	.75	96	0.102	Flow regime probe
T6	29	1.24	.75	49	0.091	
T11	36	1.13	.75	84	0.091	
T15	49	1.665	1.27	101	0.091	*
T16	35	1.12	.88	113	0.112	
T17	33.5	1.12	.88	75	0.112	

* Movie shows CHF phenomenon. See Figs. 32 and 34 for temperature trace.

TABLE E-4

Table of Computer Runs

Computer Input	1	2	3	4	5	6
BRAD	0.002	0.006	0.006	0.004	0.002	0.002
IDIV	1	3	3	2	1	1
HLEN	10.0	10.0	10.0	10.0	2.82	2.82
MC	30	30	30	20	20	20
ALPHA	0.172	0.172	0.172	2.074	0.172	0.172
COND	10.3	10.3	10.3	68.0	10.3	10.3
FREQ	35	35	10	34	150	150
TIN	71	71	68	71	66	66
P	40.0	40.0	28.8	40	27.7	27.7
QONA	1.665	1.665	1.100	1.665	3.58	3.58
SFRAC	0.52	0.52	0.25	0.52	0.52	0.52
RIN	0.121	0.121	0.121	0.121	0.047	0.047
ROUT	0.156	0.156	0.156	0.156	0.060	0.052
W	1040	1040	614	1040	178	178
ΔT_{rise} (°F) (1 cycle)	37	76	61	9	67	70

Discussion of Computer Runs

Run 1 The input data was from the CHF test shown in Fig. 32 and the results are shown in Fig. 34. Good agreement with actual temperature is noted.

Run 2 Similar input as Run 1 but different dry spot size. The dramatic change of ΔT_{rise} indicates that bubble size is an important variable.

Run 3 The input data was from the CHF test shown in Fig. 28 and the results are shown in Fig. 29. Good agreement with actual temperature is noted.

Run 4 This run shows the important effect of metal properties on ΔT_{rise}. Note that ΔT_{rise} is only 9°F instead of 37°F for Run 1.

Run 5 Runs 5 and 6 were designed to show the diameter effect. The data is for CHF Test No.5, Table E-2. Since no wall temperature measurements were made for tube flow, the frequency for froth flow was assumed.

Run 6 For the same data with a smaller wall thickness (0.008 in.less) ΔT_{rise} is a few degrees higher than for the thicker walled tube. This indicates that the temperature variation resulting from different tube wall thicknesses, is consistent with the proposed model.

TABLE E-5

CHF DATA FOR TUBE WALL THICKNESS EXPERIMENTS

I.D. = 0.094 in. L/D = 30

Test	$G \times 10^{-6}$ lbm/hr-ft^2	P psia	$(q/A)_{cr} \times 10^{-6}$ Btu/hr-ft^2	ΔH_{sub} Btu/lbm	t in.
1	3.0	30.5	3.76	20.7	0.078
2	3.0	88	4.1	62.8	0.078
3	4.5	31	4.41	53.5	0.078
4	4.5	90	5.46	93.3	0.078
5	3.3	38	3.98	42.0	0.078
6	1.5	35	2.70	38.0	0.078
7	1.5	29	1.73	28.0	0.012
8	3.0	29	3.04	49	0.012
9	4.5	28	3.66	67.8	0.012
10	4.5	89	5.20	99.0	0.012
11	3.0	89	3.96	81.6	0.012
12	1.5	92	2.58	37	0.012

TABLE E-6

PHOTOGRAPHIC STUDY

Phase	Purpose	Test Section	Photographic Equipment
1.	Establish flow regime at CHF	Glass Annulus	Microflash and Polaroid Camera
2.	Flow regime study in boundary layer	Metal Annulus	Techtronix 502 Oscilloscope and camera
3.	Black and white Fastax Movies	Glass Annulus	Fastax camera, no oscillograph recorder
4.	Possibility of using video tape for analytical work	Glass Annulus	TV - Ampex Model VR 7100 Video tape system
5.	Colored movies for confirmation of relationship of flow regime and wall thermocouple	Glass Annulus	Fastax camera - oscillograph recorder
6.	35 mm camera for still picture confirmation of flow regime and wall thermocouple	Glass Annulus	Microflash and Contaflex 3 camera with oscillograph recorder
7.	Flow regime study of M.I.T. data points	Straight Tube	Techtronix Storage Scope Model 564 and camera

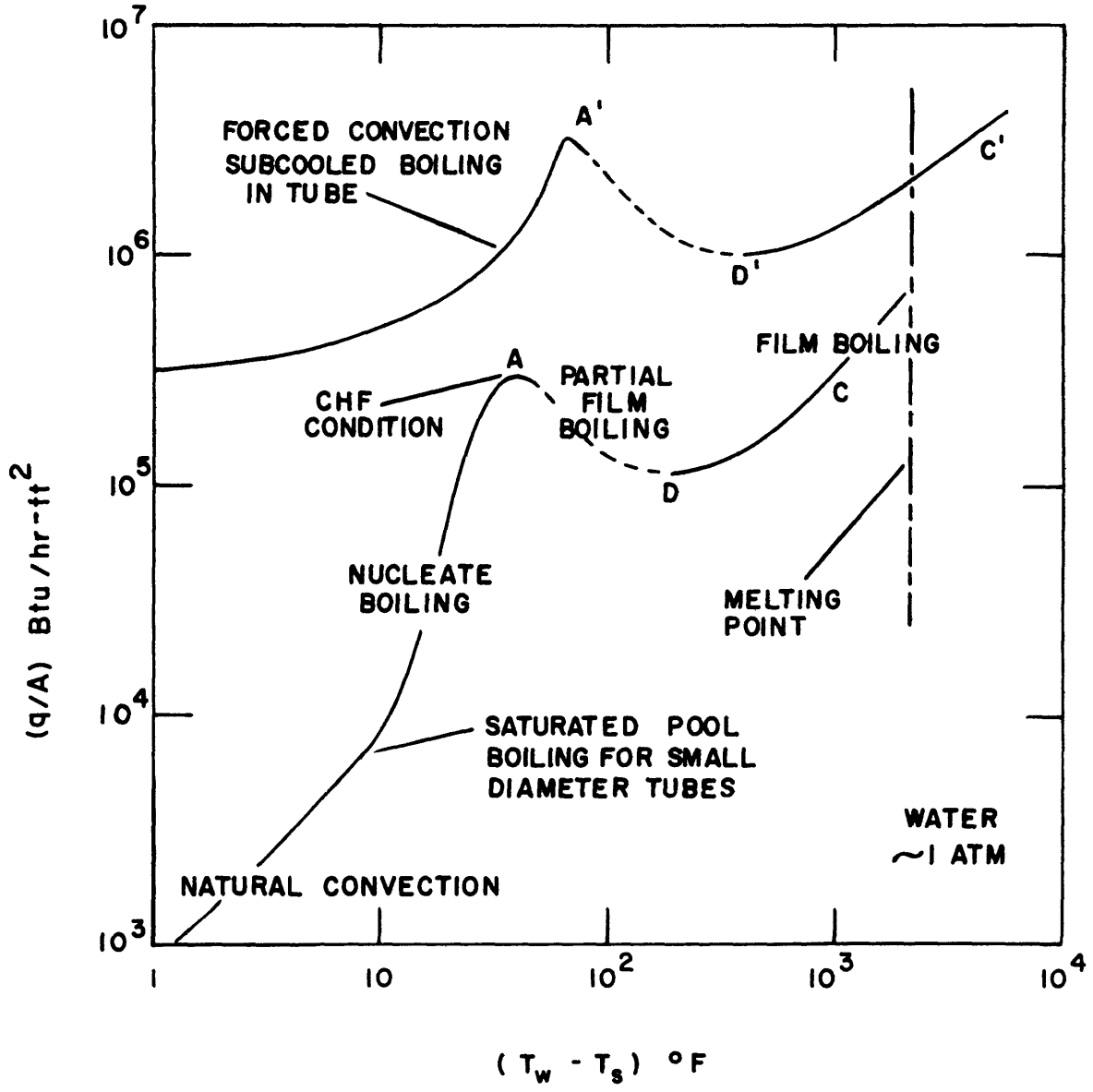

FIG. 1 BOILING CURVE FOR WATER UNDER SUBCOOLED FORCED-CONVECTION CONDITIONS

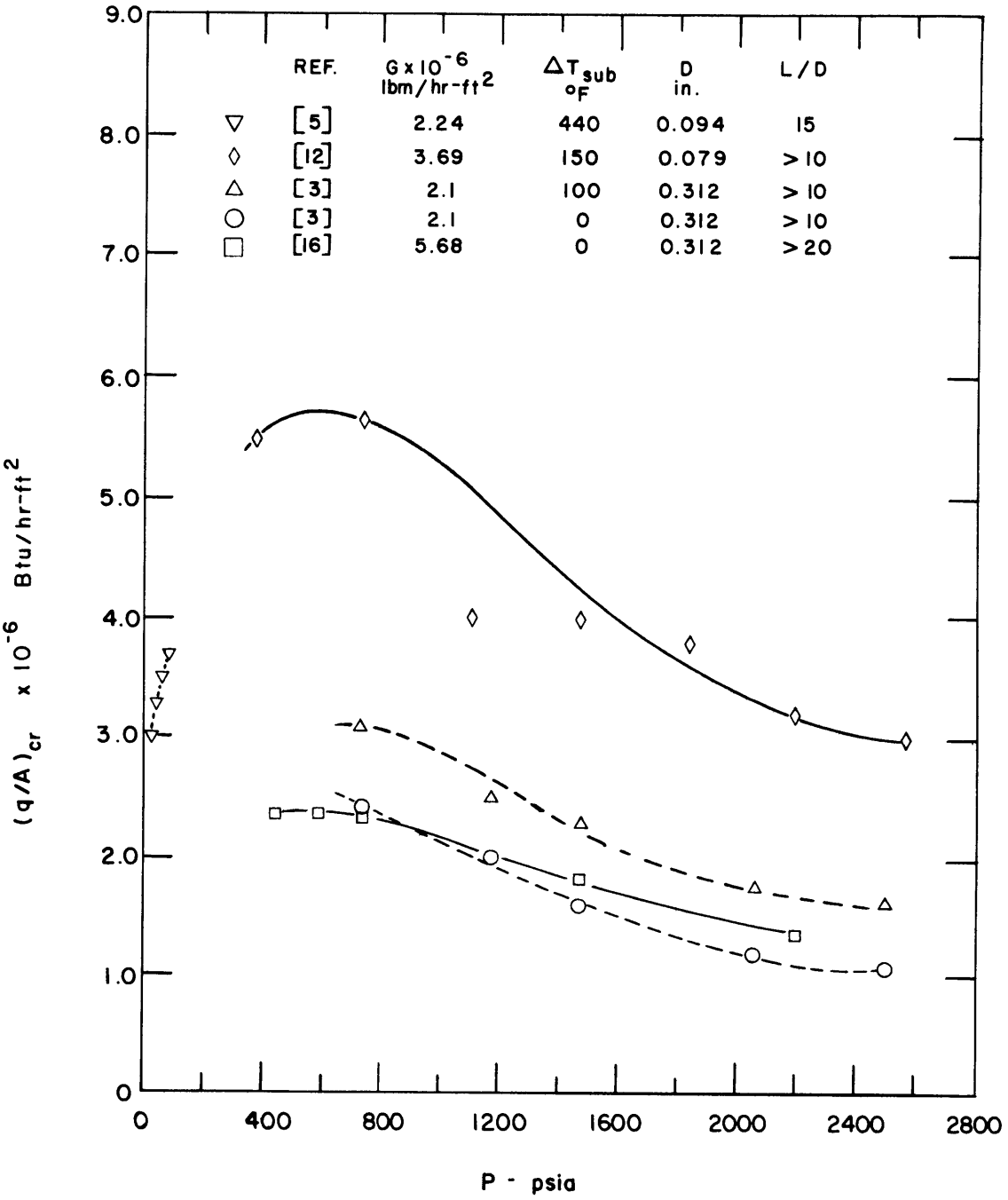

FIG. 2 EFFECT OF PRESSURE ON CHF

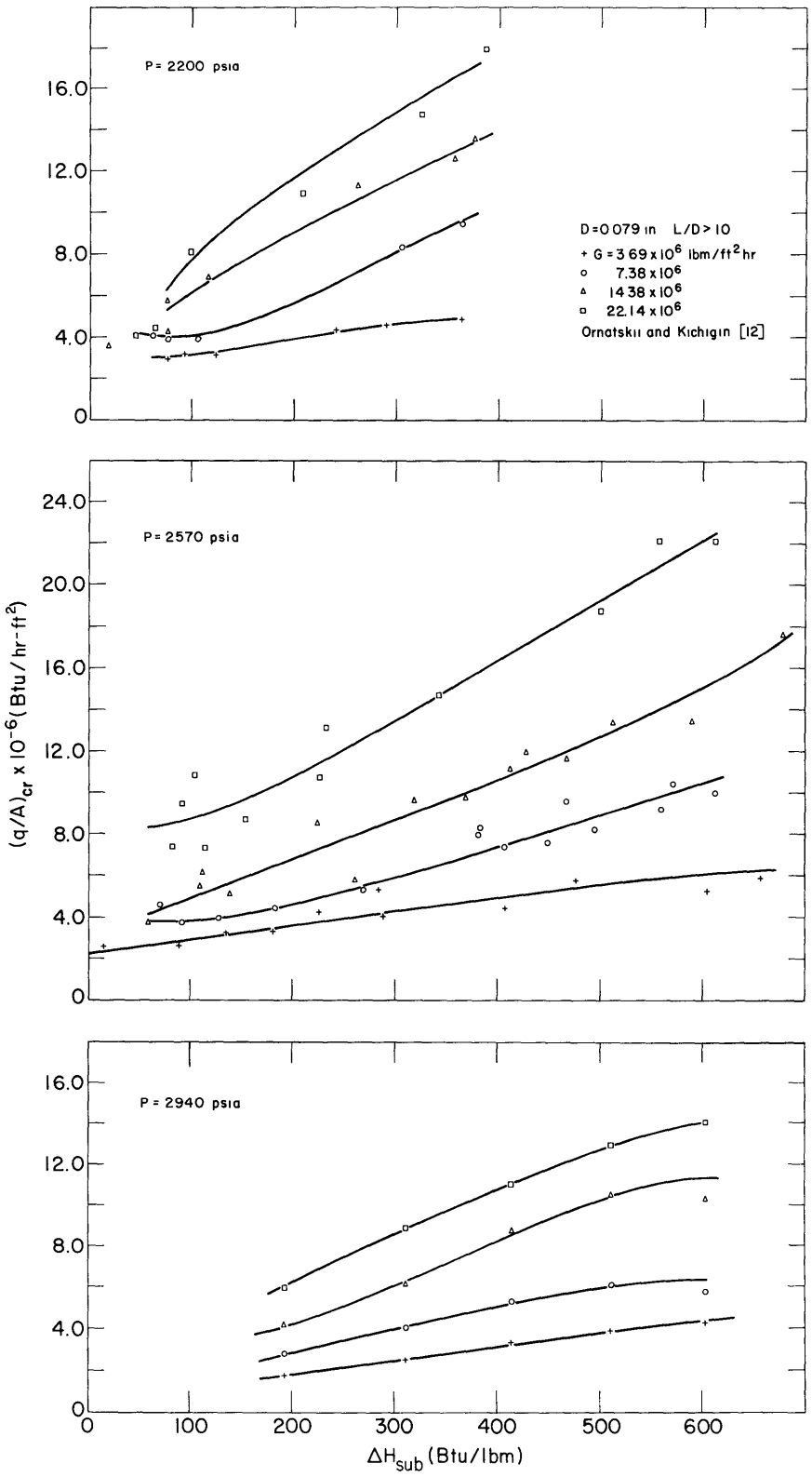

FIG. 3 EFFECT OF MASS VELOCITY ON CHF AT HIGH PRESSURES

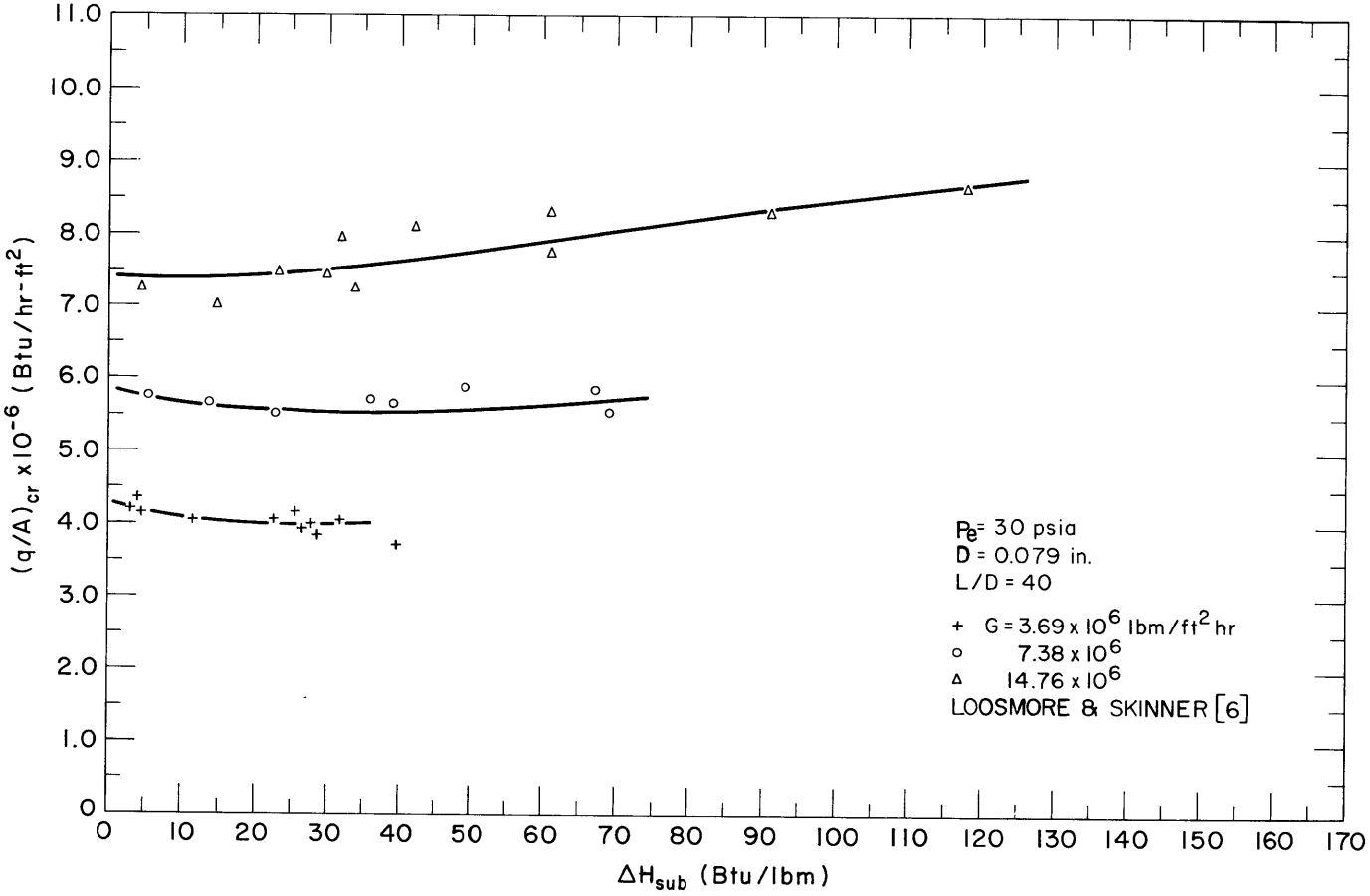

FIG. 4 EFFECT OF MASS VELOCITY ON CHF AT LOW PRESSURES

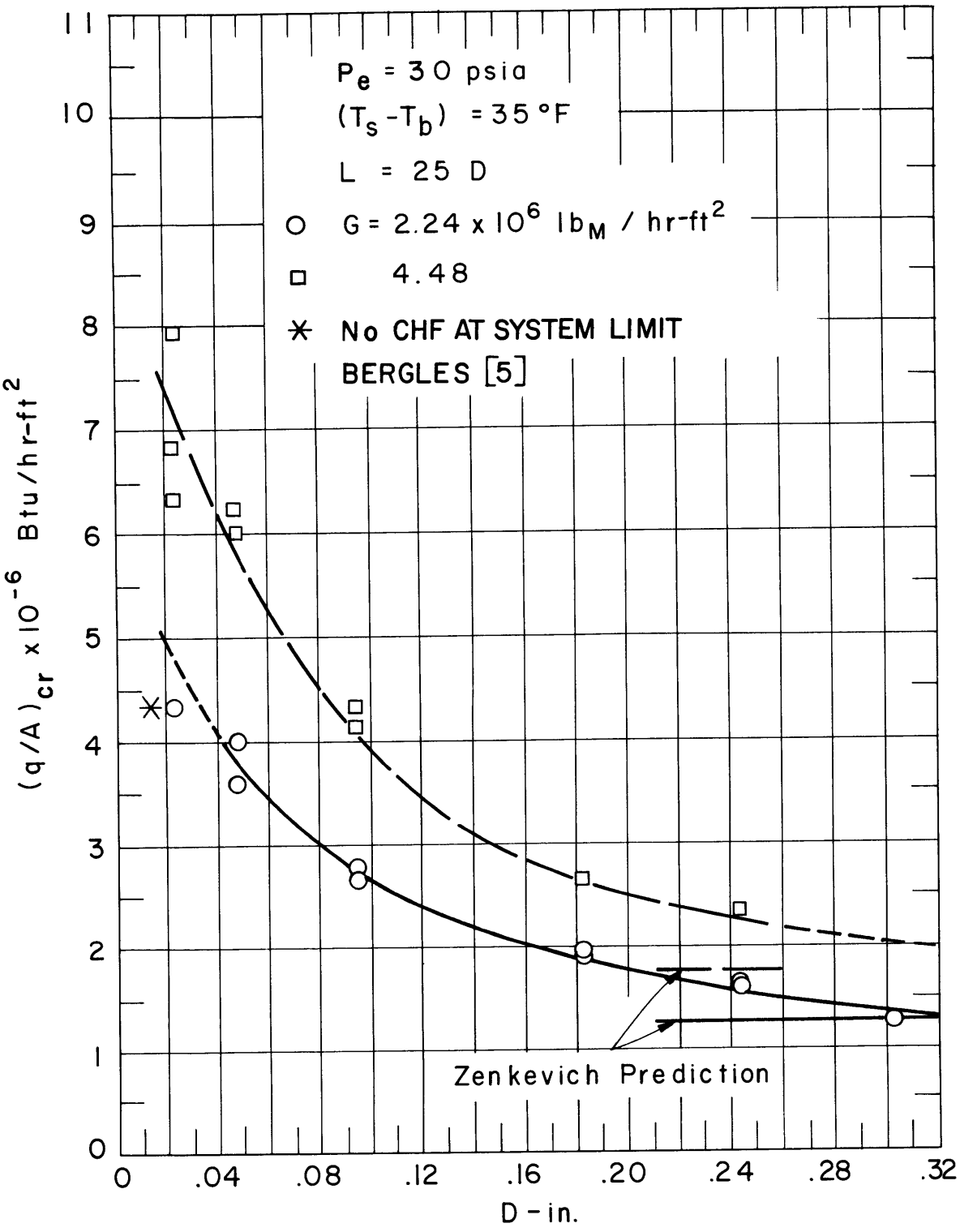

FIG. 5 EFFECT OF TUBE DIAMETER ON CHF

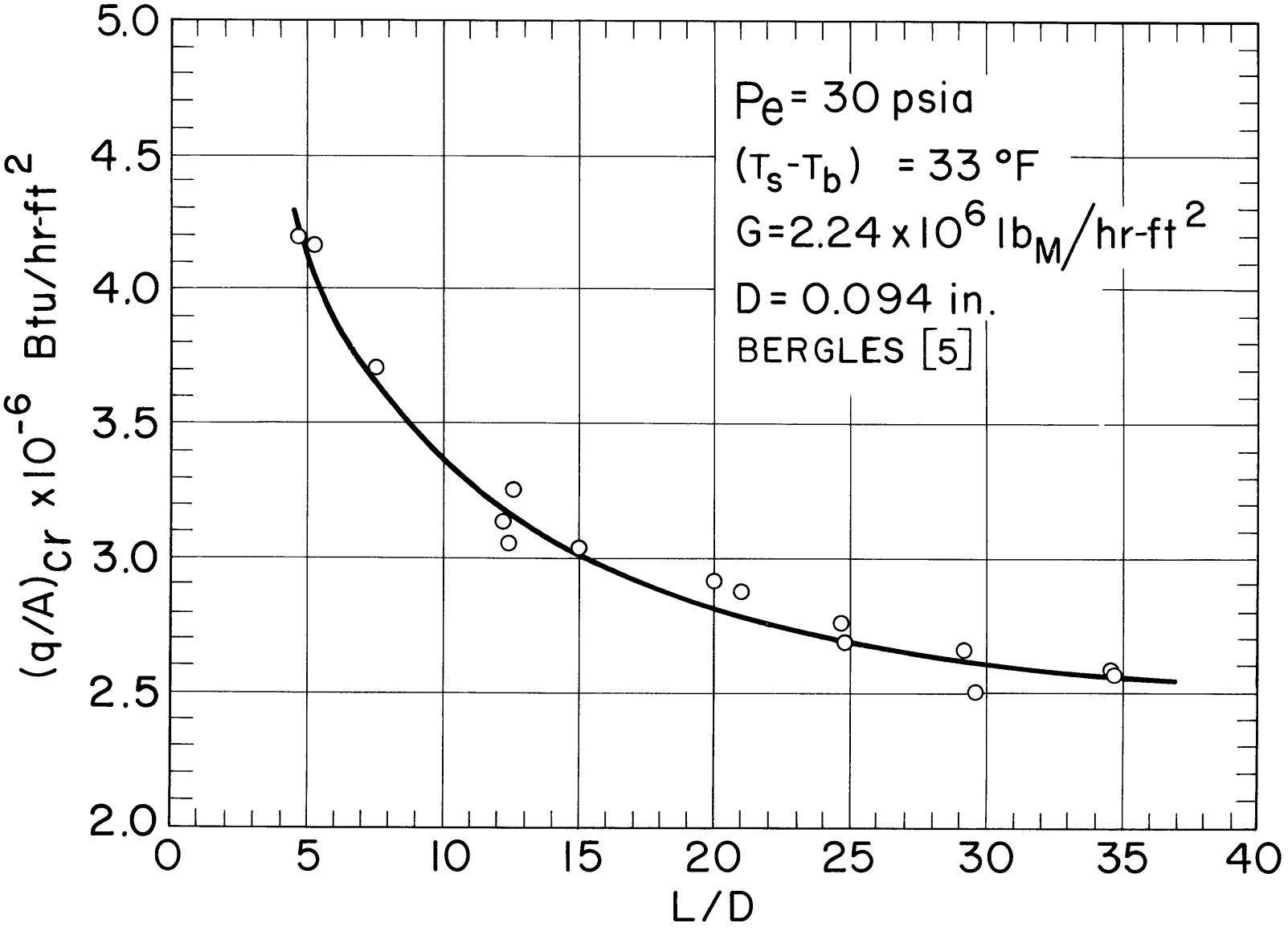

FIG. 6 EFFECT OF HEATED LENGTH ON CHF

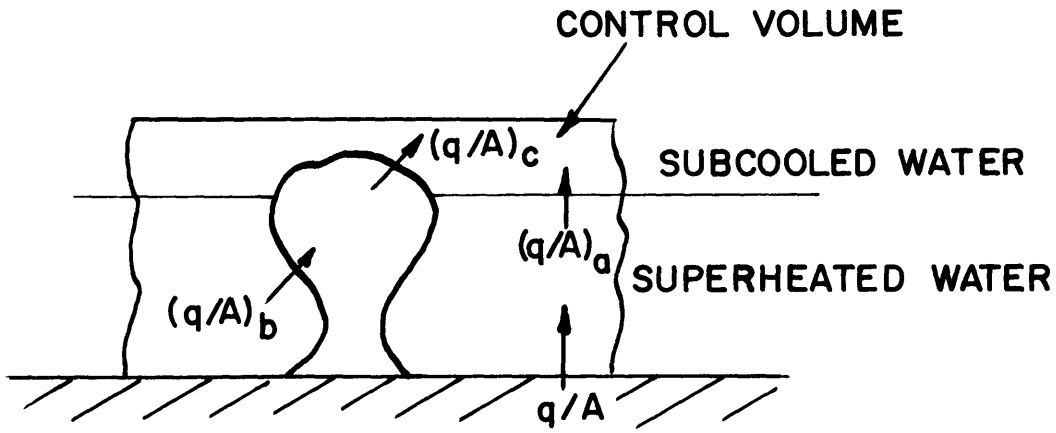

$$(q/A)_1 = (q/A)_b - (q/A)_c$$

$$(q/A)_2 = (q/A)_a + (q/A)_c$$

$$(q/A)_{cr} = (q/A)_1 + (q/A)_2$$

$$= C_1 \rho_v H_{fg} v_v^* + C_2 C_1 \rho_1 \Delta T_{sub} v_1^*$$

$$= \text{Latent Heat} + \text{Sensible Heat}$$

C_1, C_s = Constants

v_v^*, v_1^* = Critical Vapor and Liquid Velocities, Respectively

FIG. 7 SIMPLIFIED SCHEMATIC OF CHANG'S CHF MODEL

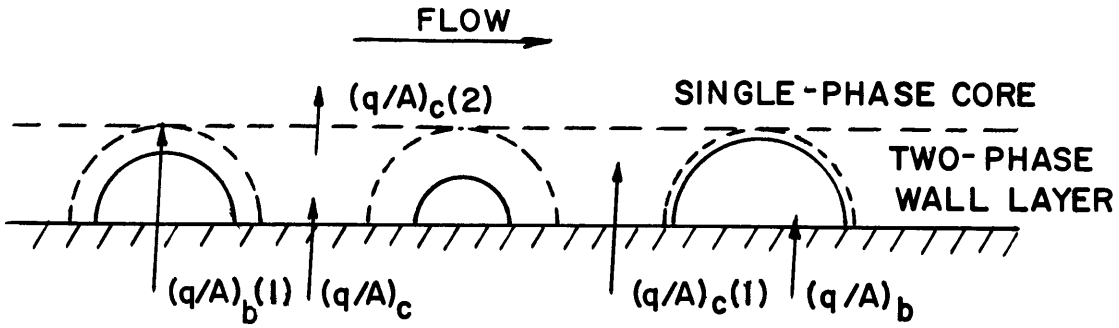

$(q/A)_c(2)$ (the convective heat flux from the outer portion of the two phase wall layer to the turbulent core) = $(q/A)_b(1)$ (the heat flux due to vaporization of liquid at the inner portion of the wall layer and condensation at the outer portion) + $(q/A)_c(1)$ (the convective heat transport through the liquid between the bubbles) = $(q/A)_b$ (the heat flux from the surface beneath the bubbles) + $(q/A)_c$ (the convective heat flux from the surface between the bubbles at any instant)

FIG. 8 BANKOFF'S SEQUENTIAL RATE PROCESS MODEL OF CHF

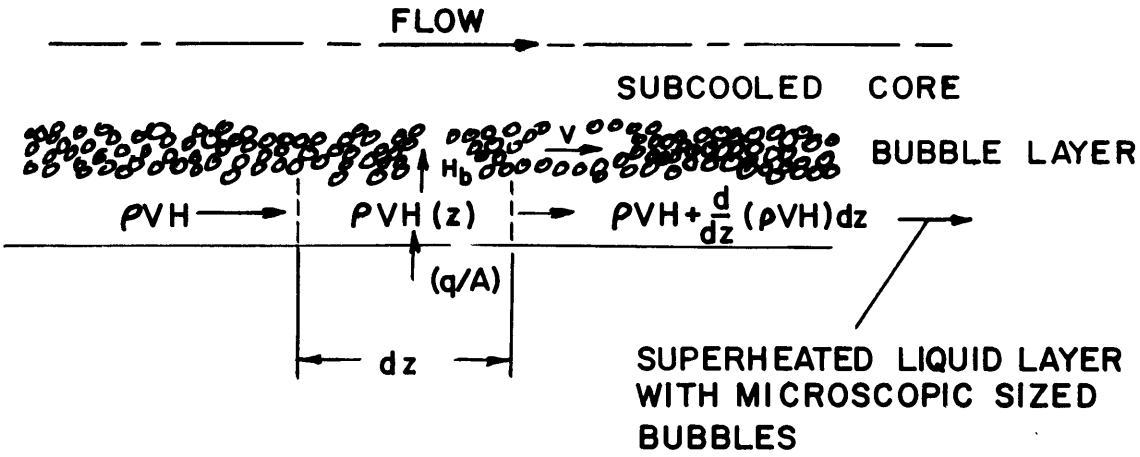

The superheat of the superheated layer and the local heat flux determine the temperature of the wall and thus critical heat flux conditions.

FIG. 9 TONG'S MODEL OF CHF UNDER SUBCOOLED CONDITIONS

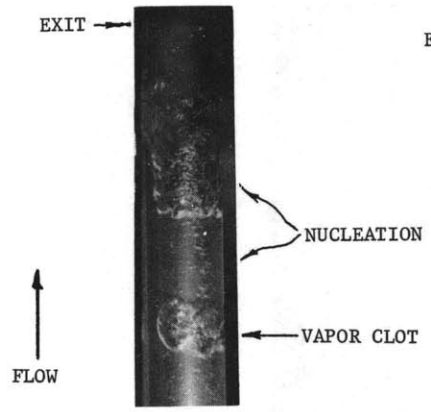

PHOTO I

$q/A = 0.4 \times 10^6$ lbm/hr-ft^2

G = 0.405 x 10^6 Btu/hr-ft^2

P = 21 psia

ΔH_{sub} = 64 Btu/lbm

SLUG FLOW

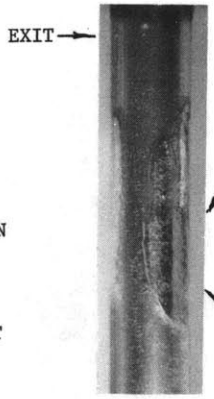

PHOTO II

$q/A = 0.458 \times 10^6$ Btu/hr-ft^2

G = 0.4 x 10^6 lbm/hr-ft^2

P = 21.5 psia

ΔH_{sub} = 54.15 Btu/lbm

SLUG FLOW

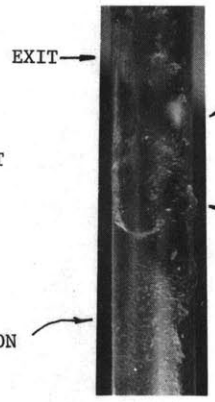

PHOTO III

$q/A = 0.546 \times 10^6$ Btu/hr-ft^2

G = 0.4 x 10^6 lbm/hr-ft^2

P = 21.5 psia

ΔH_{sub} = 45.52 Btu/lbm

CHF CONDITION

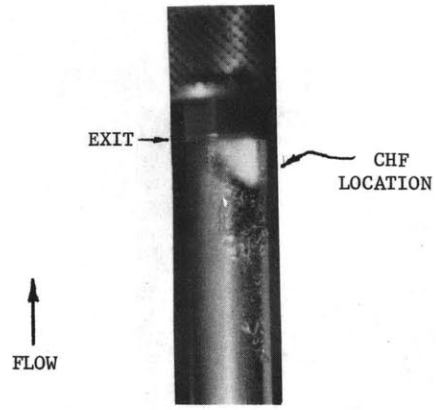

PHOTO IV

$q/A = 0.89 \times 10^6$ Btu/hr-ft^2

G = 0.7 x 10^6 lbm/hr-ft^2

P = 34 psia

ΔH_{sub} = 69 Btu/lbm

CHF CONDITION

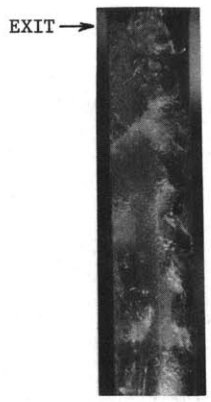

PHOTO V

$q/A = 1.35 \times 10^6$ Btu/hr-ft^2

G = 1.1 x 10^6 lbm/hr-ft^2

P = 44 psia

ΔH_{sub} = 92 Btu/lbm

98 PERCENT OF CHF

FIG. 10 PHOTOGRAPHS OF THE FLOW STRUCTURE

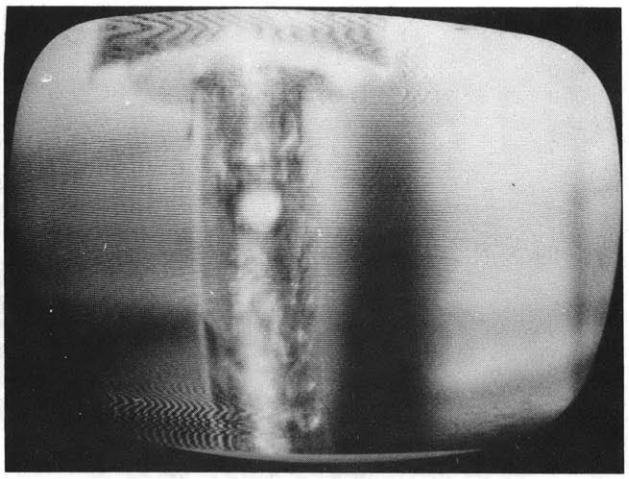

PHOTO VI

$q/A = 1.626 \times 10^6$ Btu/hr-ft^2

$G = 1. \times 10^6$ lbm/hr-ft^2

$P = 67$ psia

$\Delta H_{sub} = 85.9$ Btu/lbm

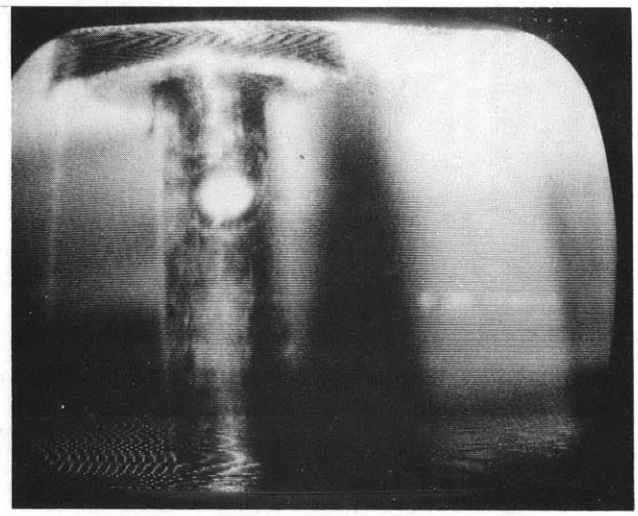

PHOTO VII

Same Conditions Approximately

.1 Sec Later

FIG. 11 CHF AS VIEWED ON VIDEO TAPE

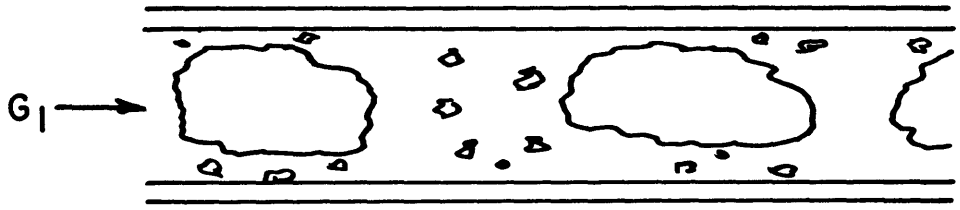

SLUG FLOW

FROTH FLOW

$$G_1 < \sim 2.5 \times 10^6 \text{ lbm/hr-ft}^2 < G_2$$

$$P_1 = P_2$$

$$\Delta H_{sub_1} = \Delta H_{sub_2}$$

FIG. 12 ILLUSTRATION OF SLUG AND FROTH FLOW

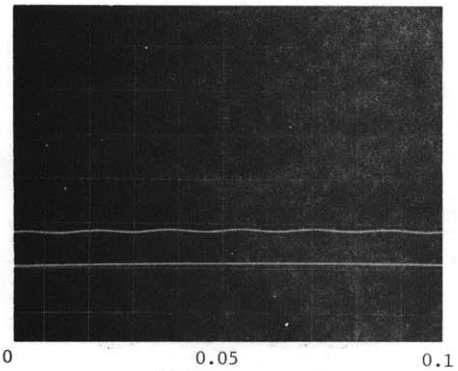

PHOTO I

FORCED CONVECTION WATER
ZERO POWER

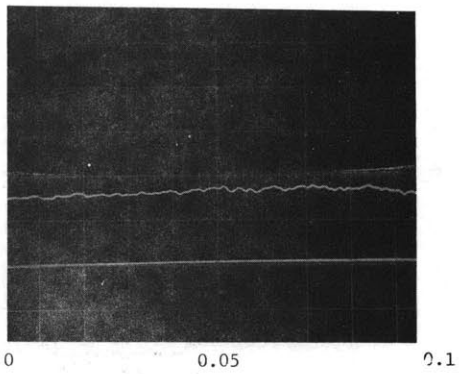

PHOTO II

P ~ 45 psia, G = 1.5 x 10^6 lbm/hr-ft^2
T_{in} = 60 °F, X = -13.4 %

BUBBLY FLOW

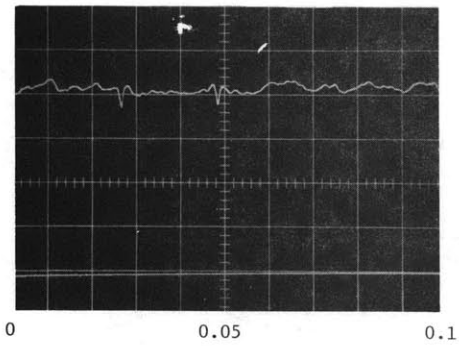

PHOTO III

P ~ 88, G = 1.0 x 10^6, T_{in} = 69, X = -10.4

BUBBLY TO SLUG TRANSITION

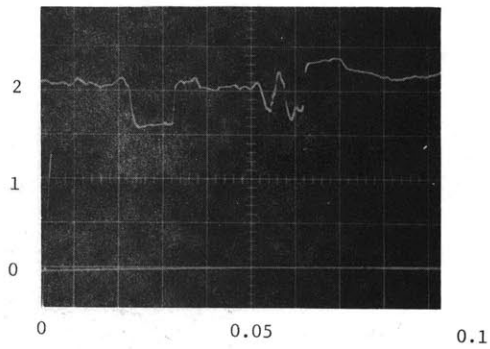

PHOTO IV

P ~ 76, G = 1.0 x 10^6, T_{in} = 71, X = -7.13

SLUG FLOW

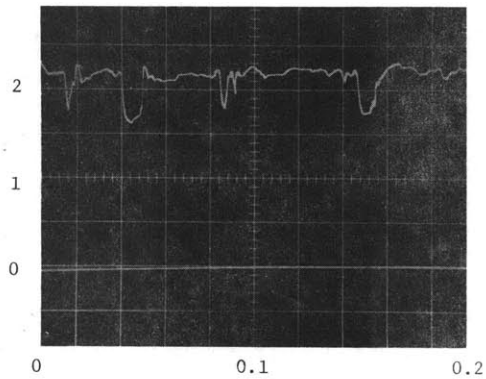

PHOTO V

P ~ 82, G = 1.0 x 10^6, T_{in} = 71, X = -7.49

SLUG FLOW

FIG. 13 FLOW REGIMES OBSERVED BY THE ELECTRICAL RESISTANCE PROBE

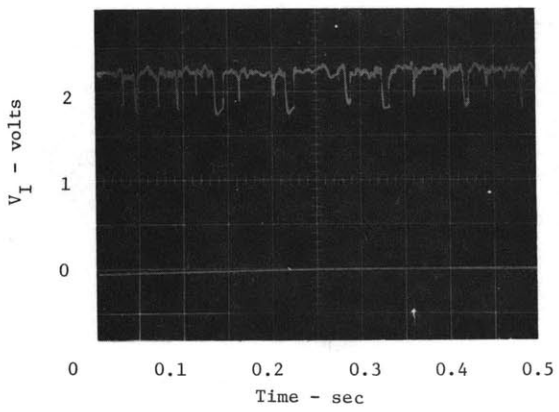

PHOTO VI

P = 91, G = 1.0×10^6, T_{in} = 71, X = -8.62

SLUG FLOW

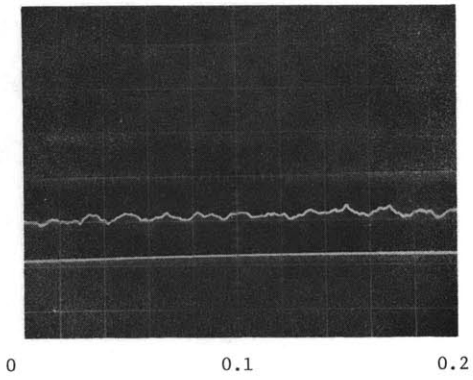

PHOTO VII

P = 45, G = 3.4×10^6, T_{in} = 62, X = -18.7

BUBBLY FLOW

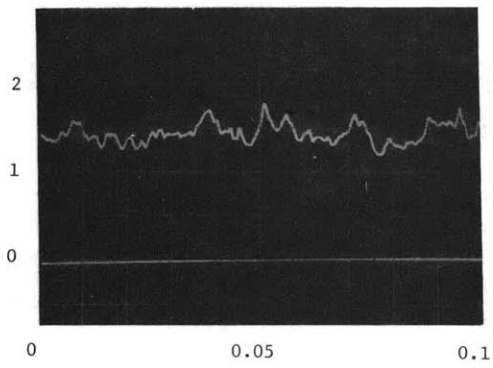

PHOTO VIII

P = 53, G = 3.4×10^6, T_{in} = 78, X = -10.3

FROTH FLOW

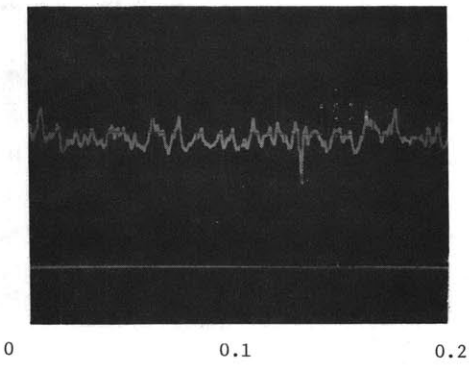

PHOTO IX

P = 53, G = 3.4×10^6, T_{in} = 82, X = -9.94

FIG. 14 FLOW REGIMES OBSERVED BY THE ELECTRICAL RESISTANCE PROBE

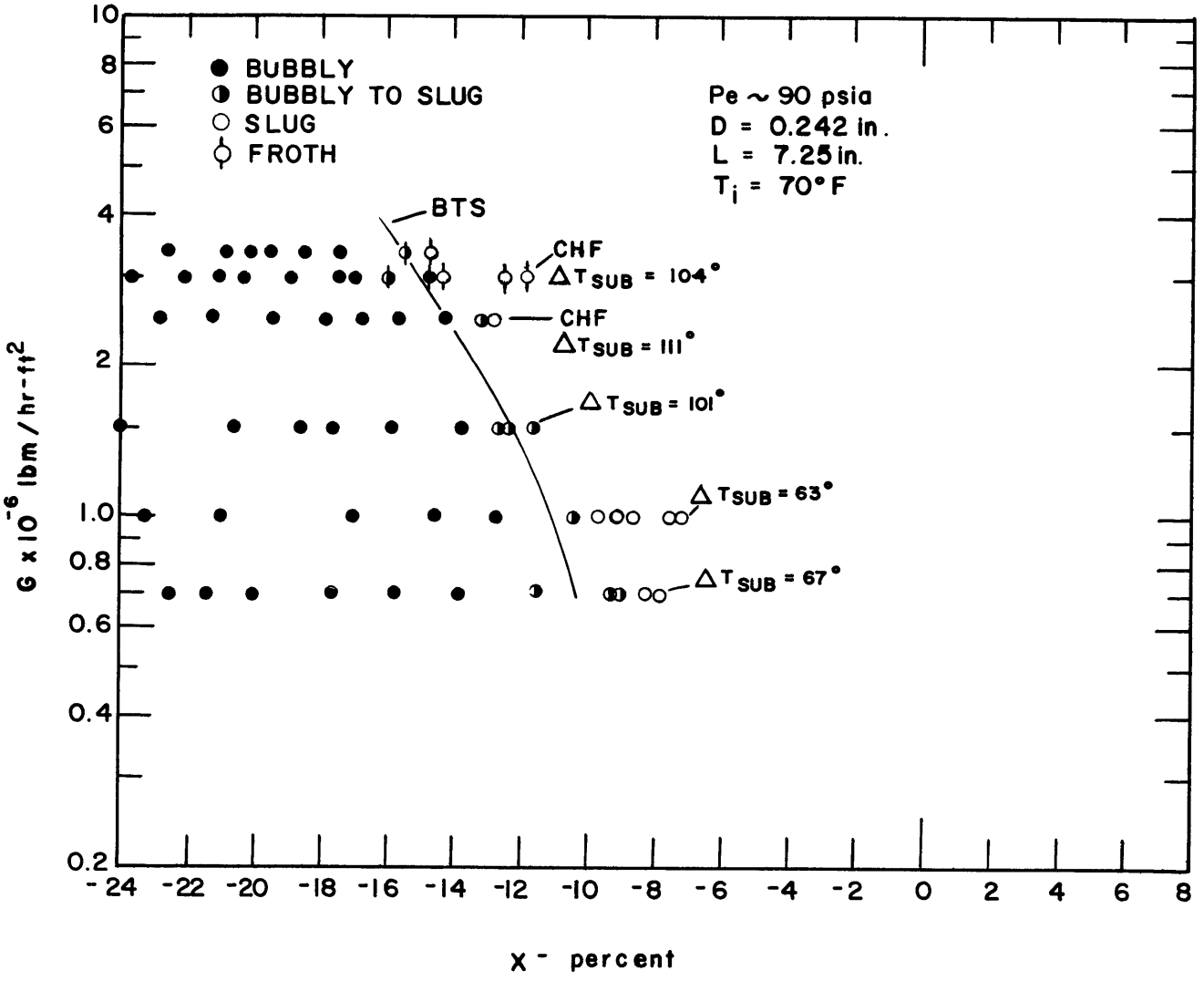

FIG. 15 FLOW REGIME MAP - HIGH PRESSURE, T_{in} = 70°F

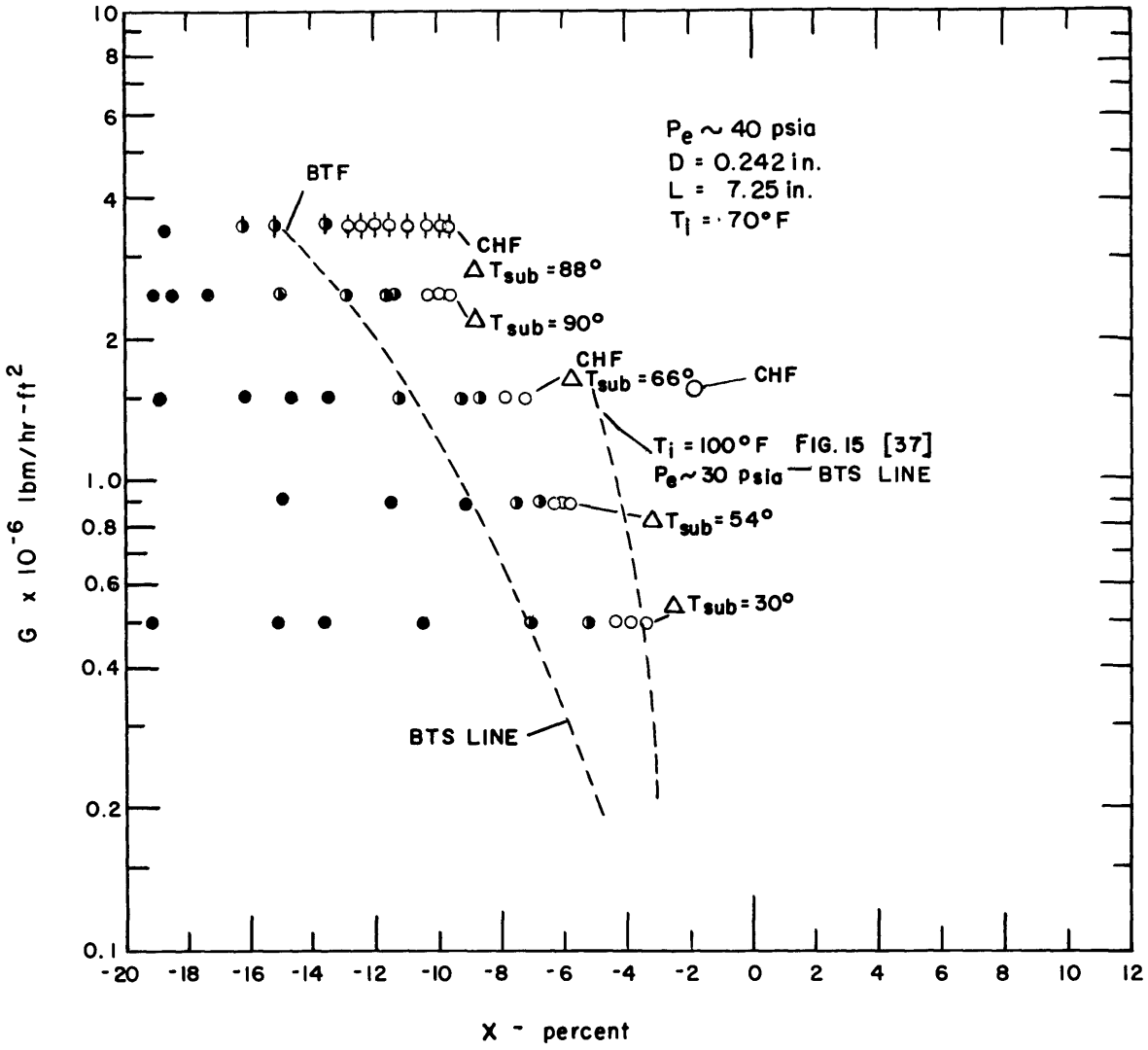

FIG. 16 FLOW REGIME MAP - LOW PRESSURE, T_{in} = 70°F

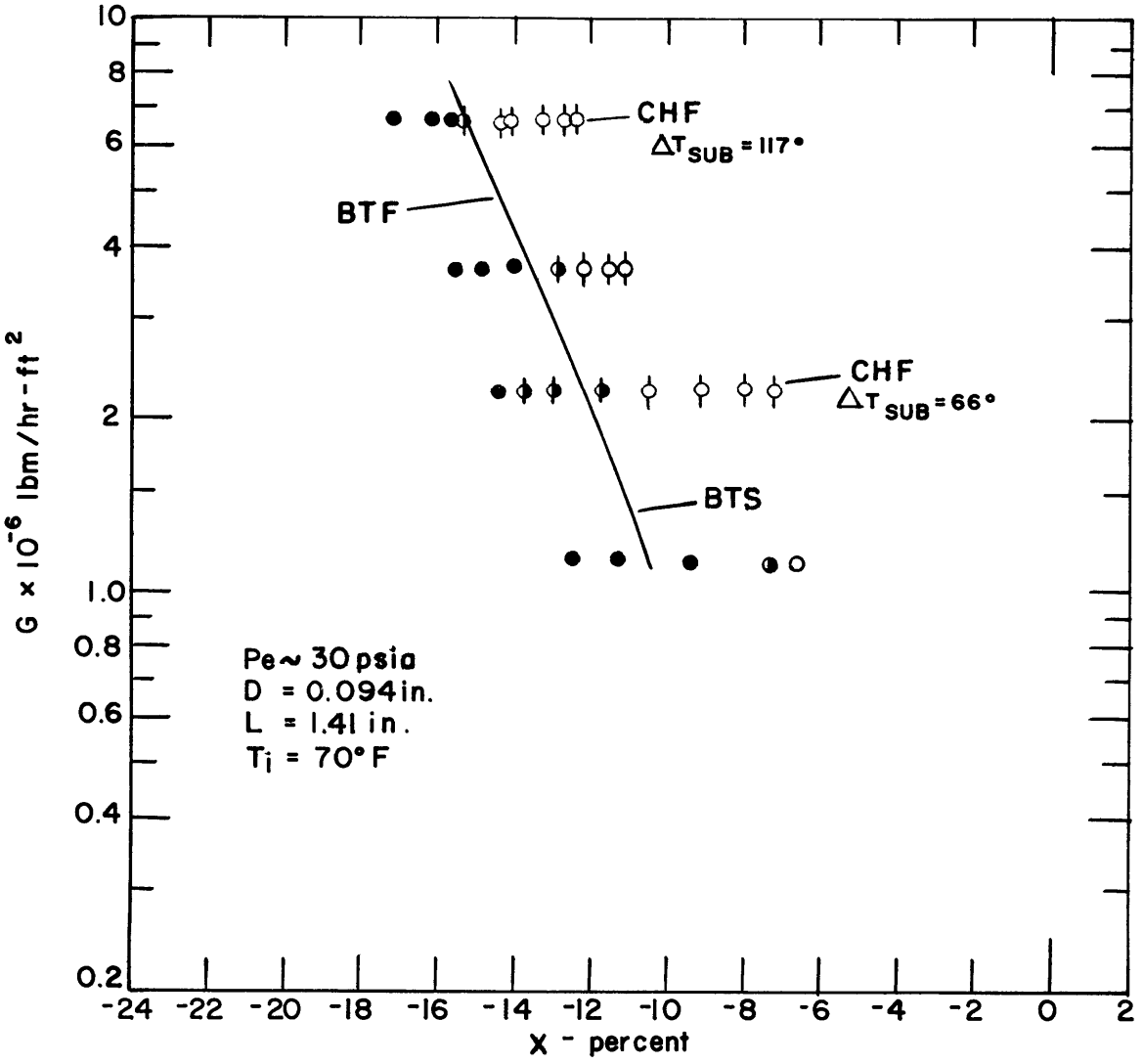

FIG. 17 FLOW REGIME MAP - L/D = 15

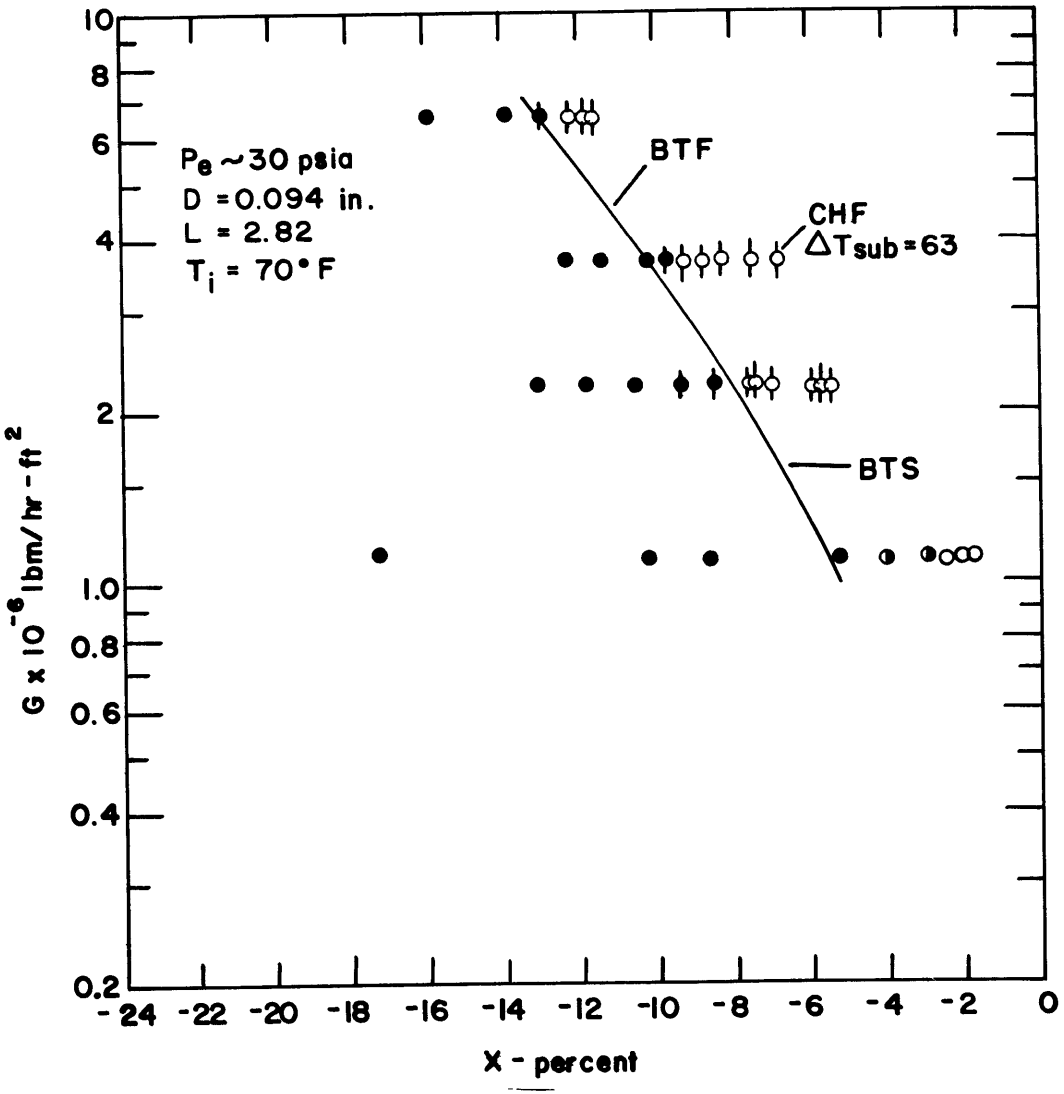

FIG. 18 FLOW REGIME MAP - L/D = 30

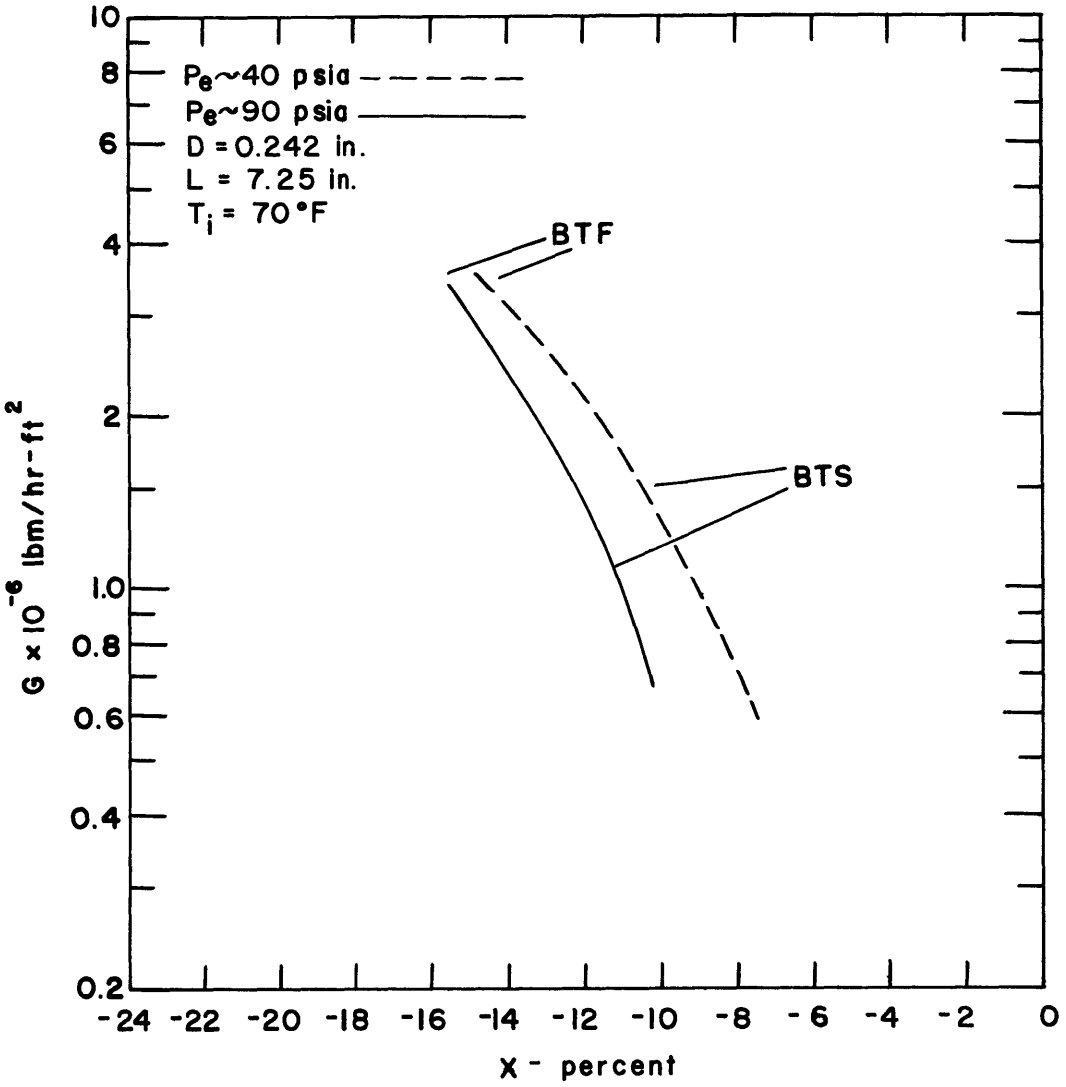

FIG. 19 EFFECT OF PRESSURE ON THE FLOW REGIME BOUNDARIES

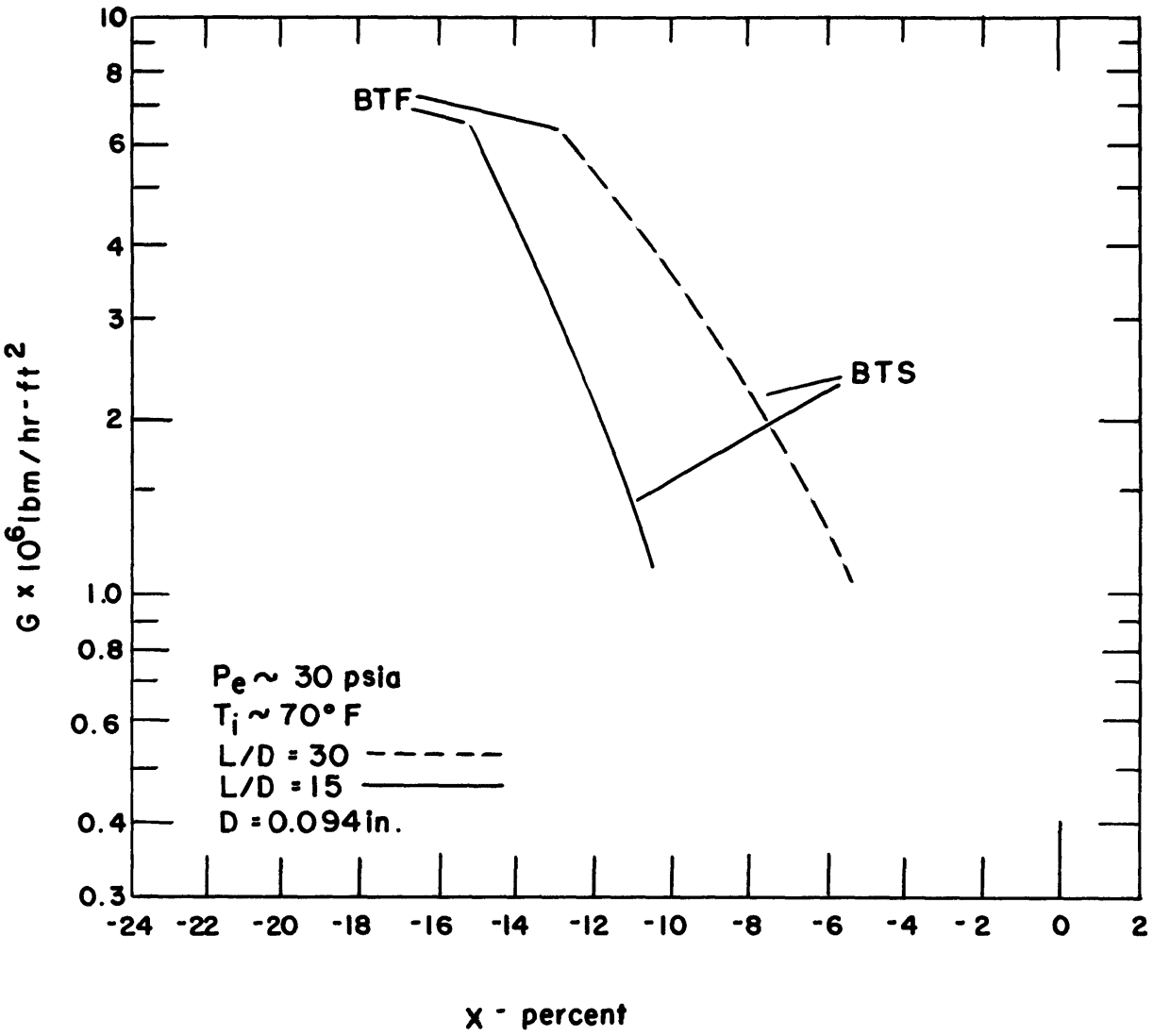

FIG. 20 EFFECT OF LENGTH ON THE FLOW REGIME BOUNDARIES

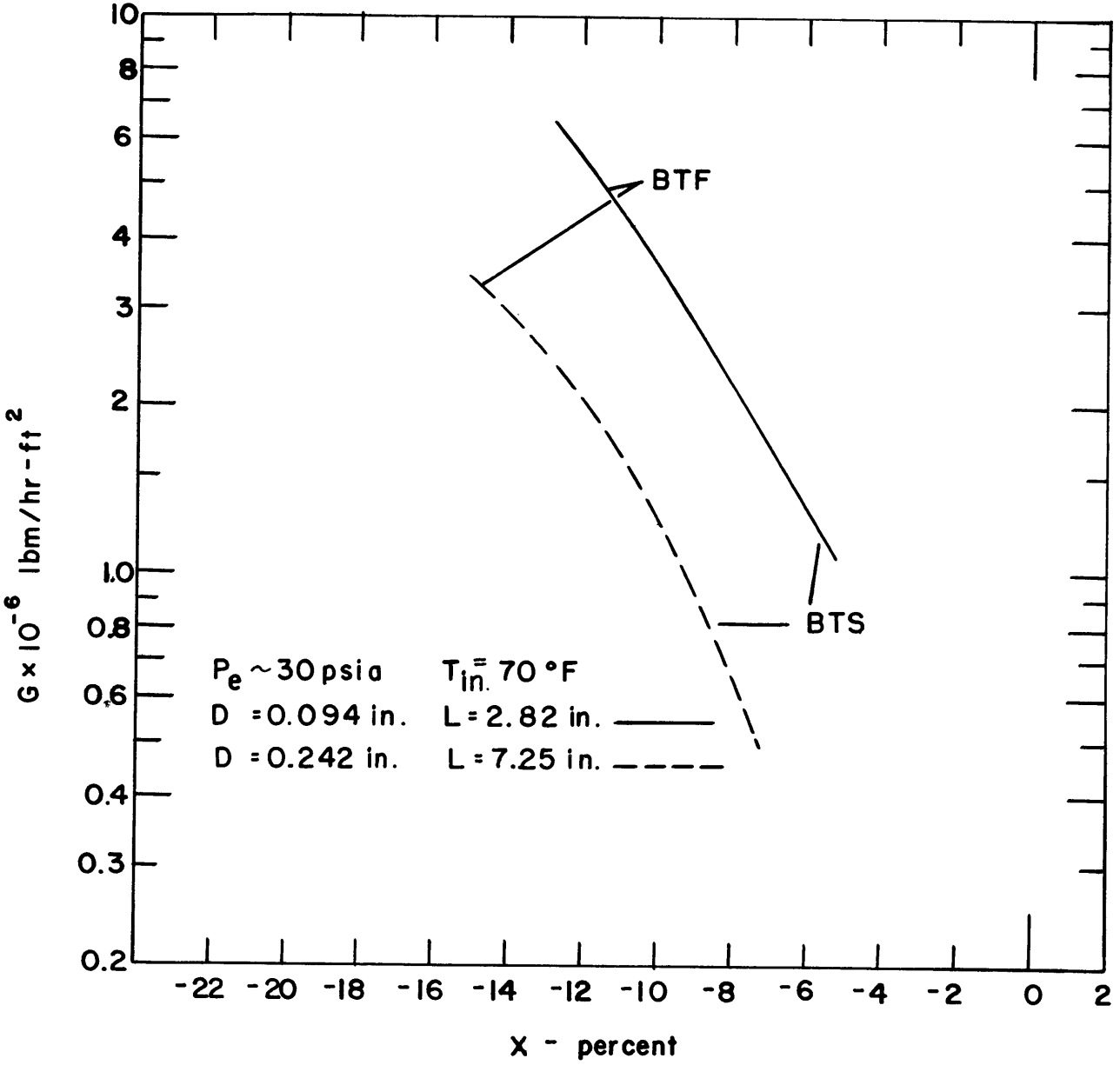

FIG. 21 EFFECT OF DIAMETER ON THE FLOW REGIME BOUNDARIES

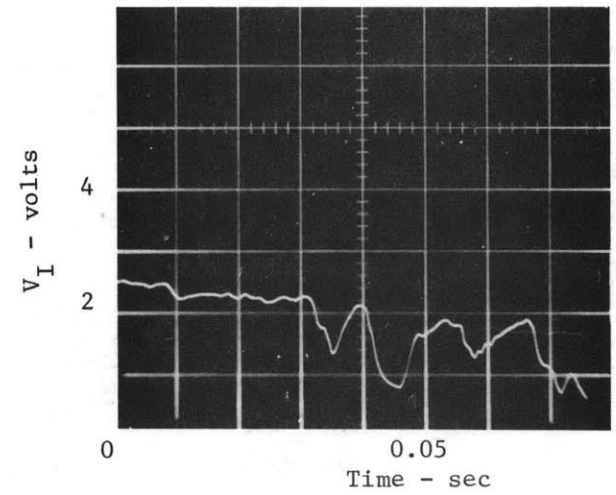

PHOTO I

Slug Flow

Probe 0.011 in. from wall

P = 60 psia
G = 1.25×10^6 lbm/hr-ft^2
T_{in} = 96 °F
X = -12.4 %

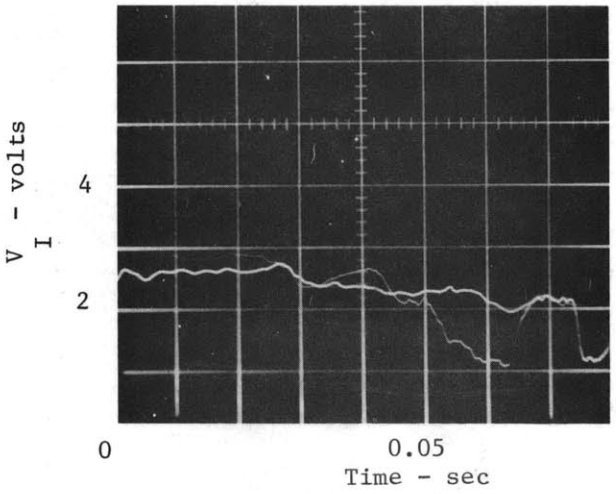

PHOTO II

Slug Flow

Probe 0.0015 in.

from wall

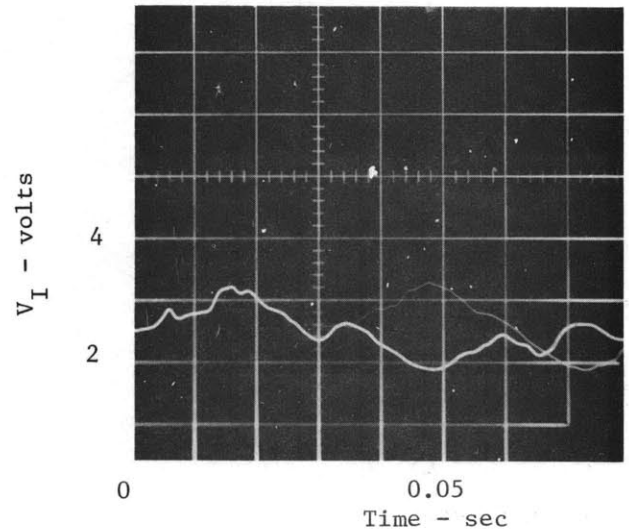

PHOTO III

Bubbly Flow

Probe 0.001 in.

from wall at CHF

X = -12.36 %

FIG. 22 EXAMINATION OF FLOW STRUCTURE IN SUPERHEATED LIQUID FILM

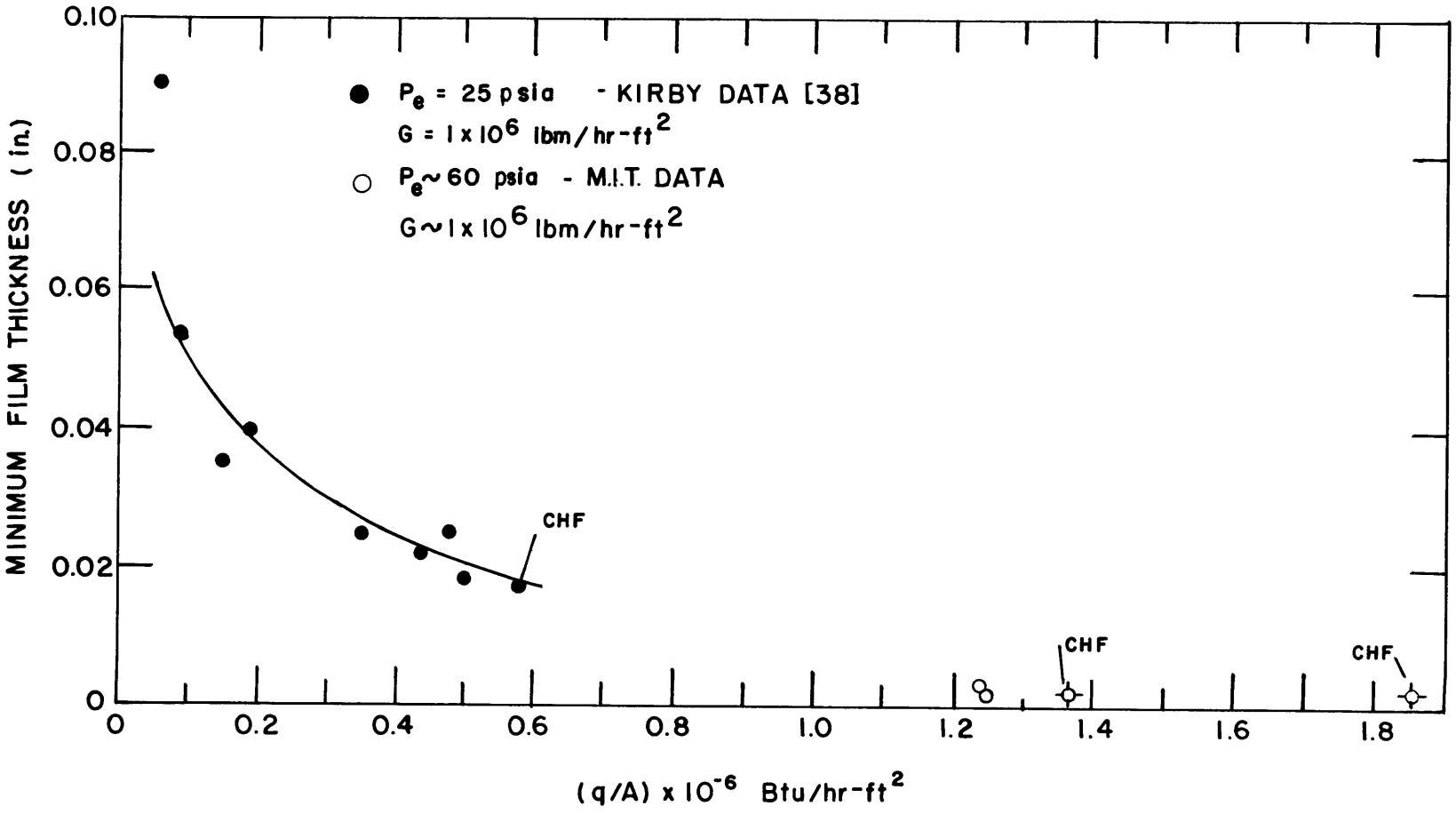

FIG. 23 CRITICAL FILM THICKNESS VERSUS HEAT FLUX

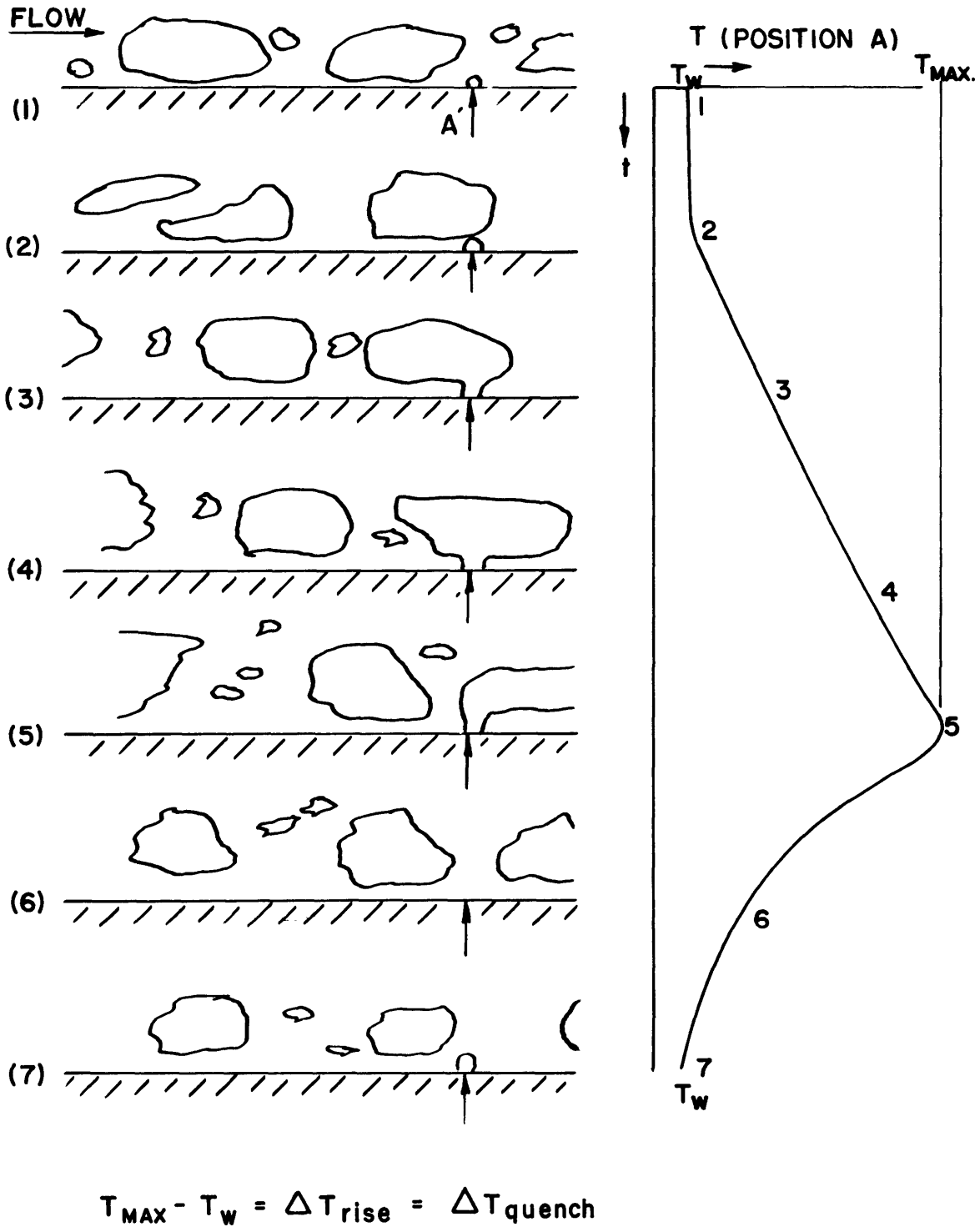

FIG. 24 SCHEMATIC RELATING FLOW MODEL AND SURFACE TEMPERATURE VARIATION

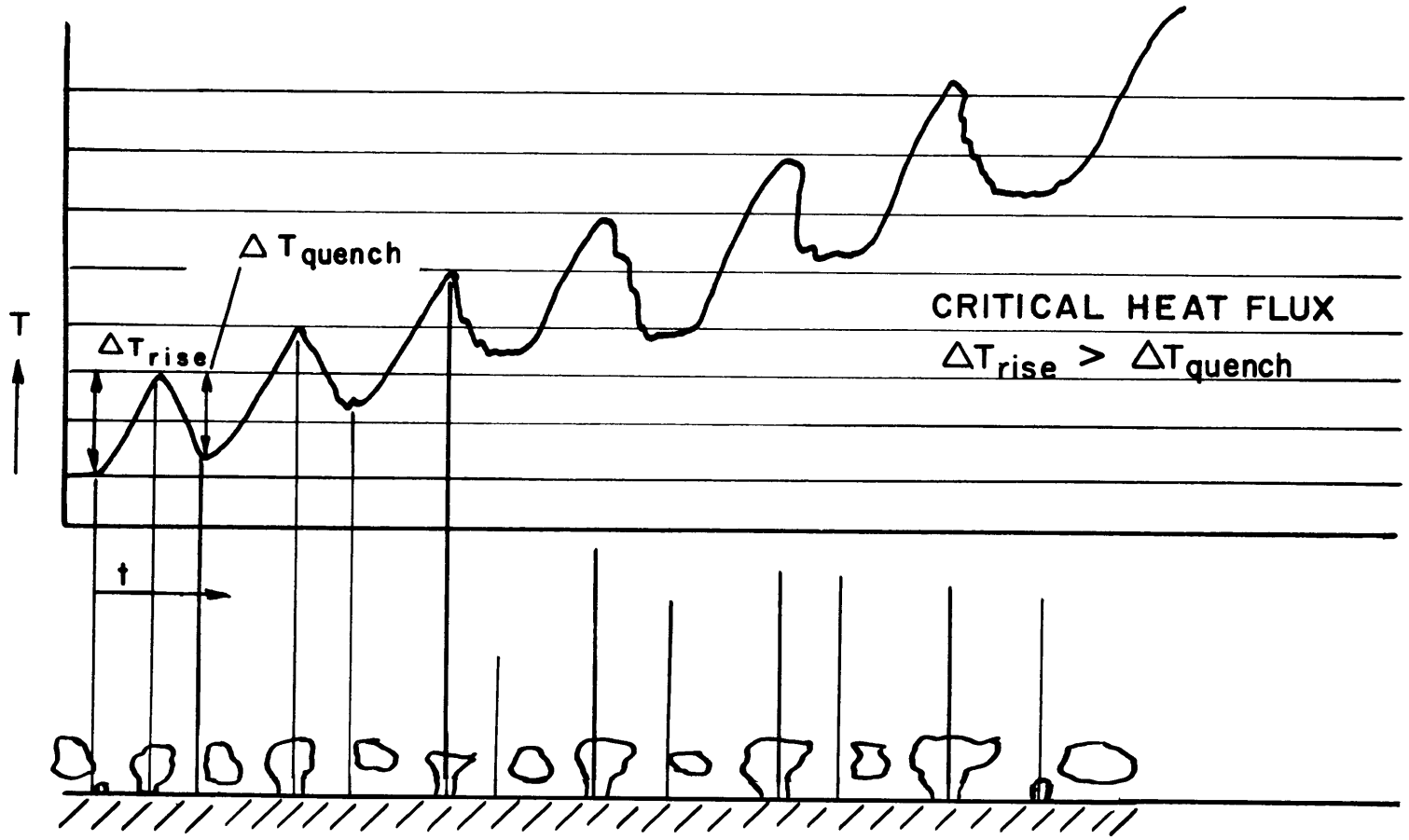

FIG. 25 ILLUSTRATION OF CHF PHENOMENON

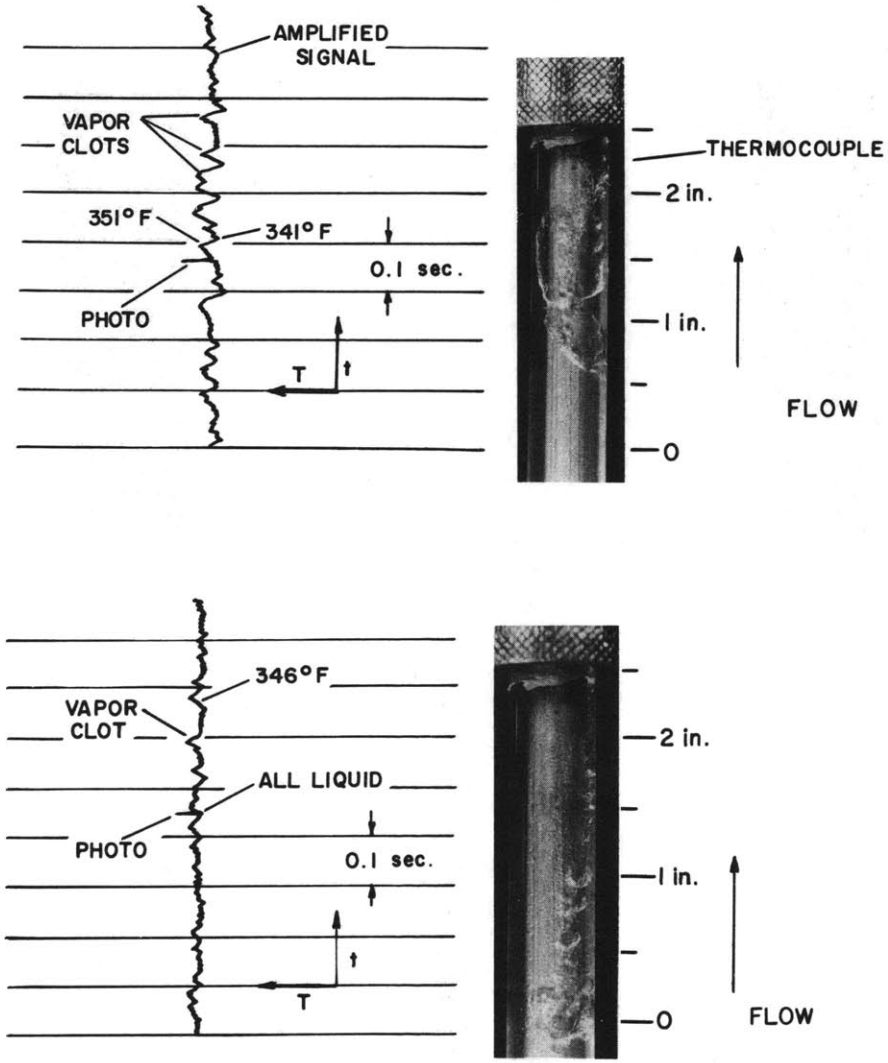

FIG. 26 MICROFLASH PHOTOS WITH SIMULTANEOUS TEMPERATURE TRACES

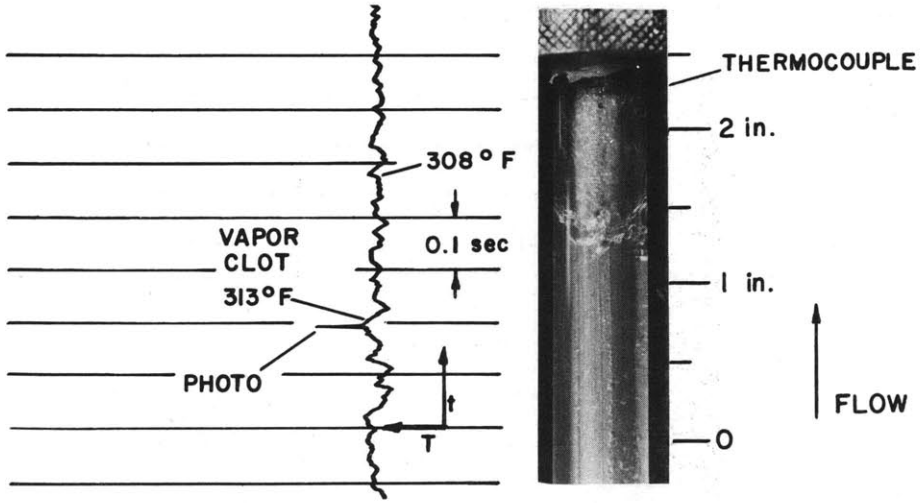

PHOTO III

$q/A = 0.936 \times 10^6$ Btu/hr-ft^2

$G = 0.59 \times 10^6$ lbm/hr-ft^2

P = 32 psia

$\triangle T_{sub}$ = 88 ° F

PHOTO IV

$q/A = 0.96 \times 10^6$ Btu/hr-ft^2

$G = 0.59 \times 10^6$ lbm/hr-ft^2

P = 30 psia

$\triangle T_{sub}$ = 62°F

PHOTO V

$q/A = 1 \times 10^6$ Btu/hr-ft^2

$G = 0.59 \times 10^6$ lbm/hr-ft^2

P = 30 psia

$\triangle T_{sub}$ = 56 °F

FIG. 27 MICROFLASH PHOTOS WITH SIMULTANEOUS TEMPERATURE TRACES

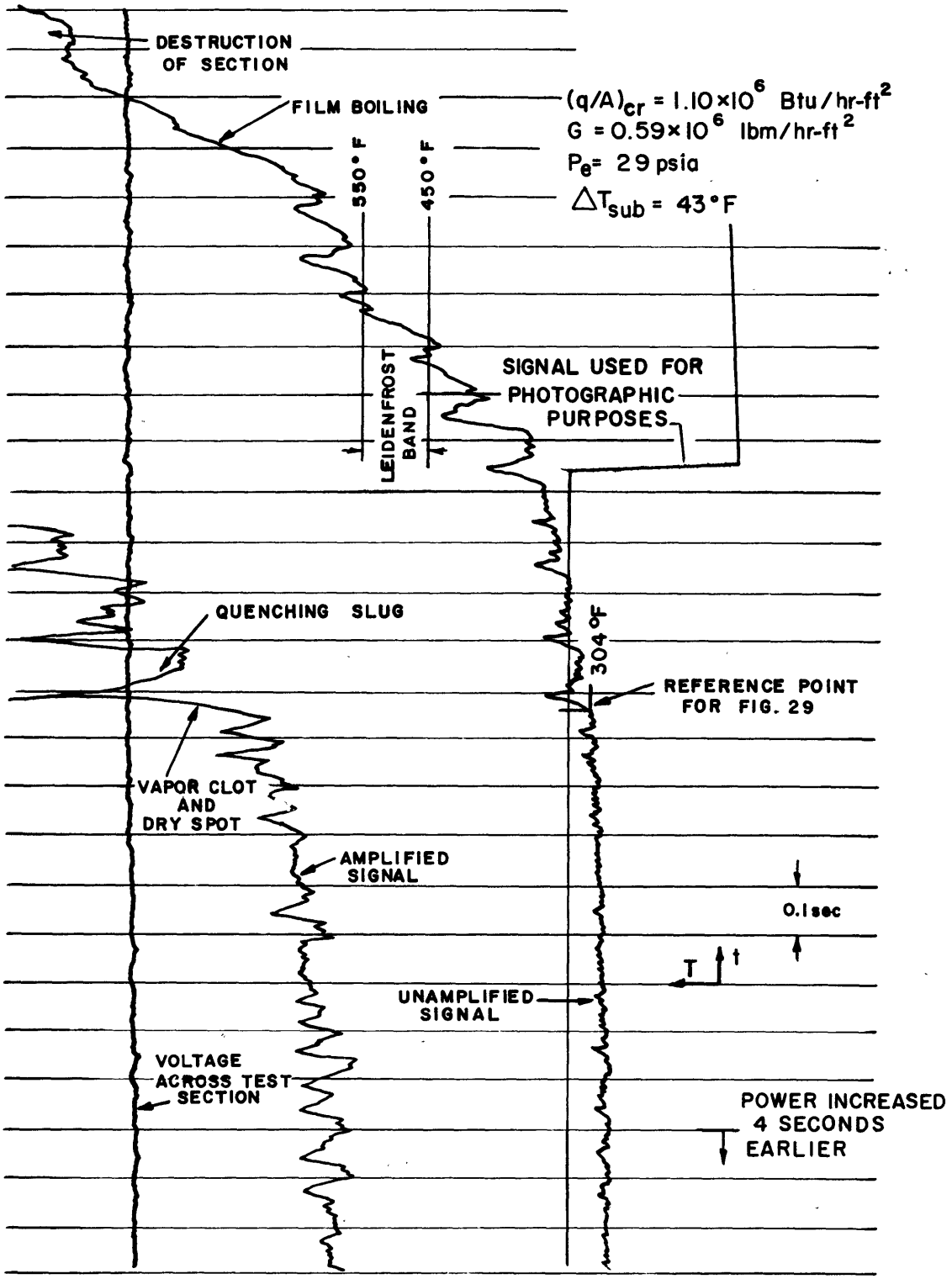

FIG. 28 SURFACE TEMPERATURE TRACE AT CHF (TEST P-12)

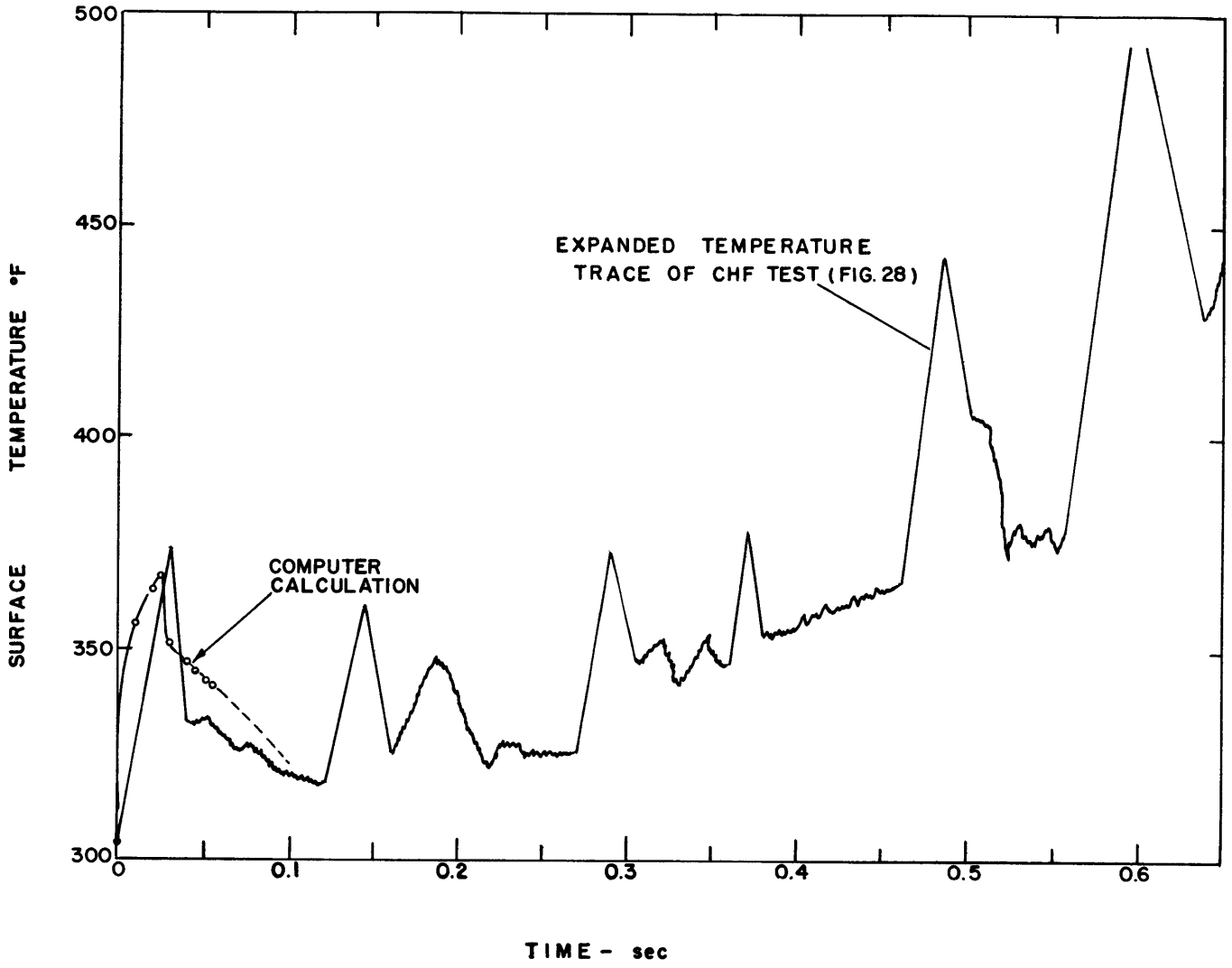

FIG. 29 EXPANDED SCALE SHOWING SURFACE TEMPERATURE VARIATION AT CHF (TEST P-12)

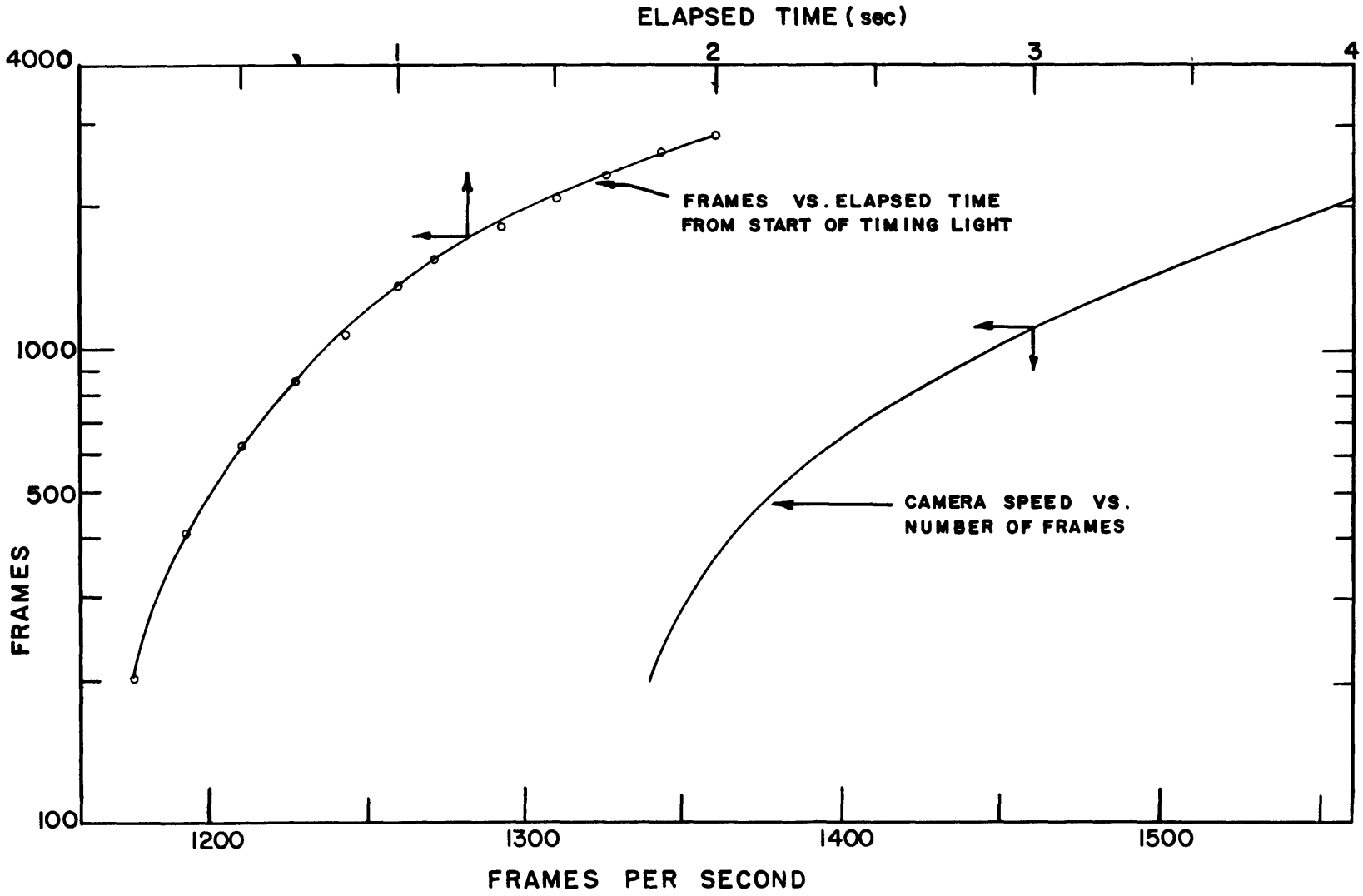

FIG. 30 CAMERA SPEED AND NUMBER OF FILM FRAMES AS A FUNCTION OF ELAPSED TIME

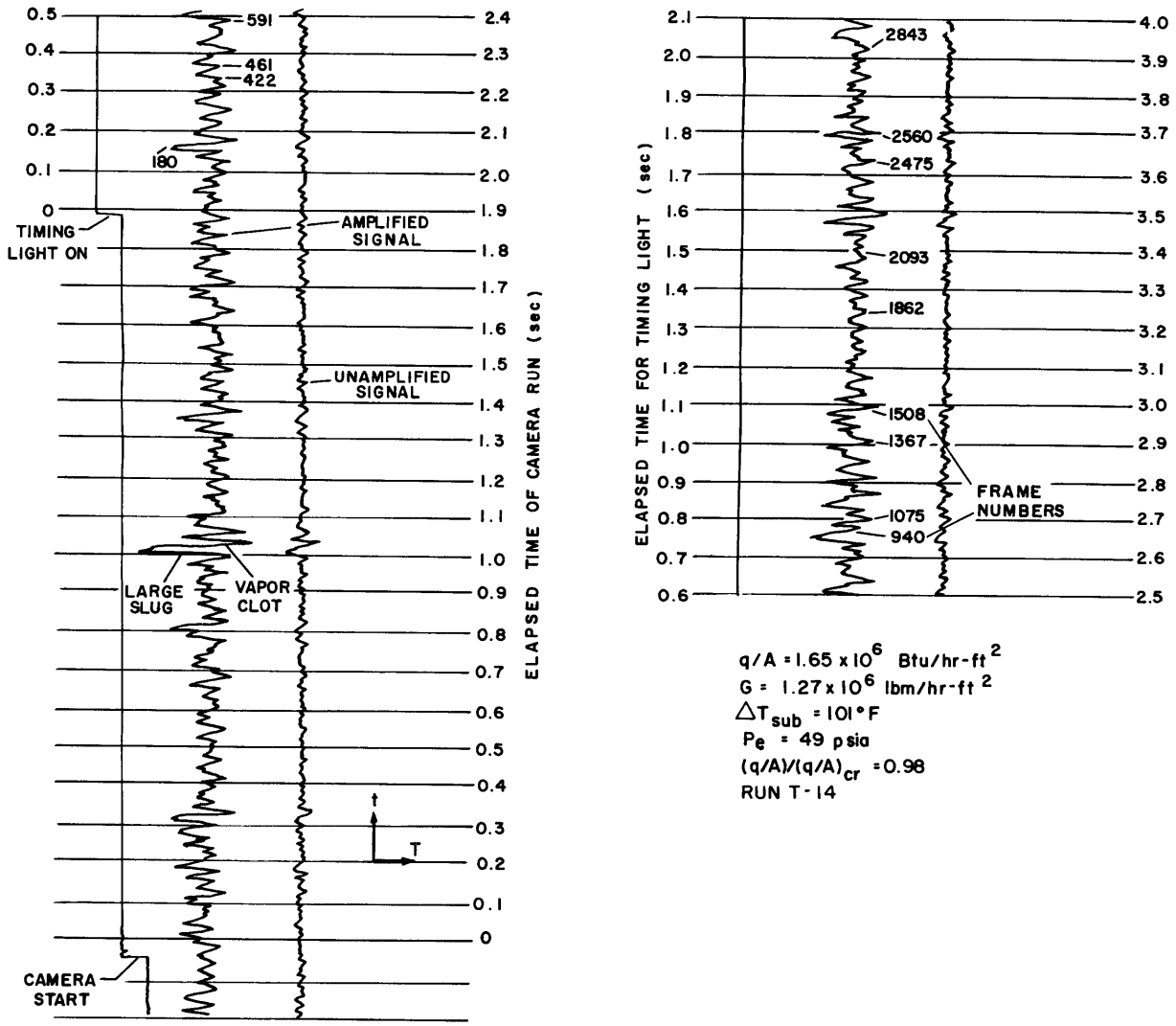

FIG. 31 WALL TEMPERATURE TRACE FOR MOVIE RUN

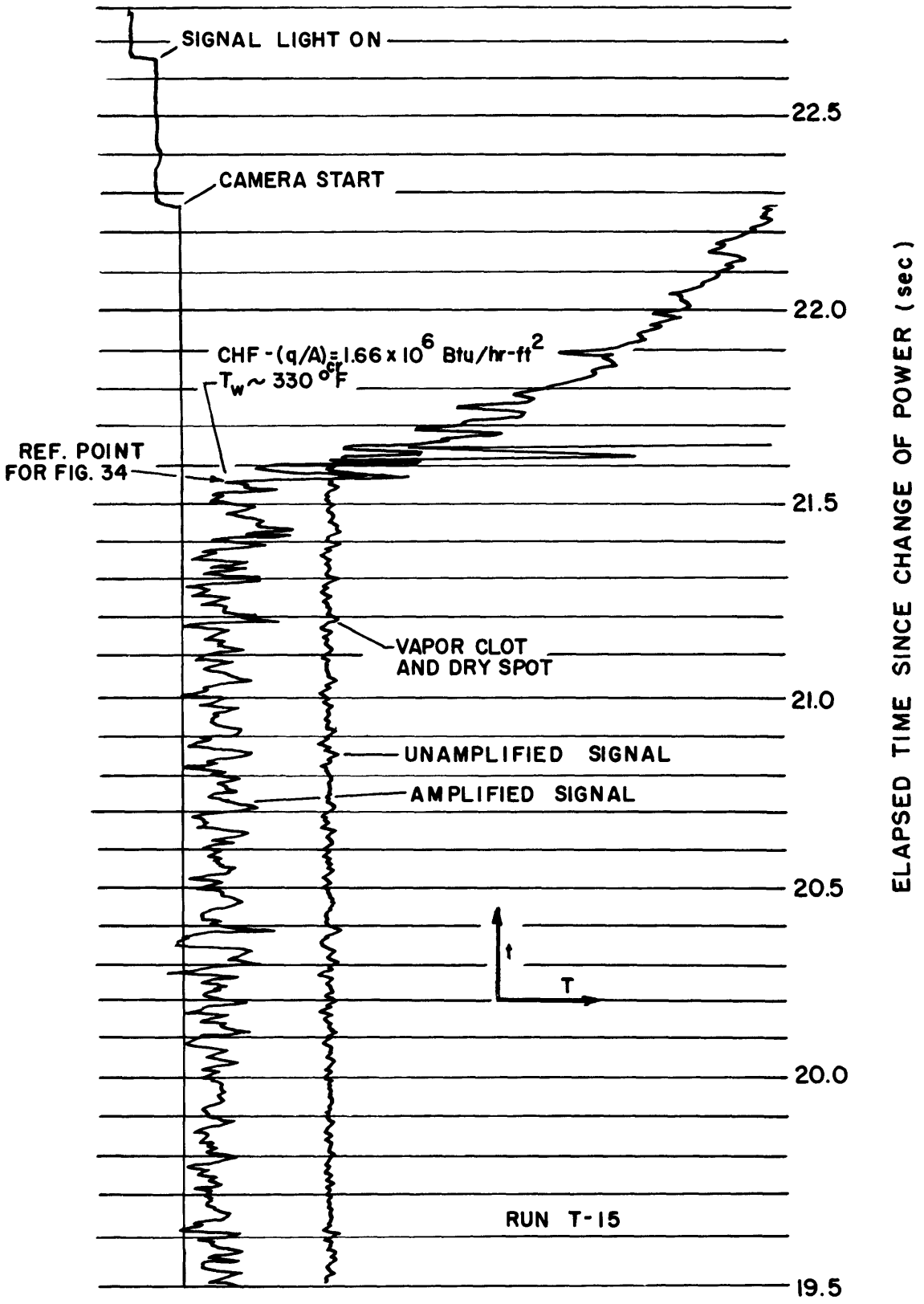

FIG. 32 WALL TEMPERATURE TRACE AT CHF DURING MOVIE RUN

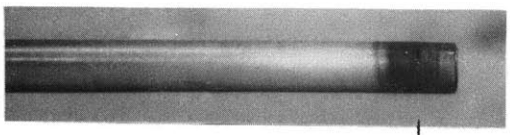

PIN-HOLE

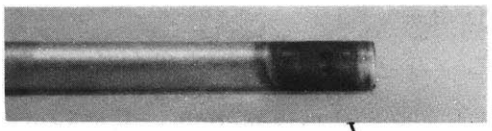

TWO PIN-HOLES

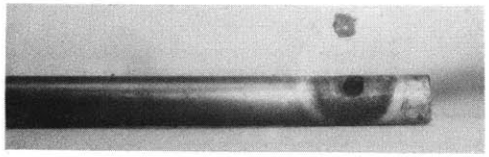

NOTE PIN-HOLE IN
METAL BLOWN OUT

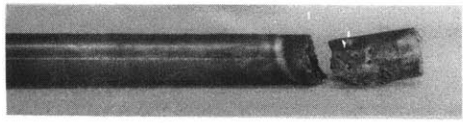

PIN-HOLES IN
FRACTURED TEST SECTION

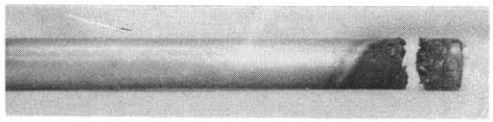

FRACTURED TEST SECTION

FIG. 33 PIN-HOLES OBSERVED IN DESTROYED TEST SECTIONS

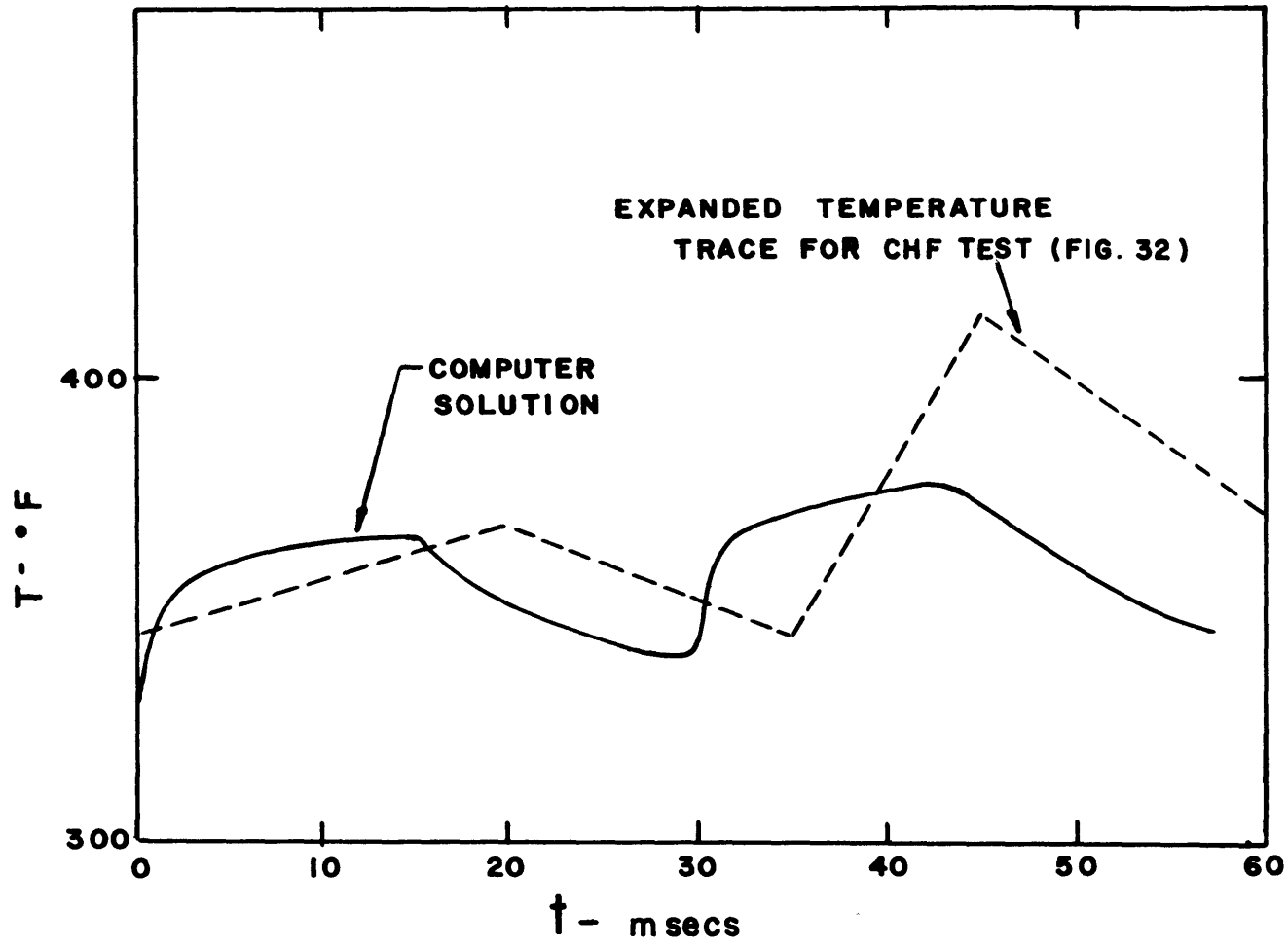

FIG. 34 CALCULATED TEMPERATURE VARIATION AT CHF DURING MOVIE RUN

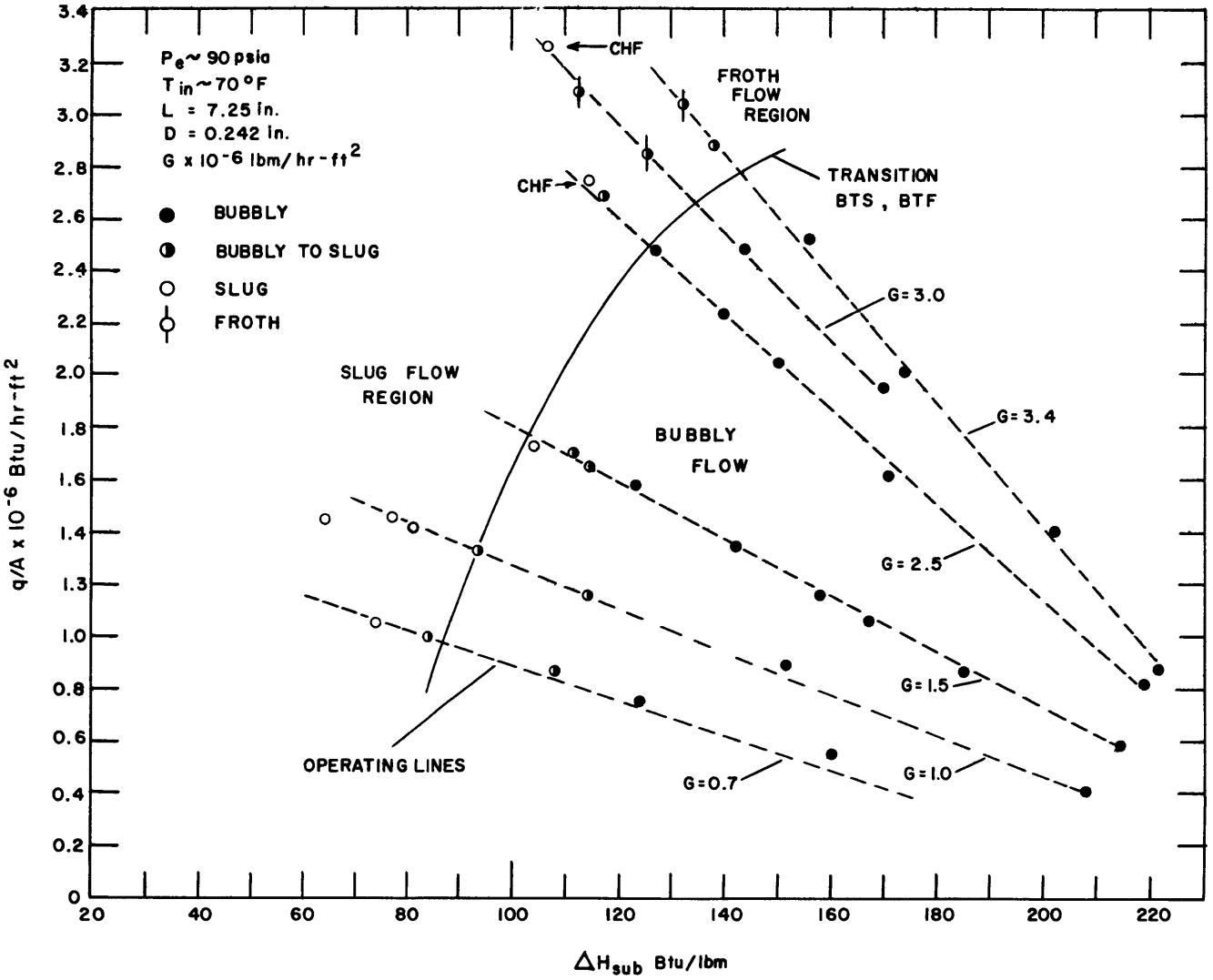

FIG. 35 FLOW REGIME BOUNDARIES ON HEAT FLUX VERSUS SUBCOOLING COORDINATES

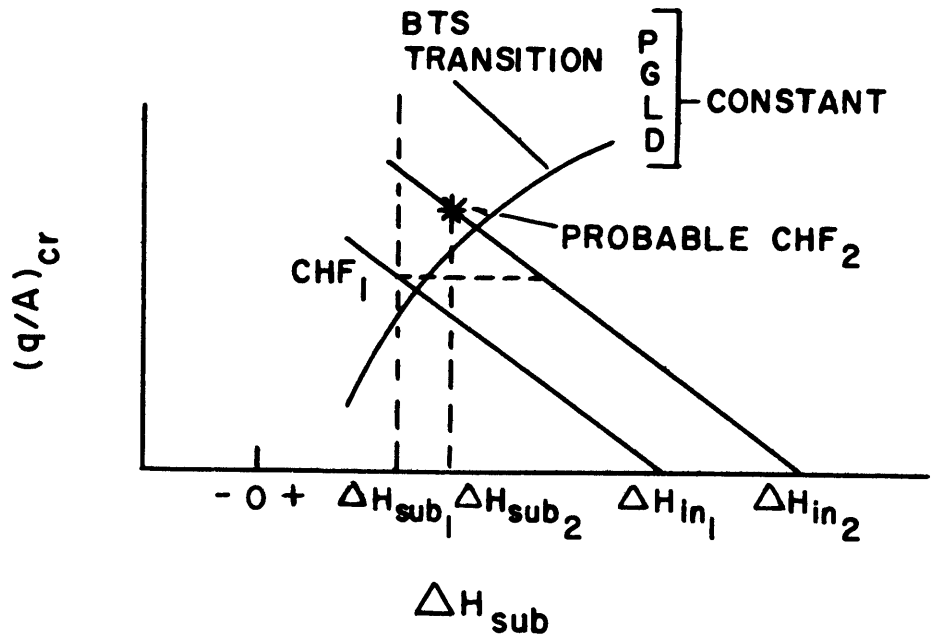

FIG. 36 SUBCOOLING EFFECT ON CHF AS RELATED TO FLOW REGIME BOUNDARY

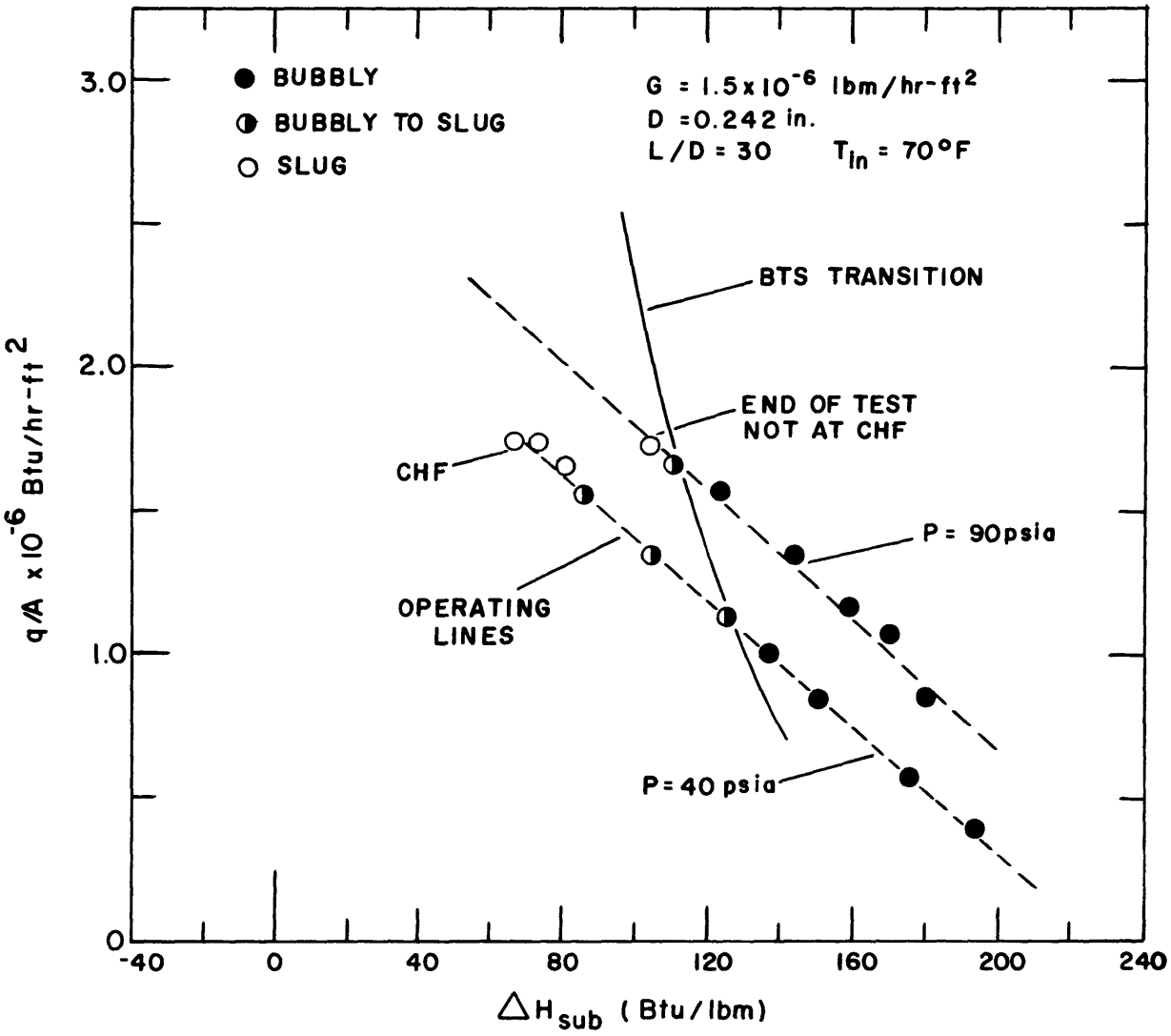

FIG. 37 HEAT FLUX VERSUS SUBCOOLING SHOWING PRESSURE EFFECT

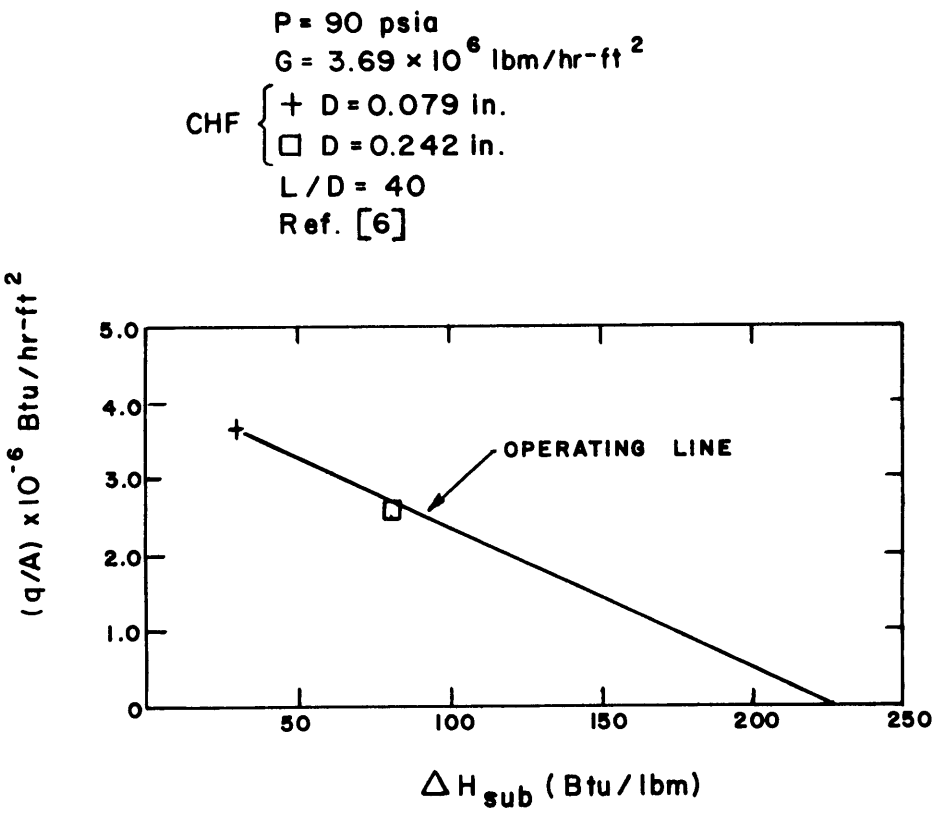

FIG. 38 DIAMETER EFFECT ON CHF

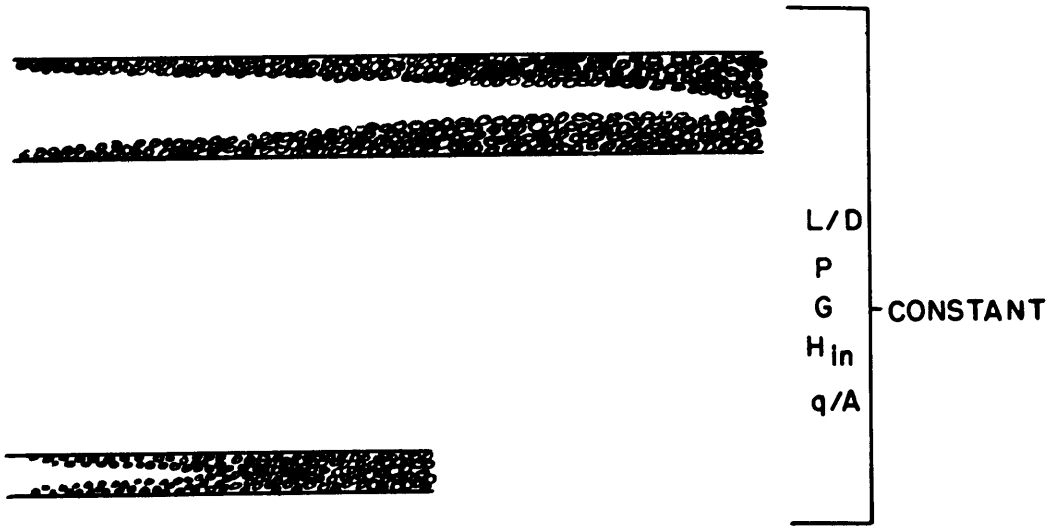

FIG. 39 DIAMETER EFFECT ON VOID FRACTIONS

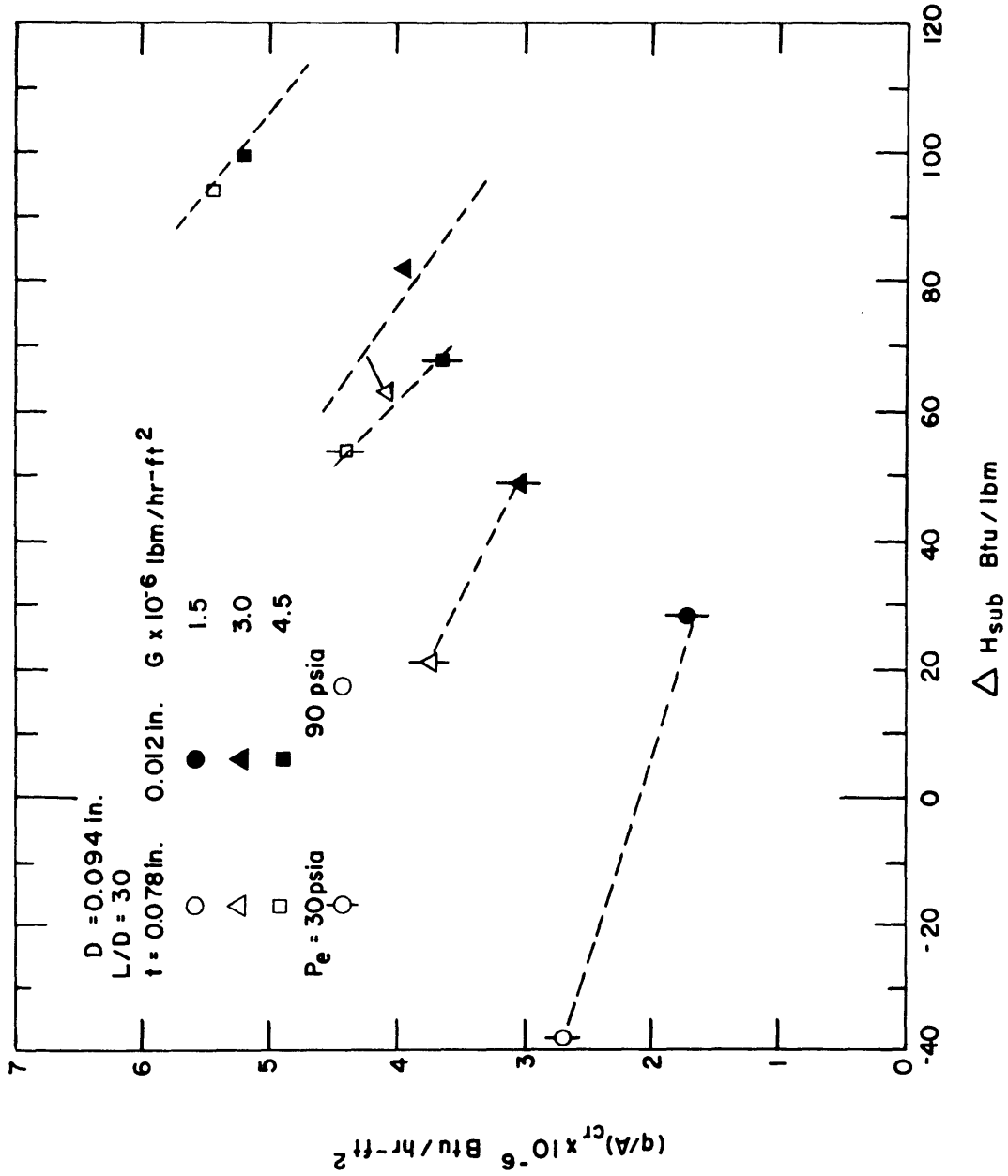

FIG. 40 EXPERIMENTAL RESULTS OF WALL THICKNESS EFFECTS ON CHF

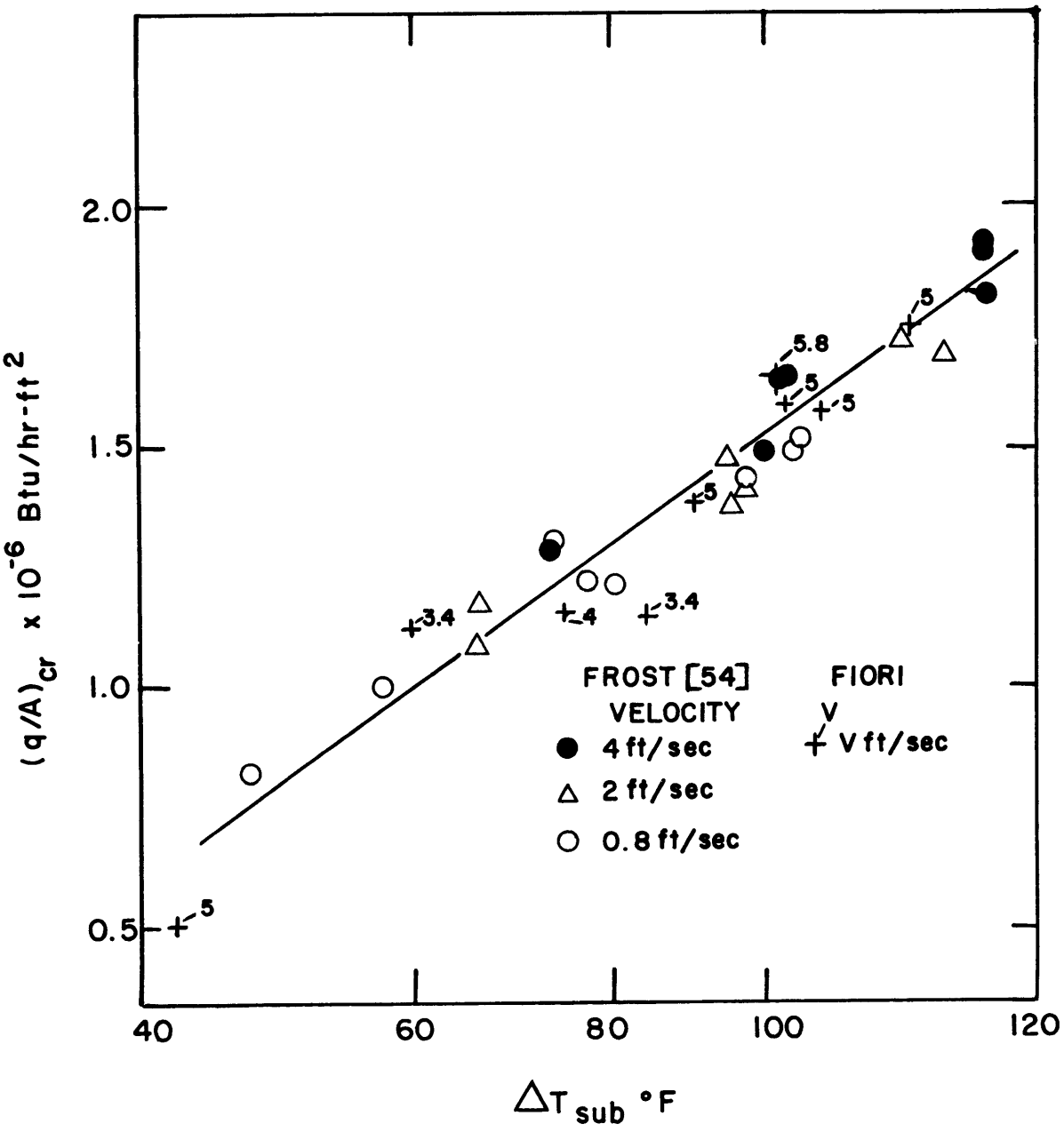

FIG. 41 COMPARISON OF FROST'S [54] CHF ANNULAR DATA WITH PRESENT STUDY

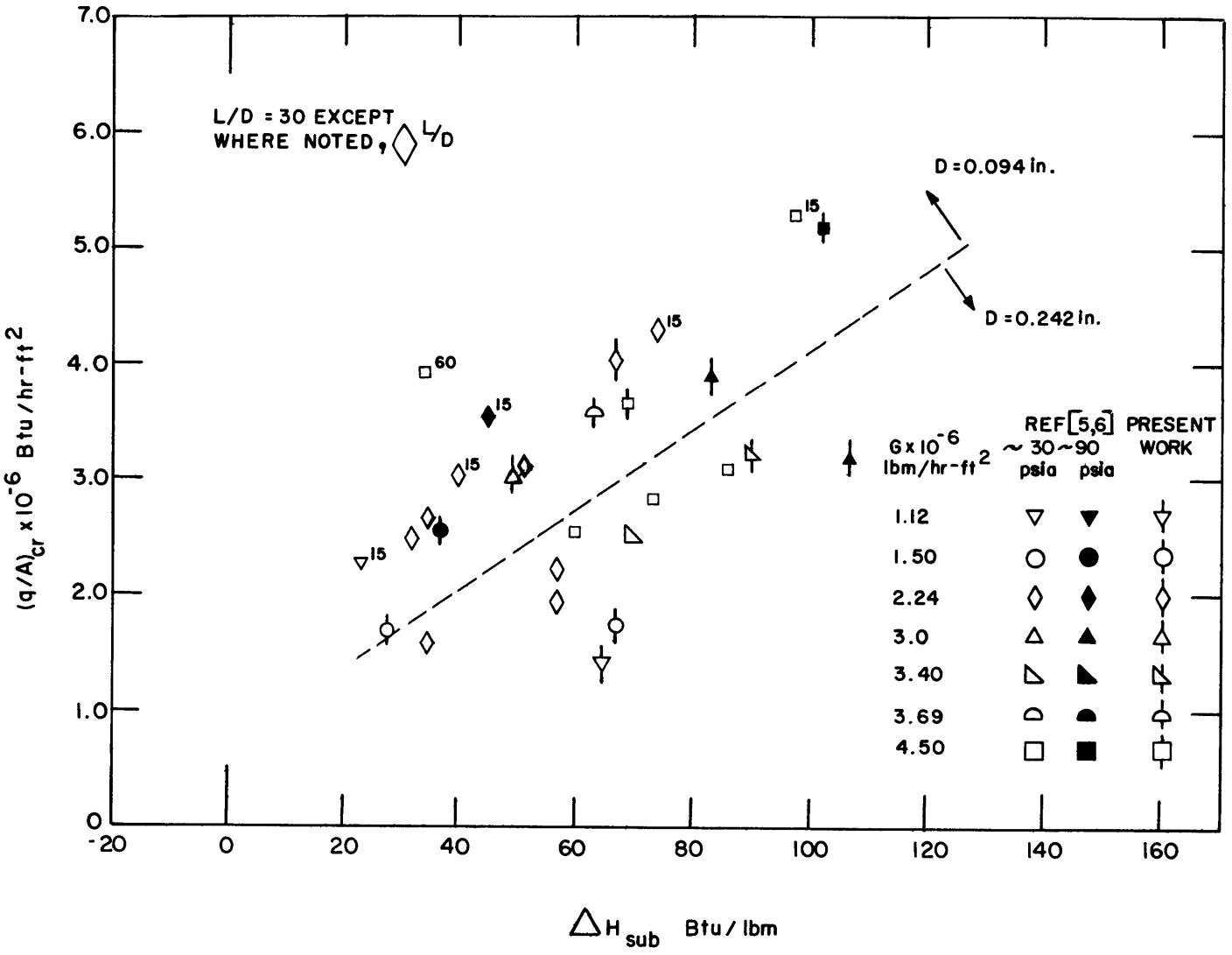

FIG. 42 COMPARISON OF M.I.T. CHF DATA WITH PRESENT STUDY

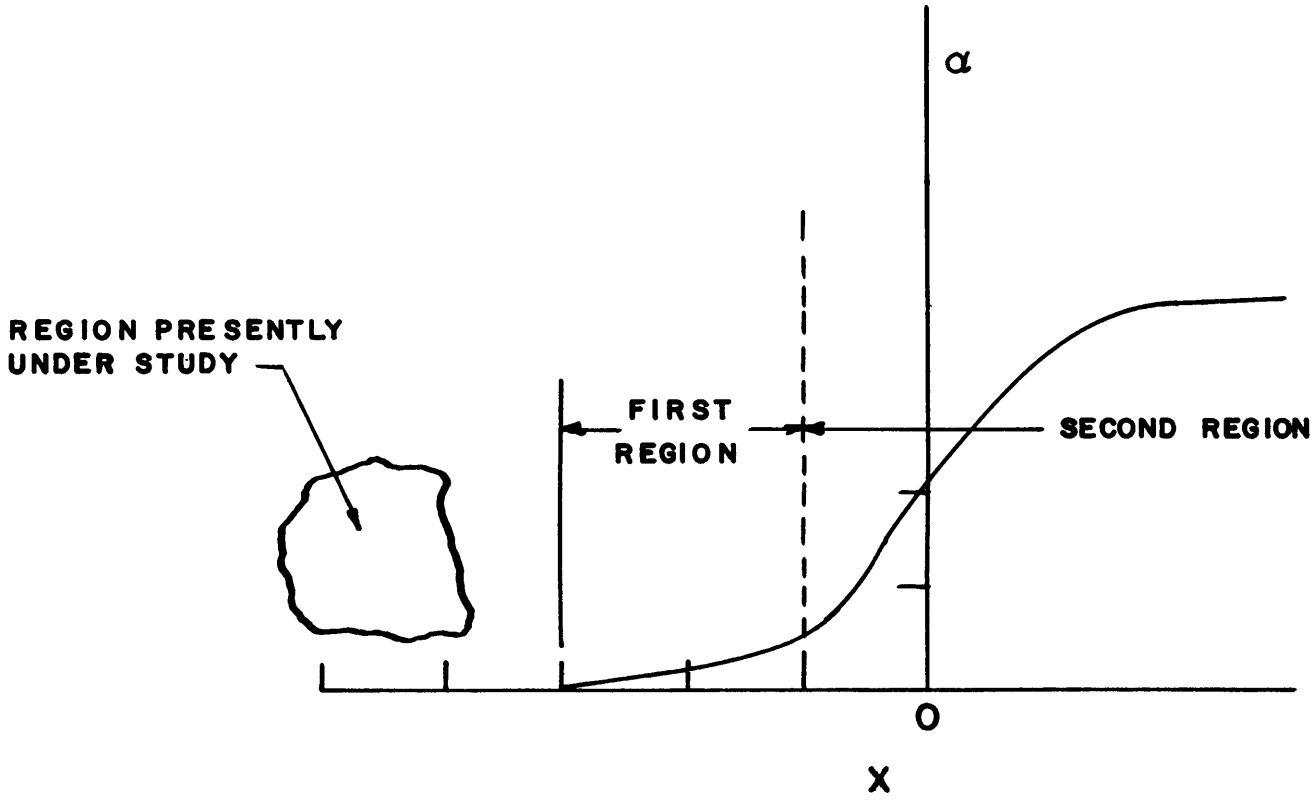

FIG. 43 GENERALIZED VOID FRACTION PREDICTION FOR FORCED-CONVECTION BOILING IN TUBES

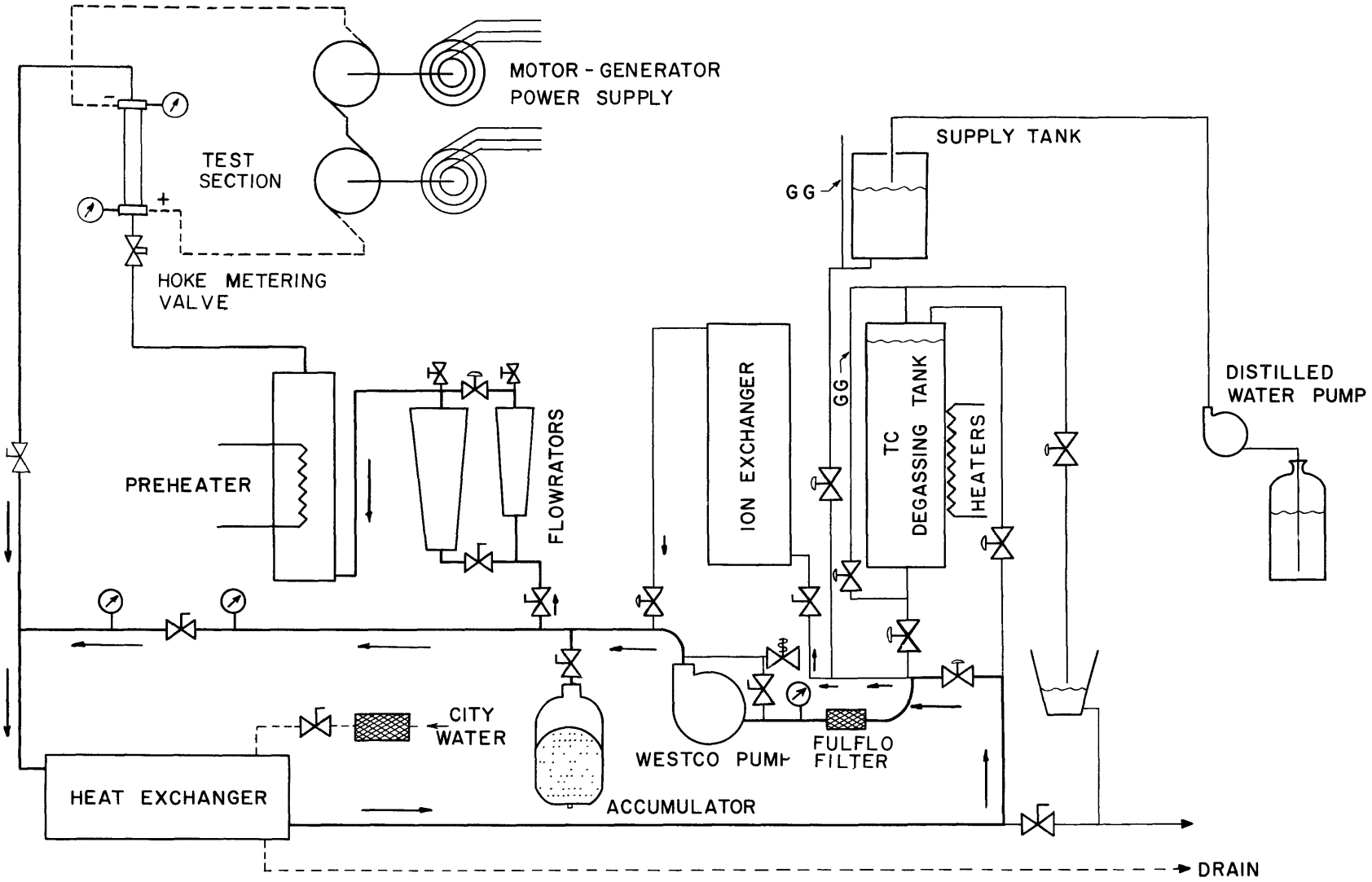

FIG. 44 SCHEMATIC LAYOUT OF EXPERIMENTAL FACILITY

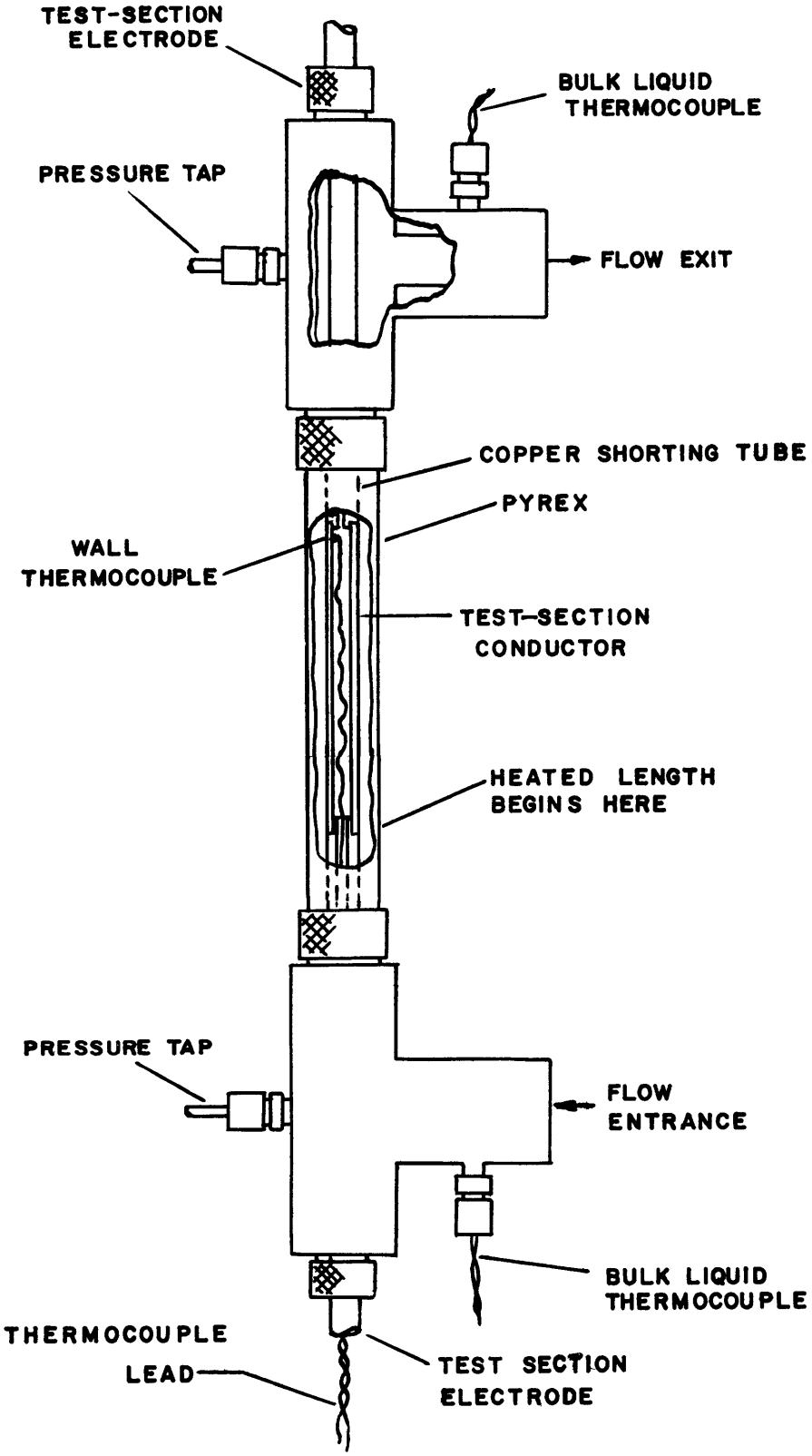

FIG. 45 GLASS ANNULAR TEST SECTION

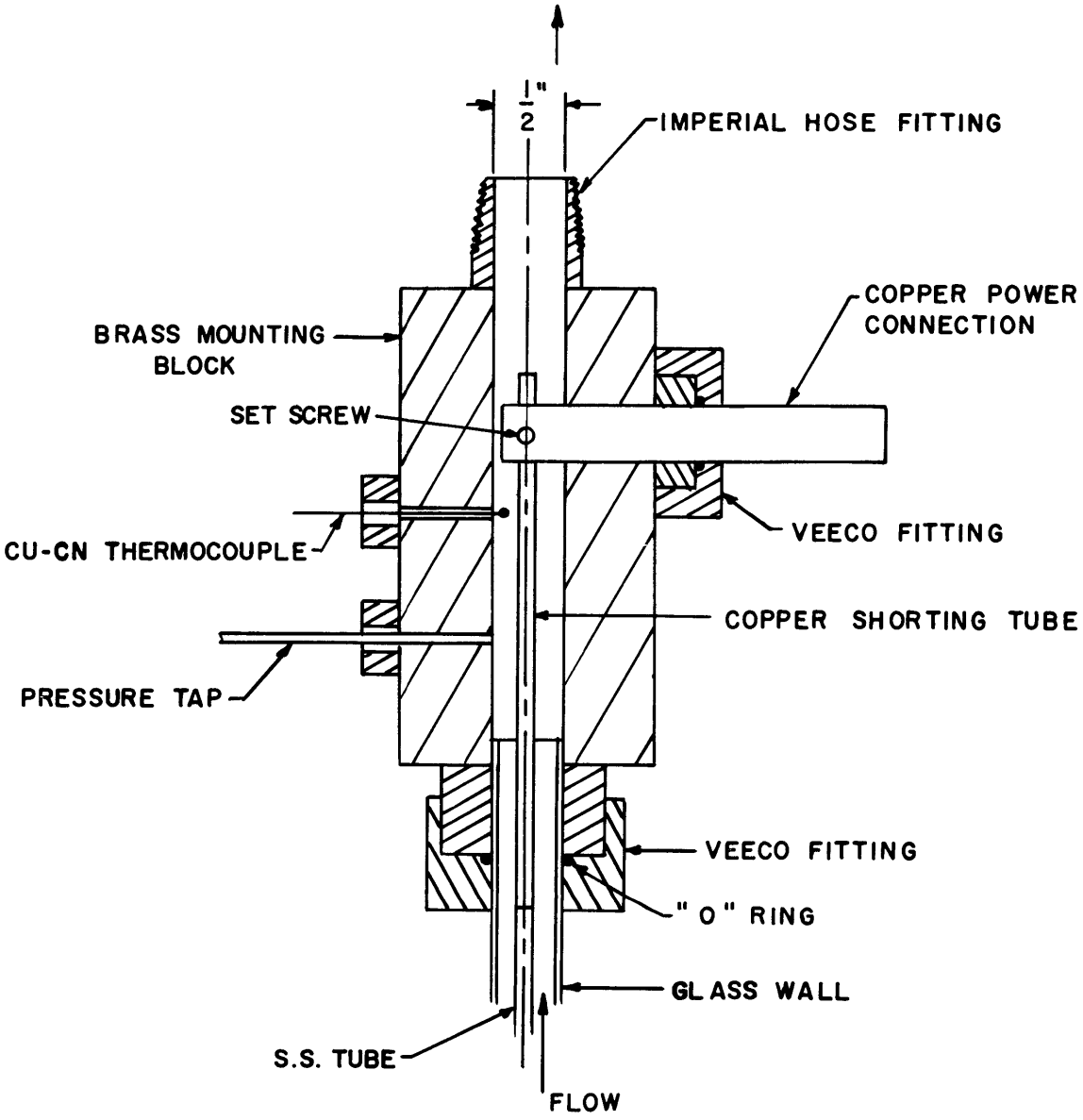

FIG. 46 MODIFIED EXIT PLENUM FOR ANNULAR TEST SECTION

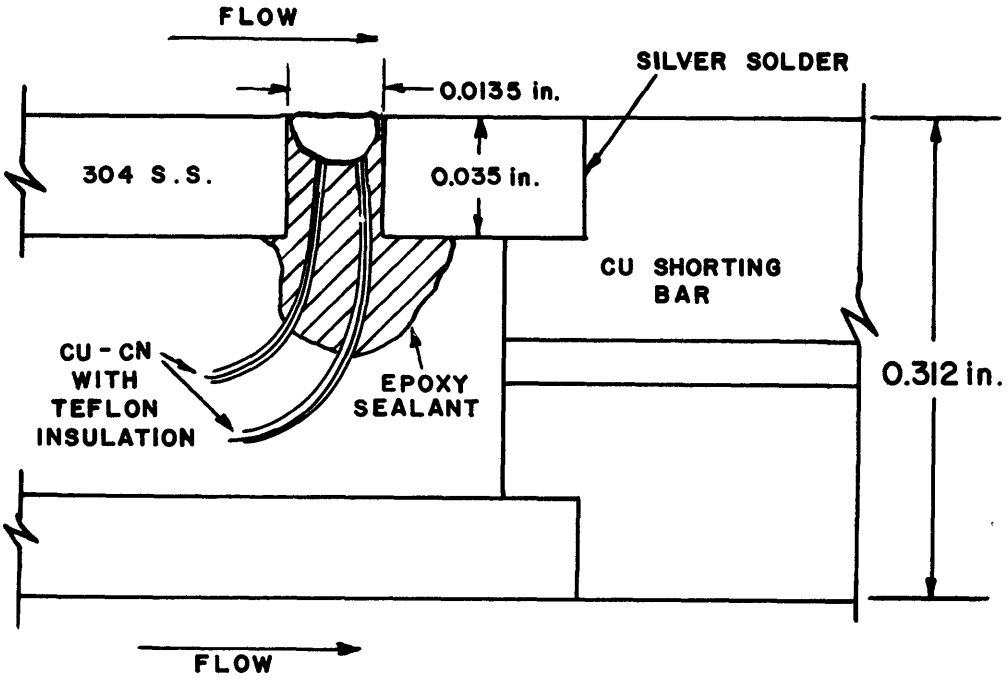

FIG. 47 DETAILS OF WALL THERMOCOUPLE CONSTRUCTION

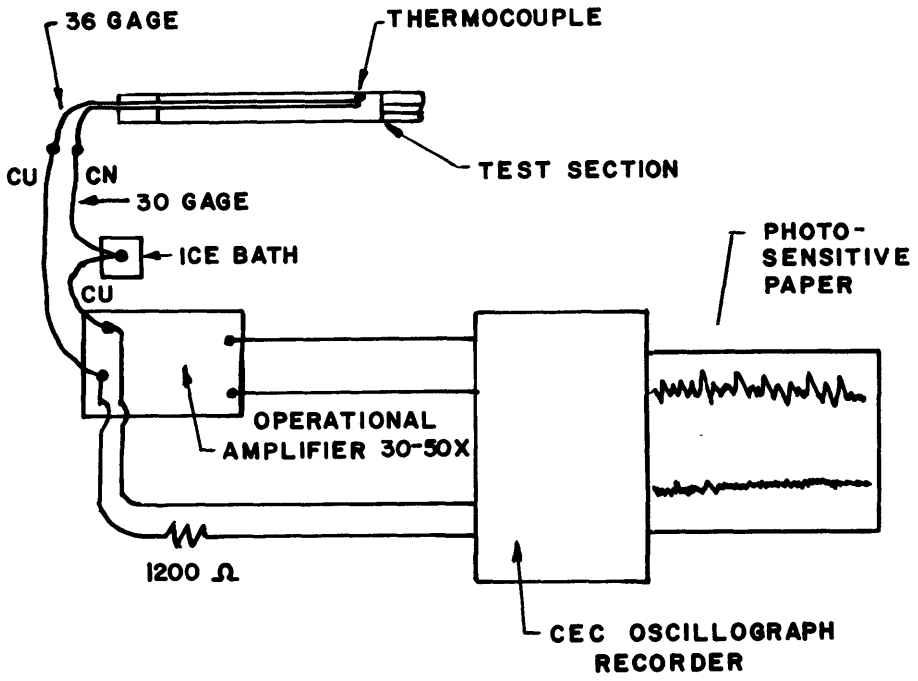

FIG. 48 WALL THERMOCOUPLE INSTRUMENTATION

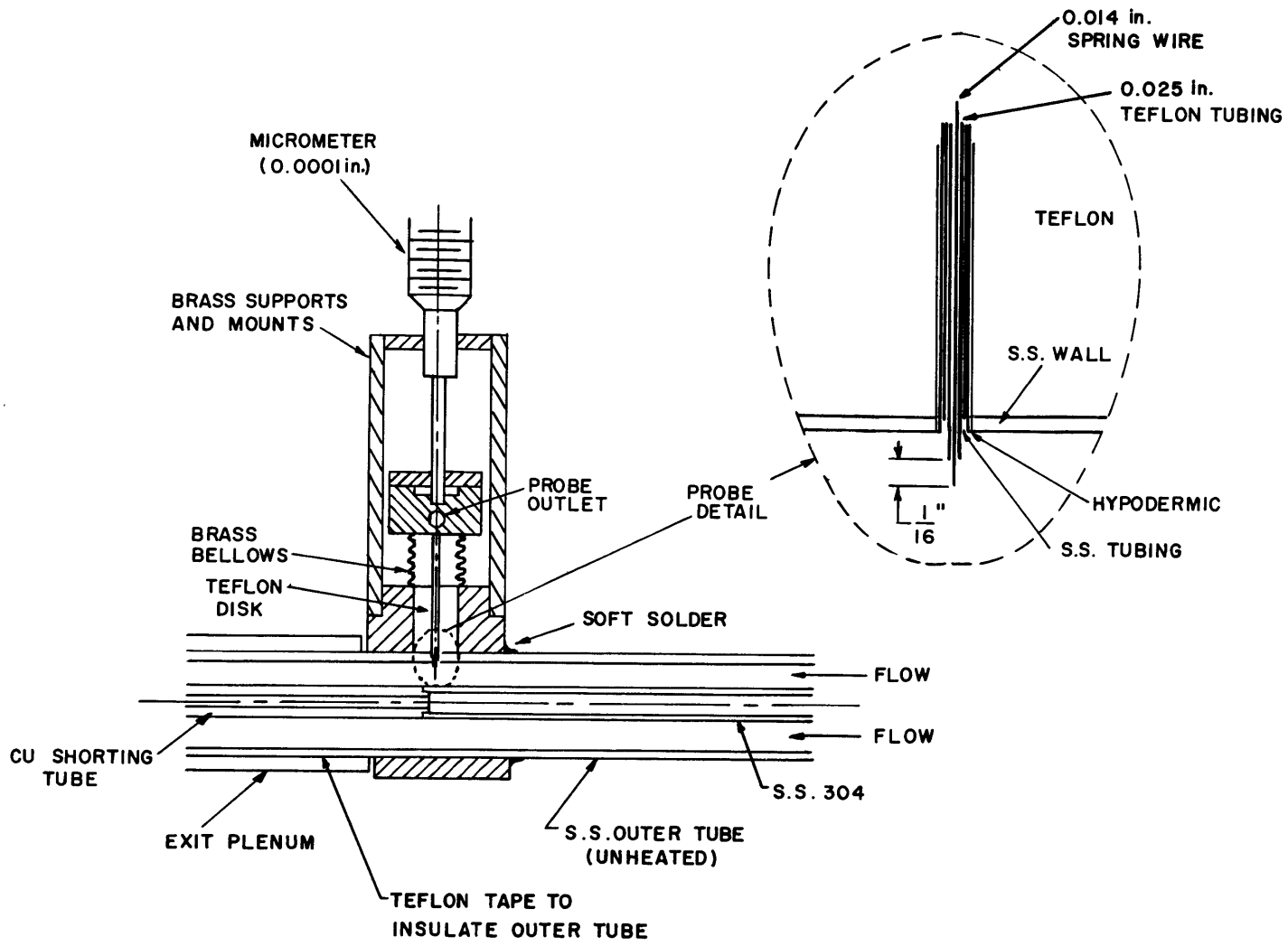

FIG. 49 MOVEABLE ELECTRICAL-RESISTANCE-PROBE ASSEMBLY FOR ANNULAR TEST SECTION GEOMETRIES

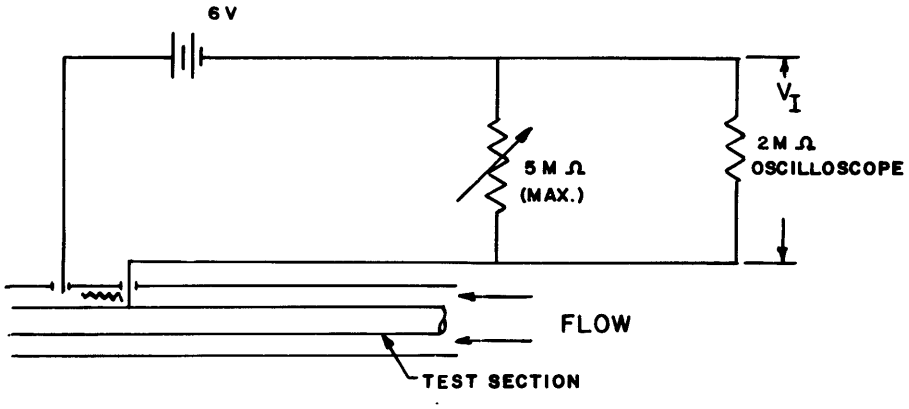

FIG. 50 ELECTRICAL-RESISTANCE-PROBE CIRCUIT

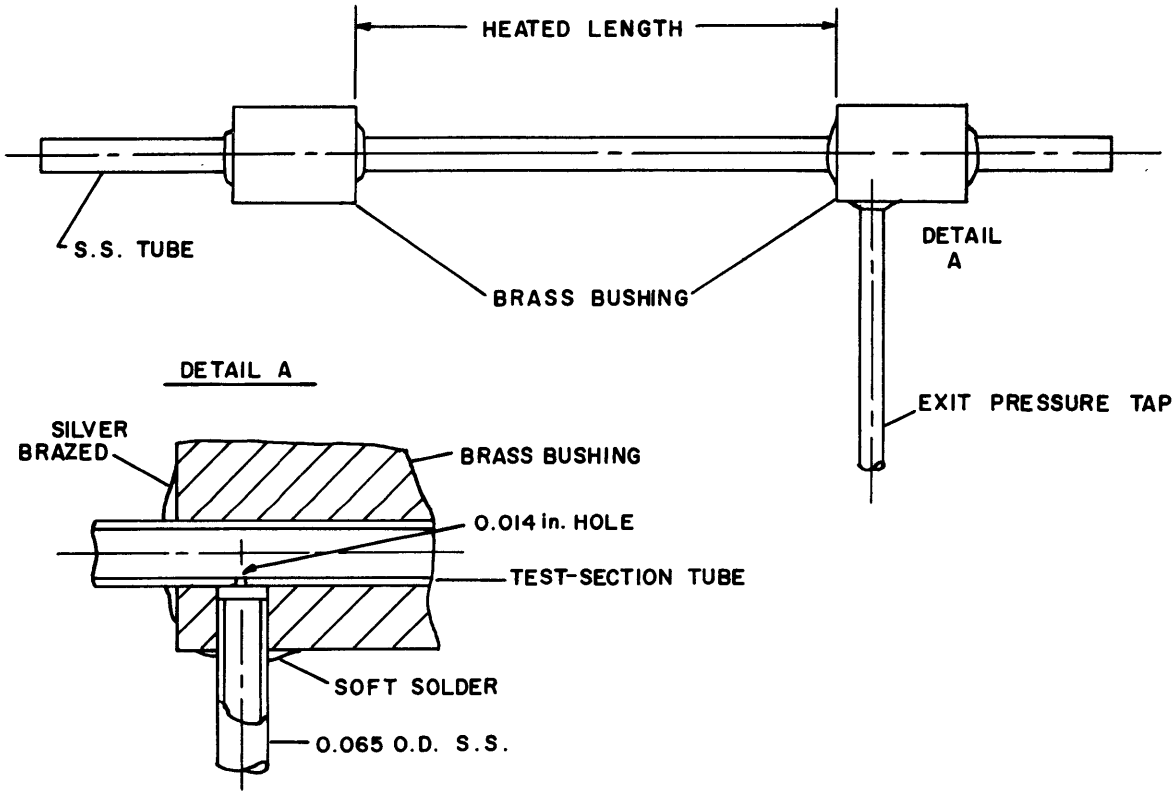

FIG. 51 DETAILS OF STANDARD TUBULAR CHF TEST SECTIONS

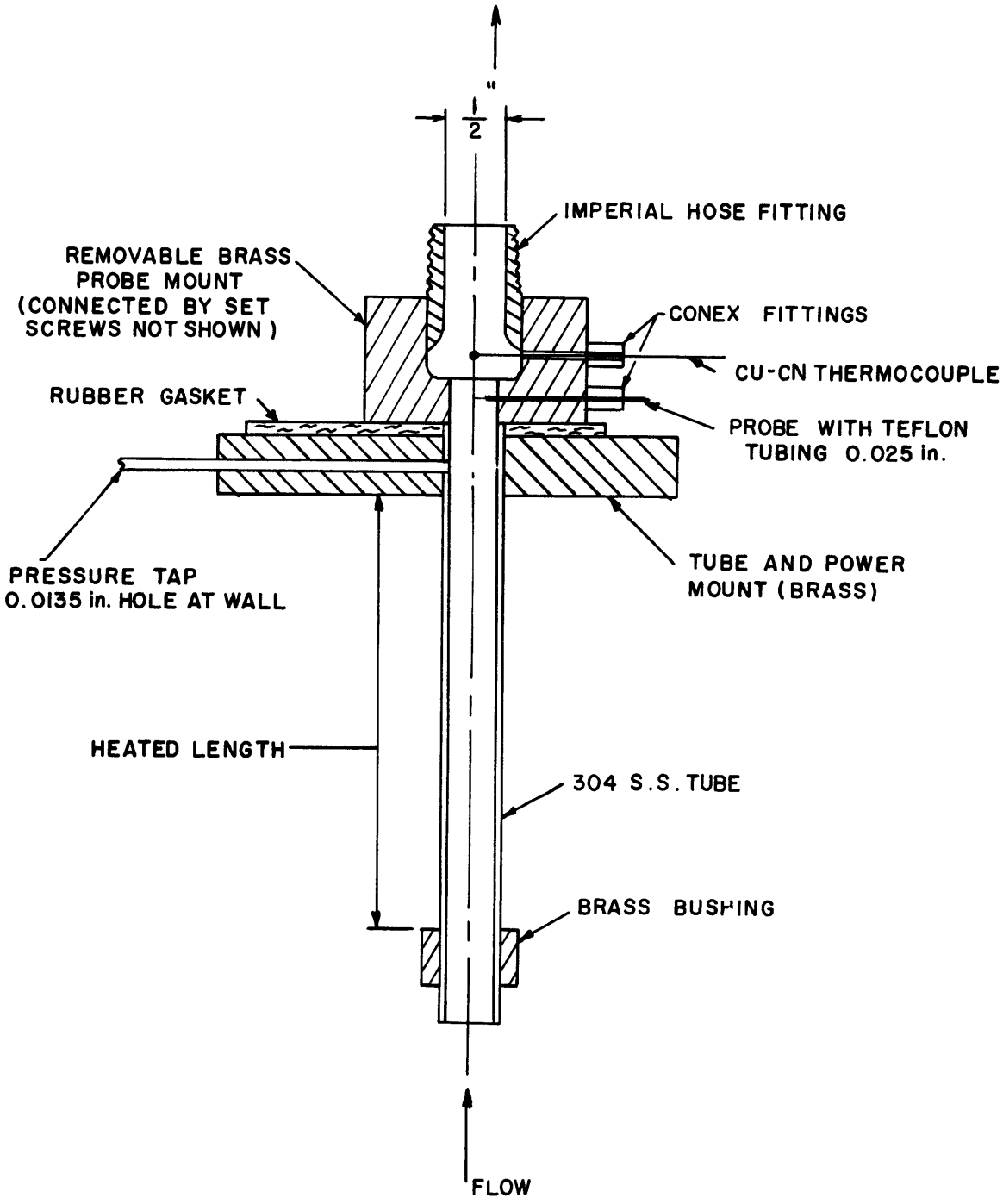

FIG. 52 ELECTRICAL-RESISTANCE-PROBE ASSEMBLY FOR TUBULAR TEST SECTIONS

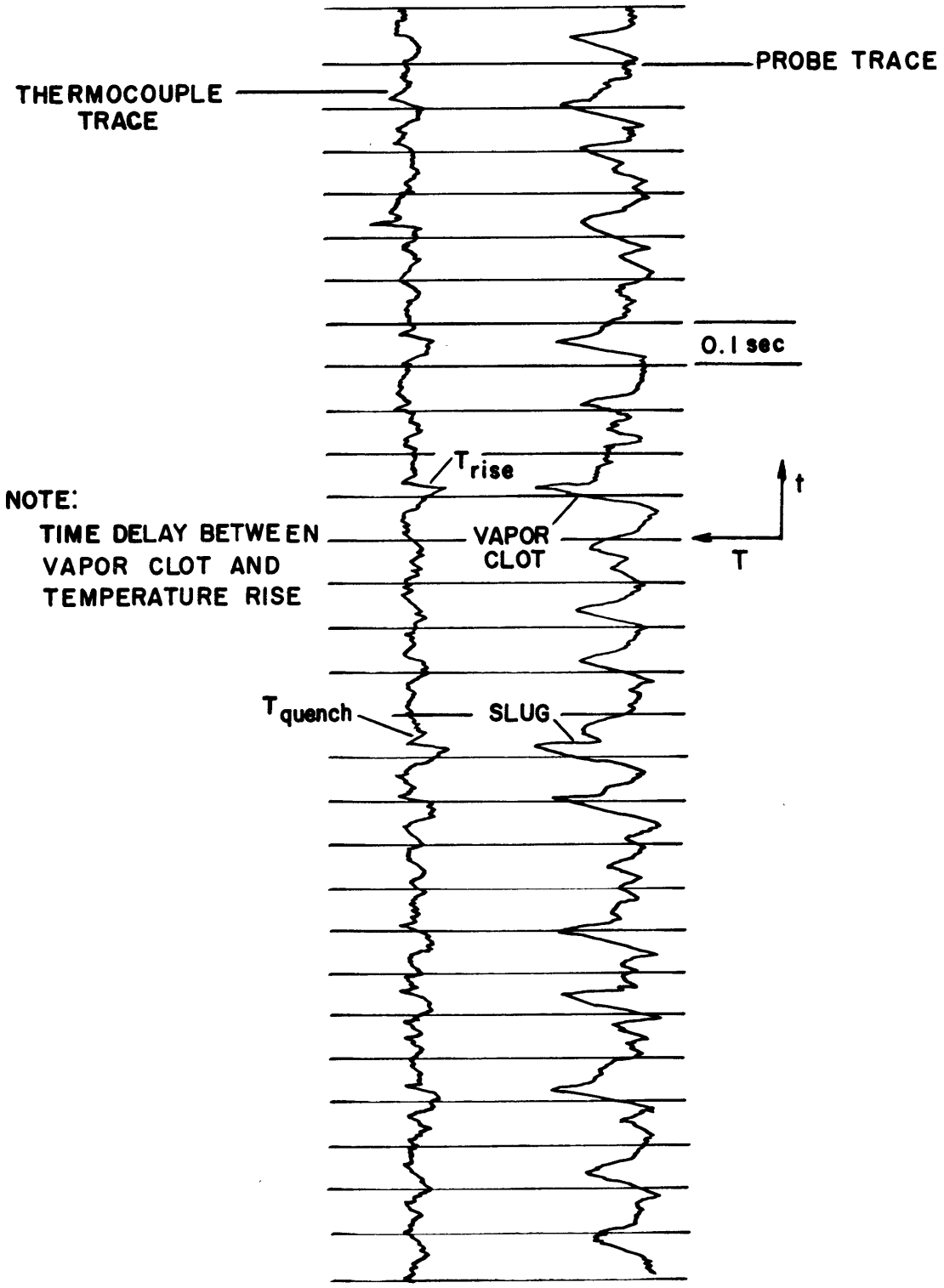

FIG. 53 WALL TEMPERATURE TRACE WITH SIMULTANEOUS FLOW REGIME PROBE TRACE

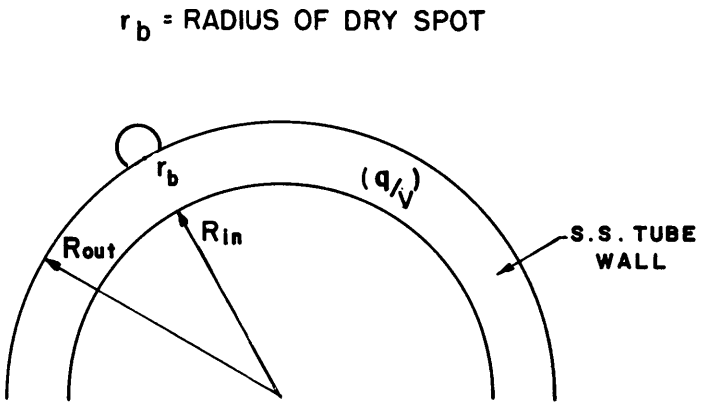

FIG. 54 SKETCH OF BUBBLE ON CURVED HEATED SURFACE

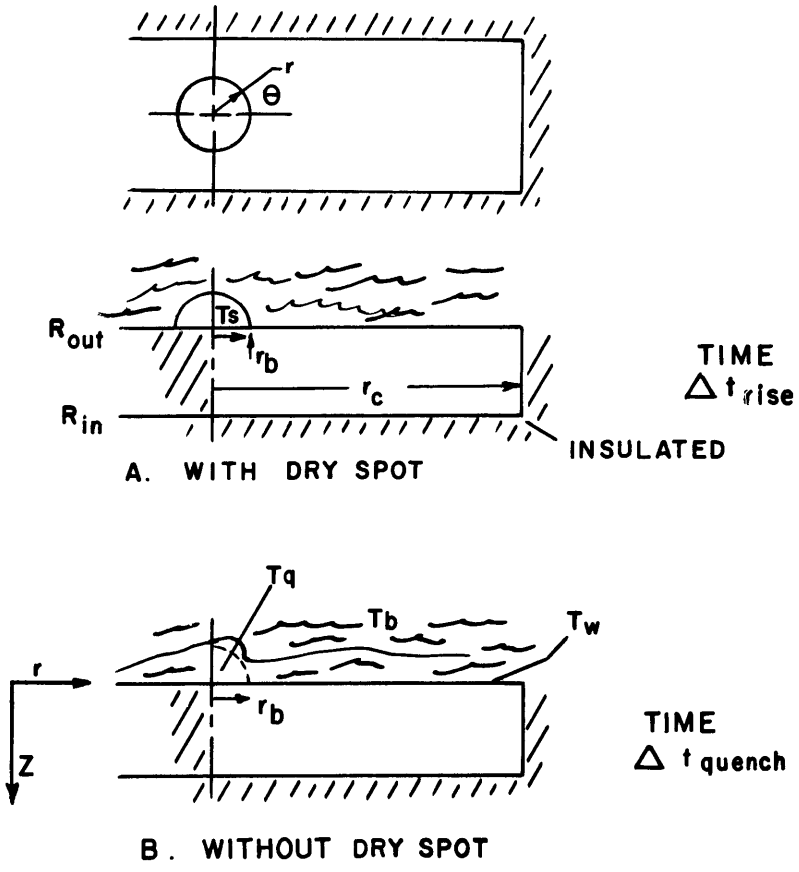

FIG. 55 FLAT PLATE APPROXIMATION TO TUBULAR WALL GEOMETRY

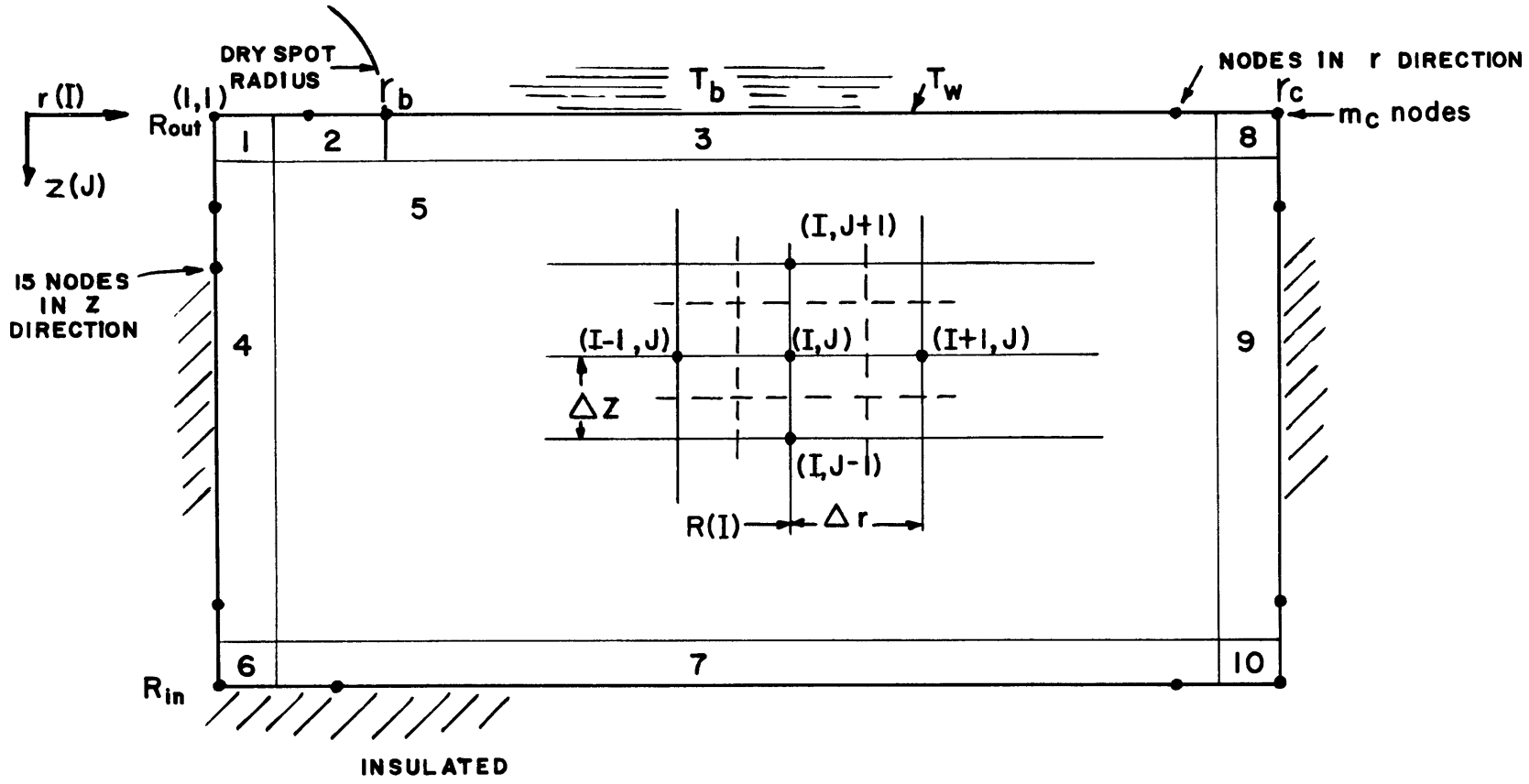

FIG. 56 SCHEMATIC OF TUBE WALL DIVISIONS FOR THE COMPUTER PROGRAM

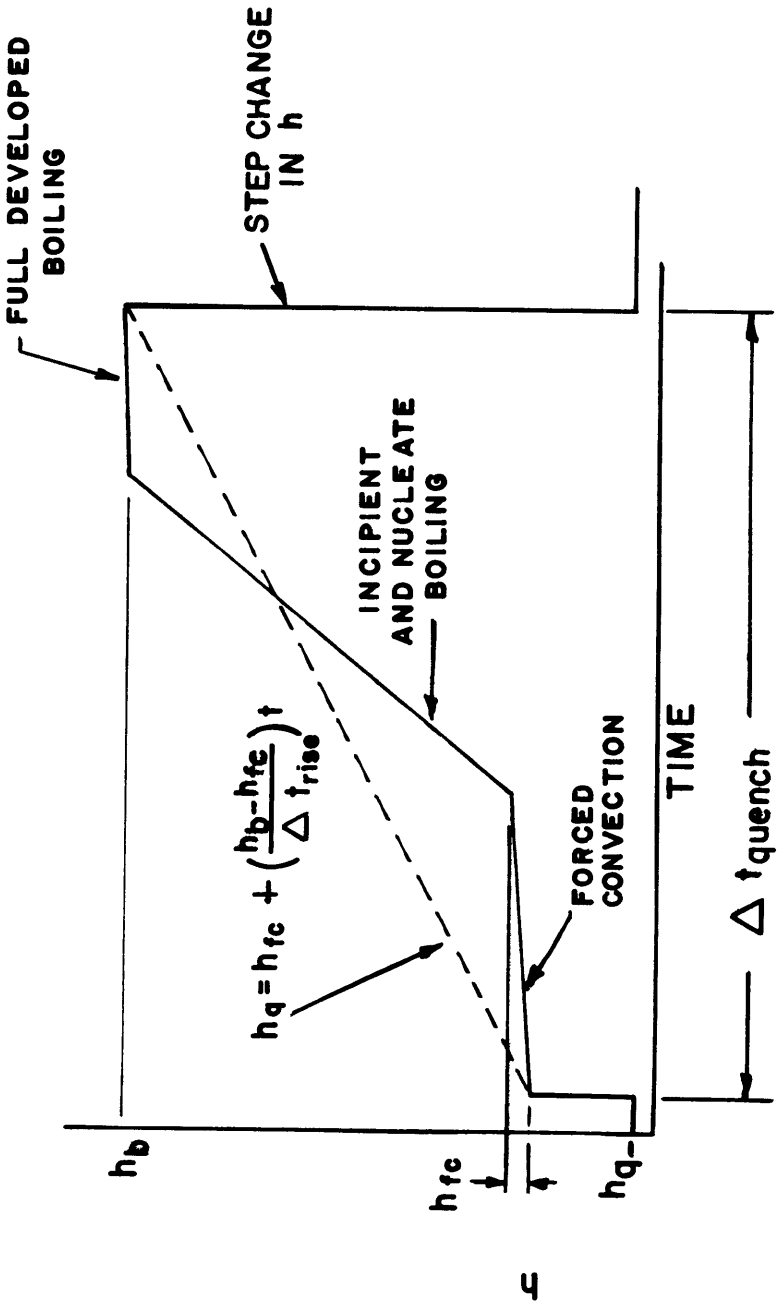

FIG. 57 VARIATION OF HEAT-TRANSFER COEFFICIENT WITH TIME

REFERENCES

1 W. H. McAdams, W. E. Kennel, C. S. Minden, R. Carl, P. M. Picornell and J. E. Dew, "Heat Transfer at High Rates to Water with Surface Boiling," Industrial and Engineering Chemistry, vol. 41, No. 9, 1949, pp. 1945 - 1953.

2 F. C. Gunther, "Photographic Study of Surface-Boiling Heat Transfer to Water with Forced Convection",ASME Transactions, vol. 73, 1951, pp. 115-123.

3 V. E. Doroshchuck and F. P. Lantsman, "The Effect of Channel Diameter on Critical Heat Flux", Teploenergetika No. 8, 1963.

4 A. D. Ornatski, "The Effect of Length and Tube Diameter on Critical Heat Flux in Subcooled Forced Convection", Teplo-energetika, no. 6, 1960.

5 A. E. Bergles, "Subcooled Burnout in Tubes of Small Diameter", ASME Paper 63-WA-182, 1963.

6 C. S. Loosmore and B. C. Skinner, "Subcooled Critical Heat Flux for Water in Round Tubes", SM thesis in Mech. Eng., M.I.T., June 1965.

7 S. Mirshak, W. S. Durant, and R. H. Towell, "Heat Flux at Burnout", DP-335, Savannah River Lab., February 1959.

8 R. V. Macbeth, "Part 4: Application of a Local Condition Hypothesis to World Data for Uniformly Heated Round Tubes and Rectangular Channels", AEEW-R 267, August 1963.

9 E. Burck and W. Hufschmidt, "Measurement of the Critical Heat Flux Density of Subcooled Water in Tubes at Forced Flow", EURATOM Report No. EUR 2432. d, 1965.

10 J. Longo, "A Statistical Study of Subcooled Burnout Including the Effects of Local Hot Spots", KAPL-1744, October 1957.

11 B. A. Zenkevich, "The Generalization of Experimental Data on Critical Heat Fluxes in Forced Convection of Subcooled Water", J. Nucl. Energy, Part B: Reactor Technology, vol. 1, 1959, pp. 130-133.

12 A. P. Ornatskii and L. S. Vinyarskii, "Heat Transfer Crisis in a Forced Flow of Under heated Water in Small Bore Tubes", Trans. from Teplofizika Vysokikh Temperatur, vol. 3, No. 3, May 1965, pp. 444-451.

13 W. S. Durant and S. Mirshak, "Roughening of Heat Transfer Surfaces as a Method of Increasing Heat Flux at Burnout", DP-380, July 1959.

14 D. H. Lee, "An Experimental Investigation of Forced Convection Burnout in High Pressure Water - Part III. Long Tubes With Uniform and Non-Uniform Axial Heating", AEEW - R355, 1965.

15 G. C. Vliet and G. Leppert, "Critical Heat Flux for Subcooled Water Flowing Normal to a Cylinder", ASME Paper No. 62-WA-174,1962.

16 I. T. Aladyev, Z. L. Miropolsky, V. E. Doroshchuck and M. A. Styrikovich, "Boiling Crisis in Tubes", International Developments in Heat Transfer, Part II, ASME, 1961, pp. 237-243.

17 G. F. Hewitt, H. A. Kearsey, P. M. C. Lacey, and D. J. Pulling, "Burnout and Film Flow in the Evaporation of Water in Tubes", AERE-R4864, March 1965.

18 F. Mayinger, O. Schad, and E. Weiss, "Investigations into the Critical Heat Flux in Boiling", Report No. 09.03.01, MAN, May 1966.

19 R. S. Daleas and A. E. Bergles, "Effects of Upstream Compressibility on Subcooled Critical Heat Flux", ASME Paper No. 65-HT-67.

20 J. S. Maulbetsch and P. Griffith, "A Study of System-Induced Instabilities in Forced-Convection Flows with Subcooled Boiling", M.I.T. Engineering Projects Laboratory, Report No. 5382-35, 1965.

21 R. T. Jacobs and J. A. Merrill, "The Application of Statistical Methods of Analysis for Predicting Burnout Flux", Nucl. Sci. Eng., vol. 8, 1960, pp. 480-496.

22 R. V. MacBeth, B. Thompson, "Boiling Water Heat Transfer Burnout in Uniformly Heated Round Tubes: A Compilation of World Data with Accurate Correlations", AEEW-R356, July 1964.

23 P. Griffith, "The Correlation of Nucleate Boiling Burnout Data", ASME Paper No. 57-RT-21, 1957.

24 W. R. Gambill, "Generalized Prediction of Burnout Heat Flux for Flowing Subcooled, Wetting Liquids", AIChE preprint 17, Fifth National Heat Transfer Conference, Houston, 1962.

25 L. Bernath, "A Theory of Local Boiling Burnout and its Application to Existing Data," AIChE Preprint 110 for Third National Heat Transfer Conference, 1959.

26 H. L. Wessel, "Investigation of Forced-Convection Subcooled Boiling," SB thesis in Mech. Eng., M.I.T., May 1964.

27 S. Levy, "Prediction of the Critical Heat Flux in Forced Convection Flow," GEAP-3961, June 1962.

28 W. H. Jens and D. A. Lottes, "Analysis of Heat Transfer, Burnout, Pressure Drop and Density Data for High Pressure Water," ANL-4627, May 1951.

29 Y. P. Chang, "Some Possible Critical Conditions in Nucleate Boiling," ASME Paper No. 62-HT-37, 1962.

30 N. Zuber, M. Tribus, and J. W. Westwater, "The Hydrodynamic Crisis in Pool Boiling of Saturated and Subcooled Liquids,"International Developments in Heat Transfer , Part II, ASME, 1961, pp.27-.

31 S. G. Bankoff, "On the Mechanism of Subcooled Nucleate Boiling," Part I Preliminary Considerations, Part II Sequential Rate Process Model," AIChE preprint No. 19 and No. 20 for Fourth National Heat Transfer Conference, August 1960.

32 L. S. Tong, H. B. Currin, P. S. Larsen,and O. G. Smith, "Influence of Axially Non-Uniform Heat Flux on DNB," AIChE preprint No. 17 for Eighth National Heat Transfer Conference, 1965.

33 D. P. Jordan and G. Leppert, "Pressure Drop and Vapor Volume with Subcooled Nucleate Boiling," Int. J. Heat Mass Transfer, vol. 5,1962, pp. 751-761.

34 M. A. Styrikovich and E. I. Nevstrueva, "An Approximate Estimation of Circulation and Temperature Characteristics of Two-Phase Pulsation Flows with Surface Boiling," Proceedings of the Third Int. Ht. Trans. Conf., vol. IV., AIChE 1966, pp. 207-215.

35 M. A. Styrikovich and E. I. Nevstrueva, "Some New Methods of Examining Boiling Mechanisms and the Crisis in Boiling," High Temperature vol. 2, No. 3, May-June 1964. Translated from Teplofizika Vysokikh Temperatur, vol. 2, No. 3, pp. 437-445, May-June 1964.

36 T. Sato, Y. Mayashida, and T. Motoda, "The Effect of Flow Fluctuation on Critical Heat Flux," Proceedings, Proceedings of the Third Int. Ht. Trans. Conf., vol. IV, AIChE pp. 226-233.

37 M. P. Fiori and A. E. Bergles, "A Study of Boiling Water Flow Regimes at Low Pressure," M.I.T. Engineering Projects Laboratory, Report No. 5382-40, February 1966.

38 G. J. Kirby, R. Staniforth, and J. H. Kinneir, "An Investigation into a Possible Mechanism of Subcooled Burnout," AEEW-M 725, March 1966.

39 L. S. Tong, L. E. Efferding, and A. A. Bishop, "A Photographic Study of Subcooled Boiling Flow and DNB of Freon-113 in a Vertical Channel," ASME Paper No. 66-WA/HT-39, 1966.

40 M. S. Styrikovich and E. I. Nevstrueva, "Investigation of Vapor-Content Distribution in Boiling Boundary Layers by the Beta-Radioscopy Method," Soviet Physics Doklady, vol. 5 No. 1, July-August 1960.

41 M. G. Cooper and A. J. P. Lloyd,"Transient Local Heat Flux in Nucleate Boiling," Proceedings of the Third Int. Ht. Trans. Conf., vol. IV, AIChE, 1966, pp. 193-203.

42 R. S. Dougall and T. E. Lippert, "An Investigation into the Role of Thermal Fluctuations on Bubble Nucleation in Pool Boiling." ASME Paper No. 67-WA/HT-31, 1967.

43 B. D. Marcus and D. Dropkin, "Measured Temperature Profiles within the Superheated Boundary Layer above a Horizontal Surface in Saturated Pool Boiling of Water," Journal of Heat Transfer, vol. 87, 1965, pp. 333-.

44. R.W. Bobst and C. P. Colver, "Temperature Profiles Up to Burnout Adjacent to a Horizontal Heating Surface in Nucleate Pool Boiling Water," AIChE preprint No. 30, for Ninth National Heat Transfer Conference, August 1967.

45 R. Semeria and J. C. Flamano, "Utilisation D'un Micro Thermo-couple pour l'etude de L'eballition Locale de L'eau en Convection Libre," Grenoble Center of Nuclear Studies, Report No. 81, December 1967.

46 G. J. Kirby, R. Staniforth,and J. H. Kinneir, "A Visual Study of Forced Convection Boiling," Part 2 - Flow Patterns and Burnout for a Round Test Section," AEEW-R-506, 1967.

47 A. E. Bergles and M. Suo, "Investigation of Boiling Water Flow Regimes at High Pressure," Proceedings of the 1966 Heat Transfer and Fluid Mechanics Institute, Stanford University Press, 1966, pp. 79-99.

48 A. E. Bergles and J. P. Roos, "Critical Heat Flux and Film Thickness Observations for High Pressure Water in Spray Annular Flow," Proceedings of the International Symposium on Two-Phase Cocurrent Flow, University of Waterloo, 1968.

49 Y. Y. Hsu, F. F. Simon and J. F. Lad, "Destruction of a Thin Liquid Film Flowing Over a Heating Surface," AIChE preprint No. 5 for the Symposium on Heat Transfer Part I, Fifty-First National Meeting, San Juan, Puerto Rico, September 1963.

50 P. J. Berenson and R. A. Stone, "A Photographic Study of the Mechanism of Forced Convection Vaporization," Chemical Engineering Progress Symposium Series 57, vol. 61, 1965, pp. 213-217.

51 G. F. Hewitt and P. M. C. Lacey, "The Breakdown of the Liquid Film in Annular Two-Phase Flow," AERE-R4303, August 1963.

52 G. F. Hewitt, M. A. Kearsey, P. M. C. Lacey and D. J. Pulling, "Burnout and Nucleation in Climbing Film Flow," AERE-R4374.

53 B. S. Gottfried, C. J. Lee, and K. J. Bell, "The Leidenfrost Phenomenon: Film Boiling of Liquid Droplets on a Flat Plate," Int. J. Heat Mass Transfer, vol. 9, 1966, pp. 1167-1187.

54 W. Frost, C. P. Costello, Jr., and C. H. Kippenham, "The Effect of Reduced Liquid-Vapor Surface Tension on Forced Convection Boiling," Univ. Washington, Dept. of Mech. Eng. Technical Report No. 65-1, July 1965.

55 E. P. Quinn and C. L. Swan, "Visual Observations of Fluid Behavior in High-Pressure Transition Boiling Flows," GEAP 4636, May 1965.

56 G. D. McPherson, "Axial Stability of the Dry Patch Formed in Dryout of a Two-Phase Annular Flow," Paper presented to the Canadian Congress of Applied Mechanics, 26 May 1967, Univ. of Laval, Quebec, Canada.

57 R. Cole and H. L. Shulman, "Bubble Growth Rates at High Jakob Numbers," Int. J. Heat Mass Transfer, vol. 9,1966, pp. 1377-1390.

58 P. Dergarabedian, "The Rate of Growth of Vapor Bubbles in Superheated Water," J. of Applied Mechanics, vol. 20, 1953, p. 537-.

59 Y. Y. Hsu, "On the Size Range of Active Nucleation Cavities on a Heating Surface," Journal of Heat Transfer, vol. 84, 1962, pp. 207-216.

60 M. S. Plesset and S. A. Zwick, "The Growth of Vapor Bubbles in Superheated Liquids," Journal of Applied Physics, vol. 25, No. 4, April 1954.

61 P. Griffith, J. A. Clark and W. M. Rohsenow, "Void Volumes in Subcooled Boiling Systems," ASME paper No. 58-HT-19, 1958.

62 G. W. Maurer, "A Method of Predicting Steady State Boiling Vapor Fraction in Reactor Coolant Channels," USAEC Report WAPD-BT-19, 1960, pp.59-70.

63 R. W. Bowring, "Physical Model, Based on Bubble Detachment, Calculation of Steam Voidage in the Subcooled Region of a Heated Channel," DECD Halden Reactor Project Report No. HPR-29, December 1962.

64 G. D. McPherson and W. Murgatroyd, "Film Breakdown and Dry-out in Two-Phase Annular Flow," Proceedings of the Third Int. Ht. Trans. Conf., vol. III, AIChE, 1966, P. 111.

65 W. T. Brown,Jr., "A Study of Flow Surface Boiling," Ph.D. thesis in Mech. Eng., M.I.T., January 1967.

66 R. F. Lopina, "Two-Phase Critical Heat Flux to Low Pressure Water Flowing in Small Diameter Tubes," SM thesis in Mech. Eng., M.I.T., January 1967.

67 S. J. Green and T. W. Hunt, "Accuracy and Response of Thermo-couples for Surface and Fluid Temperature Measurements," Temperature - Its Measurement and Control in Science and Industry, vol. 3, part 2, 1962, pp. 695-721.

68 S. Hynek, "Heat Transfer to Dispersed Flow," Ph.D. thesis in Mech. Eng., M.I.T. to be completed January 1969.

69 N. E. Todreas and W. M. Rohsenow, "The Effect of Non-Uniform Axial Heat Flux Distribution," Engineering Projects Laboratory Report No. 9843-37, M.I.T., September 1965.

70 A. E. Bergles and L. S. Scarola, "Effect of a Volatile Additive on the Critical Heat Flux for Surface Boiling of Water in Tubes," Chemical Engineering Science, vol. 21, 1966, pp. 721-723.

ERRATA

Page 43, line 3, change "were" to "was"

Page 44, line 14, correct spelling to "combination"

Page 50, line 4, add period at end of sentence

Page 52, line 12, correct spelling to "contradictory"

Page 97, line 6, should read,"Runs 5 and 6 were designed to show the wall thickness effect. The"

Page 101,Fig. 2, In symbol table under ΔT_{sub}, change 440 to 44

Page 151, Fig.57, On ordinate of figure change h_q to h_s